An Investigation of Indoor Positioning Systems and their Applications

Zixiang Ma

Submitted for the degree of Doctor of Philosophy

School of Electronic Engineering and Computer Science

Queen Mary, University of London

2018

Declaration

The work presented in the thesis is the author's own.

DATE: September 2018

SIGNATURE: Zixiang Ma

Abstract

Activities of Daily Living (ADL) are important indicators of both cognitive and physical well-being in healthy and ill humans. There is a range of methods to recognise ADLs, each with its own limitations. The focus of this research was on sensing location-driven activities, in which ADLs are derived from location sensed using Radio Frequency (RF, e.g., WiFi or BLE), Magnetic Field (MF) and light (e.g., Lidar) measurements in three different environments. This research discovered that different environments can have different constraints and requirements. It investigated how to improve the positioning accuracy and hence how to improve the ADL recognition accuracy. There are several challenges that need to be addressed in order to do this.

First, RF location fingerprinting is affected by the heterogeneity smartphones and their orientation with respect to transmitters, increasing the location determination error. To solve this, a novel Received Signal Strength Indication (RSSI) ranking based location fingerprinting methods that use Kendall Tau Correlation Coefficient (KTCC) and Convolutional Neural Networks (CNN) are proposed to correlate a signal position to pre-defined Reference Points (RPs) or fingerprints, more accurately, The accuracy has increased by up to 25.8% when compared to using Euclidean Distance (ED) based Weighted K-Nearest Neighbours Algorithm (WKNN).

Second, the use of MF measurements as fingerprints can overcome some additional RF fingerprinting challenges, as MF measurements are far more invariant to static and dynamic physical objects that affect RF transmissions. Hence, a novel fast path matching data algorithm for an MF sensor combined with an Inertial Measurement Unit (IMU) to determine direction was researched and developed. It can achieve an average of 1.72 m positioning accuracy when the user walks far fewer (5) steps.

Third, a device-free or off-body novel location-driven ADL method based upon 2D Lidar was investigated. An innovative method for recognising daily activities using a Seq2Seq model to analyse location data from a low-cost rotating 2D Lidar is proposed. It provides an accuracy of 88% when recognising 17 targeted ADLs. These proposed methods in this thesis have been validated in real environments.

Acknowledgements

First and foremost, I would like to take this opportunity to thank my supervisor, Dr Stefan Poslad, for his guidance, experience, impressive visions that guided my whole research all the way through and his incredible patience. I would also like to express my sincere gratitude to Dr John Bigham, Dr Laurissa Tokarchuk and Dr Jesus Requena Carrion who also gave me their incisive and invaluable comments on my PhD research.

Also, I would like to give big thanks to both the School of Electronic Engineering and Computer Science, the Queen Mary University of London and the China Scholarship Council that together offered a full PhD scholarship to me.

It is also a pleasure to thank my research colleagues and friends who have helped me and made this journey much more enjoyable, in particular, Dr Yansha, Dr Khuong, Dr Xingjian, Dr Qiao, Xiaoshuai and Bang.

I would also gratefully acknowledge the support of NVIDIA Corporation for the donation of the GPU used for the data analytics.

Finally, the special thanks must go to my beloved family for their great love, support and understanding, as I cannot accompany them when they were facing difficulty. Their encouragement has made this journey more comfortable, without them, this thesis would not have happened. Their generous love and support are beyond words.

List of Content

List of Figures

List of Tables

List of Abbreviations

ADL	Activities of Daily Life
AOA	Angle of Arrival
AP	Access Point
BLE	BLE Low Energy
BS	Base Station
CDF	Cumulative Distribution Function
CNN	Convolutional Neural Network
CSI	Channel State Information
DBSCAN	Density-based Spatial Clustering of Applications with Noise
DNN	Deep Neural Network
DTW	Dynamic Time Warping
ED	Euclidean Distance
EKF	Extended Kalman Filter
EM	Expectation–Maximization
FPM	Fast Path Matching algorithm
GA	Genetic Algorithm
GNSS	Global Navigation Satellite System
GPS	Global Positioning System
GSM	Global System for Mobile communication
ICT	Information Communications Technology

IG	Information Gain
IMU	Inertial Measurement Unit
IPS	Indoor Positioning System
KNN	K-Nearest Neighbours Algorithm
KTCC	Kendall Tau Correlation Coefficient
LBS	Location-based Service
LOS	Line of Sight
LPWAN	Low-Power Wide Area Network
LSTM	Long Short-Term Memory
MAC	Medium Access Control
MCL	Monte Carlo Positioning
MD	Multi-Dimensional
MI	Mutual Information
MF	Magnetic Field
MP	Measured Point
MS	Mobile Station
NLOS	Non-line-of-Sight
NLP	Natural Language Processing
NN	Nearest Neighbour
OS	Operating System (mobile device)
RF	Radio Frequency
RFID	Radio Frequency Identification

RNN	Recurrent Neural Network
RP	Reference Point
RSSI	Received Signal Strength Indication
SD	Standard Deviation
TDOA	Time Difference of Arrival
TOA	Time of Arrival
TOF	Time of Flight
TP	Test Point
UAV	Unmanned Aerial Vehicle
UKF	Unscented Kalman Filter
UWB	Ultra-Wide Band
WKNN	Weighted K-Nearest Neighbours Algorithm

1 Introduction

1.1 Motivation

We are spending more and more time indoors within buildings than in the past because we work and live more indoors. Indoor spaces within buildings are becoming far more complex regarding size, heterogeneity, and as a result are becoming far more complicated to localise a person or physical asset, and to navigate within. Indoor location determination links increasingly to a range of related indoor Location-based Services (LBS), such as:

- Locating a retail asset - how does someone navigate from position A to B to retrieve a physical item or to access a service at a location service Access Point (AP) (Chapter 3,4);
- People tracking – for the owner of an indoor space to better understand better if the space is efficiently and effectively being used; for people to monitor how much physical exercise, what physical activities they do while working (chapter 5).
- Ambient assisted living-monitoring or using ADL recognition for smart home or smart healthcare, monitoring in which rooms someone remains, i.e., is someone who needs home care, visiting the kitchen often enough to get food? (Chapter 6)

The focus of this research is on the use of sufficiently accurate IPSs to enable a subset of IPS applications referred to as Location-driven ADLs (LD-ADLs). Although, some generic ADLs can be location-independent such as walking or standing, as can some sports activities such as running or cycling. Other ADLs are Location-Driven, LD-ADLs, because the location enables the activity. Here are some examples. A warehouse, retail space or library primarily supports the ADL to locate, select and retrieve a physical asset such as a book or retail goods. Some sports involve specialised equipment or physical environment fixtures, e.g., playing table-tennis requires a table, Heating water for tea or coffee requires a heating element and power source.

The accuracy for location determination to recognise Location-driven ADLs varies depending on the type of indoor environment and application. In a retail space, the accuracy is needed to follow the correct path between shelving and to locate an item within an arm span, about 1.7m. Whereas in a smaller home environment a higher accuracy is needed (to 10 s or 100 s of cms) and a location context, e.g., this location is where the heating element for boiling water is. It can also involve motion characterisation and linking these together. Note also that some ADLs are more complex than they seem involving orchestrating several more atomic ADLs into a composite one, e.g., making tea can involve getting a clean mug, filling the heating element with water, doing some other activity while waiting for the water to boil, adding tea, pouring the boiling water, waiting for tea to percolate and then getting and adding any milk or sugar.

To achieve the above goals, *this research focusses first on how to improve IPS location accuracy in three heterogeneous physical environments, retail, office and a home/kitchen type space in order to explore how the type of physical space influences and constrains the type of IPS that can be accessed and used in each different type of space*. Second, this *research focusses on how location-driven ADLs can be linked to, and enabled due to, this better location accuracy*.

In some cases, the mapping of location to LD-ADL is simple and one-to-one, e.g., the layout of a retail space into parallel shelving lends itself to navigating and retrieving a physical asset. An appropriate location accuracy is vital because if customers cannot easily and accurately find their way to retrieve a physical item or to access a service at a service point, they may terminate the service interaction. Subsequently, service demand and revenue may decrease. This has a significant societal and economic impact. Physical store retailers can use accurately estimated locations to increase their profit margins, e.g., to manage shelf replenishment more efficiently, to avoid out-of-stock incidents, and based on their analysis of shopper's activities are then more able to offer customised promotions [1].

An office layout into desktops lends itself to doing desktop activities, commonly information-driven activities whilst seated. However, depending on the layout and design of the office, additional activities may also be enabled such as having small group discussions. Note it is not physically healthy to sit at a desktop for long periods and people may move as they require food and drink periodically. Hence, people in an office may walk around inside and outside of the office and eat and drink at their desks. Hence, there is a one-to-many mapping between location and LD-ADLs.

Learning and recognising human activities is not only useful and essential for many indoor building services and user activities but is also an important indicator of both physical and cognitive well-being in healthy and ill humans, e.g., are people taking good care of themselves through eating, drinking and exercising periodically [2]? Hence, recognising ADLs in vulnerable people who do not work, whilst at home, is also important in these types of people. There is also a one to many mapping between some locations and LD-ADLs in this type of space too, e.g., someone may sit at a kitchen table to read, listen or watch audio and video feeds, to meet others or to eat and drink.

1.2 Challenges

LBS are information services that are accessible, often via mobile devices and wireless communication networks that exploit the ability to make use of the changing geographic position of mobile devices. One of the essential parts of LBS is the positioning system. However, unlike an outdoor LBS that uses a standard Global Navigation Satellite (Positioning) System (GNSS), IPS face different technical challenges in contrast to that of outdoor location determination. There is no one proven ‘global’ standard Indoor Positioning System (IPS) that can be used reliably for all indoor LBSs. IPSs have employed a range of methods to estimate a user’s location, which is shown in Figure 1-1. This classifies IPS into proximity, inertial, geometric, finger-printing and visual (top row) with examples of such classes given in lower rows.

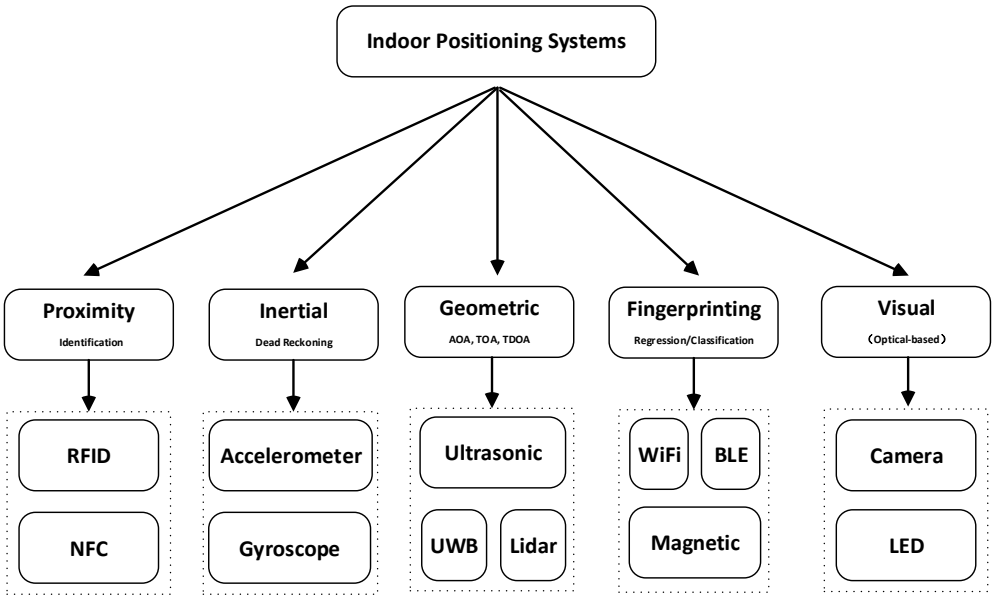

Figure 1-1 A taxonomy of methods of the most used IPS

There are several reasons for the existence of such a range of IPSs. The coverage and density of APs that can be accessed in different physical environments vary, e.g., small homes may be covered by as little as 1 WiFi AP whereas an office space may be covered by 10 s of WiFi APs. Spaces are cluttered in different ways that can attenuate AP signals in different ways, e.g., a retail space that contains metal shelving can affect WiFi, BLE, MF and light signals severely.

A higher location accuracy is often needed as physical assets tend to be packed closer together than outdoors physical assets; people move, and this increases the location determination error. There is no standard global spatial view or map, and a route plan that is accessible in a standard way. Similarly, indoor positioning methods have different limitations in different types of physical environment. For example, BLE trilateration based upon path loss methods (these can also be classified as geometric-based methods) are unsuitable for Non-Line Of Sight (NLOS) spaces; BLE and WiFi fingerprinting methods are affected by solid attenuating objects, including human bodies between the RF transmitter and receiver. MF-based fingerprinting methods are less affected by attenuation but are most effective in a space that contains lots of magnetic anomalies. Optical-based methods require a line of sight, higher data

transmission to a server and a high computation data analysis capability in a server. Thus, even if different IPSs were compared in a single physical environment, that comparison would vary across different types of physical environment with different layouts as the structure of physical objects they contain varies, e.g., these attenuate RF signals to different degrees as used by RF based IPSs (see also Section 2.2.4).

The capital and operational cost of installing and maintaining the IPS is also an important consideration. In some cases, a specific IPS infrastructure needs to be added, installed, to instrument a physical space by adding new types of APs to support that IPS service, e.g., BLE beacons. The type of AP determines how light and mobile they are and how they can be powered for how long. The physical layout determines where APs can be fixed and who has access to that space. Lightweight APs such as BLE beacons that are temporarily fixed are essentially untethered can be potentially removed by anyone who accesses that space. So, a trade-off needs to be made to select the right IPS. Moreover, even if we have 'accurate-enough' location determination results, how we analyse the data and use them to increase the application activity recognition accuracy is also a tough challenge.

The main challenges of focused indoor positioning methods are as follows:

- Proximity sensors are the more accurate positioning results they can achieve, the shorter their range. However, the short the range requires many more APs to give an adequate coverage driving up the cost.

- Inertial Measurement Units (IMUs) are effective at differentiating different types of human motion but less so at determining relative distance from a known location because they need to integrate acceleration and speed to do this, and the error increases with distance.

- RF path loss models or RSSI trilateration methods are easy to use and can offer highly accurate positioning result when they are used in a free space building environment. However, these trilateration methods need to deploy many Access Points (APs) such as transmitters or beacons to achieve a high

positioning performance, and it will severely be affected if NLOS conditions happen, which makes those methods unsuitable for complex RF spaces where there are fixed and moving attenuating RF objects.

- Location fingerprinting methods that rely on processing RF signal strength to indicate the location are more suited for NLOS RF signal environments rather than those that use RSSI path loss mode-based trilateration, as the latter is more susceptible to errors due to attenuation from physical objects in the transmitter-receiver path. For example, if a person holds an RF receiver is facing 180 degrees away from the transmitter, the signals will be attenuated going through the body, and the received signal strength will appear as if the transmitter is much further away using a free-space RF propagation model. Moreover, users are using different smartphone receivers, so the heterogeneity of RF hardware in smartphone receivers can also increase the position determination error.

- Unlike typical WiFi or BLE location fingerprinting, another type of location fingerprinting method is one that uses MF measurements are relatively unaffected by moving humans, providing more time-invariant location information, which is better suited to aisle-like spaces, e.g., used by retail outlets. However, this needs to be combined with inertial sensors, e.g., accelerometer and magnetometer or gyroscope, to calculate the heading of the user, and it usually needs time and a vast number of computations to give convergence results.

- Device-free or off-body positioning methods, e.g., using a Lidar or camera, can achieve excellent positioning accuracy within 10 cm. However, it also faces different problems, for example, multi-person tracking and heavy arithmetic computation. It is affected by objects that block the line of sight and cannot localise a person behind a nearby physical block (NLOS). This kind of technique is also quite expensive and is more suited for scenarios that require a high-accuracy, such as healthcare, or automatic driving. Moreover, such

techniques will collect vast amounts of data, so how to store, transmit and analyse this for real-time LBS applications is also a tough challenge.

For ADL recognition, there is also the following challenges:

- If traditional indoor positioning methods can offer accurate-enough estimated locations that can be used to recognise location-driven ADLs, e.g., go to the kitchen to cook dinner.

- How to minimise the privacy-intrusion through not directly or indirectly identifying individual users.

- How to collect and label a user's valid location information and the corresponding activities.

- How to recognise human activities based on the analysed information, and if the interleaved ADLs can be recognised.

1.3 Objectives, Focus and Limitations

The *focus of this research was problem-driven not solution-driven. Its focus was to investigate how indoor location-driven activities could be enabled in heterogeneous indoor environments using a novel, improved IPS designed for that actual indoor environment* using the existing state of the art IPS as a baseline. The focus is on exploring the application of IPSs in three different types of physical environment where LD-ADLs occur that first inherently require an IPS to locate something as part of that LD-ADL, e.g., to locate an item in a library or retail like space with shelves. Second to identify the physical activities of people who are in an office type space where some type people spend a major part of their working life. Third to identify the ADLs that occur at home in a kitchen as indicators of physical health. Note also the type, ownership and access to the physical environment strongly influences the effectiveness of different IPSs that can be used and how they can be installed, operated and maintained in that environment and the repeatability of experiments to different

degrees. The focus of this research was not to compare the multiple IPS (BLE, WiFi, MF and Lidar) solutions in a single indoor environment to find out which of these is the most accurate for that one type of environment. Instead, this is added to further work as this requires an equipment budget. This PhD came with no equipment budget[1].

This thesis is concerned with indoor location determination methods in different types (Library Room, PhD Office, Kitchen) indoor environment, and how to improve their positioning accuracy, in order then to enable a higher location-driven ADL recognition accuracy. Although there is a wide range of indoor space structures existing, the objective of this thesis is on the use of three specific types of indoor space structures that are application driven.

First, the focus is on retail-like space layouts, where items are organised along multiple, sometimes parallel, long corridors of person height shelving and the application aim is to locate an item on a shelf. The location accuracy needs to be of the order of an arm span, such that someone can be directed to where an item is and reach it within about 1.7 m from the shelf. Moreover, it is considered that users are usually carried smartphones, so a smartphone-based IPS is the first choice, instead of using additional specific devices. However, the smartphone hardware heterogeneity issue exists. So, a research question for this space concerns how to solve this issue.

The second type of application and space is an office where work desks are organised as an open plan space but where one side of it has spaces for meetings and for preparing snacks and drinks. Here, the applications are not so much for the inhabitants to locate things as they should quickly familiarise themselves with the use of the space. It is, for example, more to do with the managers and owners of the space, for them to understand better if it is efficiently and effectively being used. Hence, the research

[1] N.B., we bought about 55 Bluetooth beacons from another project grant, about 45 of these became lost in the library because of renovation and for other reasons.

question in this space concerns how to discriminate the activity routines (about 3 m, coarse-grained activity recognition).

The third and final type of application space focus is on small home buildings where high location accuracy is necessary to discriminate between which landmarks for activities, e.g., fridge, sink, kettle, therein a user the host is nearby to. Hence, typical fingerprinting systems cannot offer such an accurate estimated location (less than 0.5 m positioning accuracy to discriminative those mentioned objectives), so Lidar was used. Here, many home activities occur at furniture units that are on the periphery or walls of rooms. This type of space is also of interest as it tends to be used for example for sheltered human accommodation, i.e., for the elderly, those in rehabilitation and those recovering from severe depression. Hence, eHealth such as care in the community applications have the potential for a huge societal impact. It is of interest to carers if someone undertakes regular normal routine applications such as making a hot drink. If not, this could indicate a health state that needs to be addressed in some way. The research questions of this space concern how to accurate localise the user without jeopardising the users' privacy and recognise their activities.

Each of these spaces has different technical challenges, e.g., to do with security and privacy, to do with access and management of equipment such as APs, i.e., how and where APs can be located, etc.

Generally, for the simplicity and elegance to organise different studies, and because of different practical constraints, e.g., lack of a large enough number of WiFi transmitters to use trilateration to determine the location in a home environment, different techniques were used for different IPS applications and spaces. Bluetooth and MF with inertial sensors were used for the library location study (as they are smartphone compatible, users do not need to bring other sensors); Lidar (high accurate and wearable-free) was used for the home environment; WiFi (plenty WiFi APs) was used in the office study. Proximity, Ultrasonic, LED (as shown in Figure 1-1), etc were not studied. Since RF infrastructures in two experiment testbeds were already deployed (WiFi APs), massively deploying devices as RFID, NFC tags, lights would be time-

consuming and cost a lot for the maintenance work. Moreover, gaining the official permission of the space owner, in this case at work, i.e., the university, in order to deploy and replace lights (LED) is another barrier.

Table 1 Details of each experiment in this thesis

Testbed (Type)	**Accuracy (Needed)**	**Positioning Method**	**Behaviour (Type)**	**Recognition Method**
Library (Retail)	< 1.7 m (Arm)	BLE/MF+IMU Fingerprinting	Locating & Retrieving Items	----------
PhD Lab (Office)	< 3 m (Path)	WiFi Fingerprinting	Multiple ADLs	MD-DTW[2]
Kitchen (Home)	< 0.5 m (Object)	2D Lidar Positioning	Multiple ADLs	Seq2Seq[3]

Table 1 shows the details of each experiment. In the Library room, it was considered that since the user has mobile devices, location fingerprinting could be a good solution to offer arm span positioning accuracy. So it was adopted in this scenario; In the PhD office, as we only need to discriminate different paths, instead of localising a single position, so sequential WiFi fingerprints was used; In the kitchen, as it needs to discriminate between different things such as a table and a chair, the aforementioned location fingerprinting methods cannot offer such an accurate positioning result. Moreover, considering the privacy protection, Lidar was used.

[2] For more details see Section 5.3.

[3] For more details see Section 6.3.

The first and second location fingerprinting indoor positioning studies and experiments occurred in Queen Mary University of London (QMUL) Mile End road campus Library, from 2015 to 2017. This researcher needed to use this shared public space owned by QMUL for the first and second studies. There were limitations in where and how Bluetooth beacons used as transmitters could be positioned and fixed in relation to the furnishings and fixtures, as permitted by the space owners. It was not possible to keep such tethered equipment in a public shared space securely, as they could not be permanently fixed and secured. For example, due to decorating work in the library, some beacons fixed to the ceiling went missing, and some of them were stolen. Also, batteries in the beacons needed to be replaced periodically, else these became non-operational. Each of these causes the set of fingerprints that are used to determine the location to change and hence to reduce the location accuracy. The maintenance of such an additional location-specific device infrastructure to remain fully operational is a significant overhead. Although, there are privacy and security concerns when monitoring people's ADLs, because of limited time this was considered out of scope for this project. For example, even though 2D Lidar was used to detect ADLs and can protect users' privacy as humans are not identifiable, however, the location data was not encrypted.

Experiments were not carried in vast spaces (more than 500 m^2), as it is hard to have permission to hold such experiments in my university. Some IPS beacons, e.g., BLE, also have a limited range (typically less than 10 m in NLOS scenarios). However, such large spaces can be considered as being clusters of smaller spaces [3], then those clustered spaces can be treated as several small spaces in which the proposed methods can be implemented.

In this thesis, only some of the most used indoor positioning and machine learning methods were explored. There are several another positioning, and recognition methods that can be explored (see also further work, Section 7.2). For example, the library study, because of beacon maintenance issues, ended before CNN-based fingerprinting and MD-DTW-based ADL recognition could be applied to the library

data. However, KTCC and CNN location fingerprinting were tested in an office environment instead.

1.4 Thesis Outline

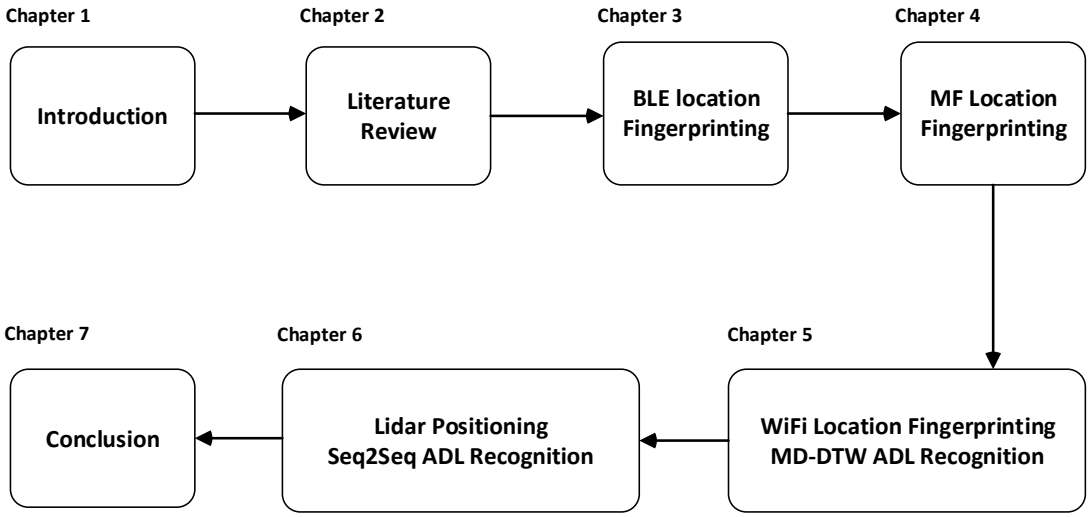

Figure 1-2 How thesis chapters are linked

In this thesis, how to accurately localise a user before accurately recognising ADLs was first investigated.

The start of the journey of this research was first driven by a problem to provide an IPS solution to support a core daily LD-ADL in a retail or library space, to navigate to and locate a physical retail or library item such as a book on a shelf. Before, researching and developing a solution for this, a comprehensive survey of the related state-of-art indoor positioning and recognition was undertaken (**Chapter 2**).

As there is no single global IPS that works effectively for all indoor areas, e.g., although WiFi seems quite pervasive in some urban areas, WiFi coverage may still be quite patchy in some indoor locations for use as a proposed global IPS because there may exist areas where the existing number of WiFi APs is limited, e.g., the targeted library space under study in late 2016 to early 2017. Subsequently, instead of using

WiFi APs in this first study, a wireless network of BLE beacons was deployed, and a RSSI ranking-based location fingerprinting method was investigated (**Chapter 3, Study 1**). This entailed planting a series of BLE beacons in a public space that were temporarily (insecurely) installed in easy to access locations. This study also considered the effect of heterogeneous RF receiver device hardware in order to improve location estimation accuracy.

In study 1, it was found that for a BLE location fingerprinting system, there was a high cost to install and maintain this added IPS infrastructure to remain operational for it because of issues to do with the orientation, attenuation, security of insecurely or temporarily fixed beacons in public areas. This was not maintainable, and a large number of BLE beacons became lost. Hence, an alternative, far lower effort IPS installation was then investigated for this library indoor space, MF-based location fingerprinting method (FPM-MI) was proposed in **Chapter 4 (Study 2)**. This exploits perturbations in the geomagnetic field caused by, e.g., structural steel elements in a building, to determine locations indoors.

However, MF location fingerprinting method, as with other positioning methods, also has its own limitations: it does not scale well in terms of space size; it is time-consuming to build the fingerprint map. Hence, another type of IPS was investigated that also required less time to build a location fingerprint map and to maintain it – as WiFi based system can be used in an area where there is good WiFi AP coverage and density. The proposed ranking method mentioned in Study 1 was also validated in this WiFi environment. Moreover, several location determination algorithms including AP selection, CNN classification and Extended Kalman Filter (EKF), were proposed in **Chapter 5** (**Study 3a**) to further increase the positioning accuracy of such a wireless RSSI location fingerprinting system. Also, in this chapter, a coarse-grained ADL recognition method using Multi-Dimensional Dynamic Time Wrapping (MD-DTW) is described (**Study 3b**).

Finally, some spaces may have poor WiFi AP coverage, especially in home environments, and there exists a requirement to maintain on-body devices which may

be problematic for some types of end-users (see Section 2.2.1). Hence, a 2D Lidar positioning system that uses Density-based Spatial Clustering of Applications with Noise (DBSCAN) was developed, which is off-body or device-free. The system can offer centimetre-level location results (**Chapter 6, Study 4a**). A state-of-art deep machine learning model (Seq2Seq) is also introduced, which was adopted for fine-grained ADL recognition **(Study 4b)**. The only drawback of using this system is that it requires a line of sight environment.

Finally, the last **Chapter** discusses insights, gives conclusions and outlines possible avenues for further work.

Table 2 A preview of different studies in this thesis

Study No	**Type**	**IPS**	**Implemented Positioning Algorithm**						**ADL Recognition**
			AP Selection	KTCC	CNN	EKF	FPM-MI	DBSCAN	
1-LD	Library	BLE		√					Single
2-LD	Library	MF					√		Single
3a-LD 3b-REC	Office	WiFi	√	√	√	√			Multiple (MD-DTW)
4a-LD 4b-REC	Home	Lidar						√	Multiple (Seq2Seq)

Table 2 gives a preview of the different studies described in this thesis to understand the structure of this thesis better. LD is short for location determination. REC is short for LD-ADL recognition.

Although several improved indoor positioning methods (BLE, WiFi, MF and Lidar) have been proposed, only simple, single, location-driven ADLs were investigated

using BLE and MF measurements, e.g., to retrieve a physical asset. In contrast, WiFi and Lidar-based positioning systems were investigated to recognise more complex, multiple location-driven ADLs.

2 Literature Survey

2.1 Introduction

Indoor positioning methods are reviewed in Section 2.2. Section 2.3 reviews the primary human activities recognition methods. A summary of the analysis is given in Section 2.4.

2.2 Indoor Positioning Methods

Table 3 Comparison of each positioning methods

Methods	**Advantages**	**Disadvantages**
WiFi (Location Fingerprinting)	Widely available	Low coverage areas exist Heavy collection effort for Radio Map
BLE (Location Fingerprinting)	Easy to deploy	Beacons are unsecure Heavy maintenance effort for beacons Heavy collection effort for Radio Map
BLE Path loss model	Easy to deploy	Lower accuracy
MF (Location Fingerprinting)	Ubiquitous	Heavy collection effort for Radio Map Not scalable to large areas
Pedestrian Dead Reckoning (IMU)	Ubiquitous	Error accumulation
RFID/NFC (Proximity)	Cheap	Not scalable to large areas
Lidar, UWB (AOA/TOA/TODA)	High accuracy	Lidar affected by NLOS Can be costly
Camera/LED (Recognition)	Higher accuracy	High computational cost Privacy invasion

Multiple IPSs, as shown in Figure 1-1 have been developed because of the lack of any Global Navigation Satellite System (GNSS) that works effectively indoors. Table 3 gives an overview of the advantages and disadvantages of each method.

The most popular IPS is a WiFi-based positioning system as it makes use of already deployed wireless AP infrastructure of transmitters and common smartphones as receivers to determine the position. It is infrastructure-free in the sense that no additional infrastructure for positioning needs to be added as the same one that is used for wireless local area networking, is used for positioning. Similarly, Bluetooth, e.g., BLE, is currently another widely used wireless indoor positioning technology that also operates in the 2.4 Gigahertz spectrum that is inexpensive and energy efficient. BLE enabled receivers, such as smartphones BLE beacons, e.g., iBeacon, or transmitters comes into range (typically less than 10 m in NLOS scenarios). Bluetooth is not infrastructure free, in the sense that it is primarily installed for IPSs. However, both IPSs need the radio map with corresponding updates, e.g., the layout is changed. But as these are the two most common IPSs, they both are the primary positioning systems under investigation.

However, using WiFi or BLE methods for an IPS is challenging as RF transmissions at low GHz frequencies are severely affected by attenuation due to the changing orientation, the number of moving humans, and other static solid objects such as metal furniture between RF receivers and transmitters. Furthermore, such RF methods depend on a deployed infrastructure of a fixed topology of RF transmitters, whose RF coverage may be variable, creating black spots where there are only weak or no RF signals, thus limiting the location accuracy. Hence, these methods still have an average accuracy beyond an arm span. Accordingly, more RF received signal invariant techniques could overcome this issue and achieve a more accurate IPS. Hence, this is in part a driver for techniques that are less invariant to RF attenuation effects. For example, MF measurements have been investigated and combined with inertial sensor measurements (e.g., with a digital compass to give the bearing). This type of IPS is barely influenced by humans and furniture [4]. Its other benefits are that also no

infrastructure requires to be deployed in the area, and location can be determined using a normal smartphone.

Another type RF positioning system, e.g., UWB, a high accuracy positioning solution, uses narrow pulses to transmit information, which makes it less affected by multipath propagation effects. However, it can be affected by other wide spectrum devices if misconfigured, e.g., digital TV [5]. Moreover, as UWB positioning systems are also not an infrastructure free system, which means the transmission range, a number of deployed UWB devices and battery life need to be considered. UWB systems are usually expensive if scaled to large areas [6, 7]. RFID and NFC are also popular RF positioning choices, as they are cheap positioning solutions, which small tags that can be taken by people to be tracked. However, the proximity and absolute positioning techniques need numerous infrastructure components installed and maintained in the system working area [8].

There are other non-RF methods:

1) An ultrasonic positioning system that uses ultrasonic technology and triangulation location technique to measure the location of a tag carried by a person, which can offer a high positioning accuracy. However, the performance of this technology is influenced by the reflection and obstacles between tags and receivers, which degrades the system accuracy. Moreover, like the UWB system, it is time-consuming to deploy and maintain such a large number of ultrasonic sensors [9].
2) A camera positioning system can use a single camera that covers a large area. However, it is privacy-invasive and needs a vast amount of computations to estimate the location. Moreover, the system is not reliable in a dynamic changing environment. Since the positions are based upon the saved vision information, this needs to be updated due to changing in the environment such as changing the place of your desk in your office [6].
3) LED positioning system uses Visible Light Communications technology [10] to send unique codes to the cameras on smartphones, which can achieve a high

positioning accuracy. However, as it requires specialised LED lights, these tend to be a better fit for new building or refurbishments.

4) A 2D Lidar IPS offers the benefit of being very accurate to determine the position. Off-the-shelf 2D Lidar positioning systems used to be expensive and are highly-integrated platforms that cannot be modified to support new applications as they are insufficiently open and flexible to be configured or programmed to support different ADL recognition. However, the price of 2D Lidar has become more affordable recently, and some are also now more open for third-party application development.

Figure 2-1 is a schematic that shows the additional infrastructures requirements to support an IPS, e.g., to install transmitters with respect to positioning accuracy of each IPS technique.

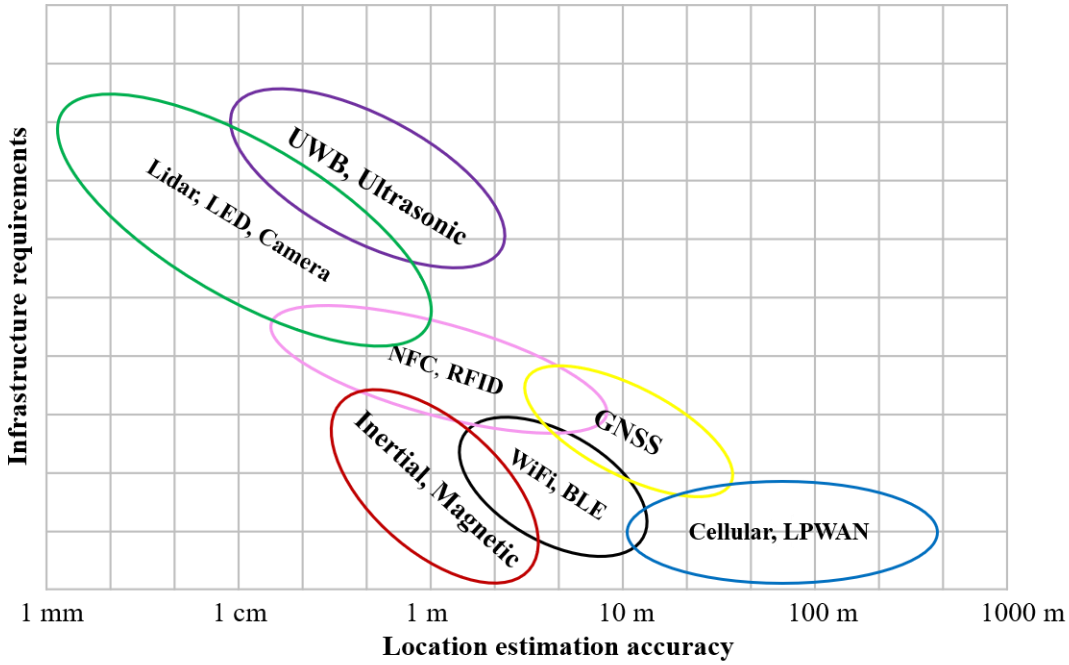

Figure 2-1 A rough infrastructure (existed) requirement to change the infrastructure to support a positioning system versus the positioning accuracy of each technique (x-axis, presented as a log scale).

2.2.1 Location Fingerprinting using BLE/WiFi RSSI

A simple way to estimate indoor location is using the RF signal path loss model via smartphones. Previous work [11-14] show such methods can provide a 0.53–3.5 m positioning accuracy. However, all these experiments were carried out in free space areas without considering the complex structure in the indoor environment where there is more likely to be RF attenuation, interference and multipath effects. As mentioned previously, WiFi is the most common smartphone-based positioning methods, as WiFi routers are already deployed in most places such as education campuses, businesses, communities, and public facilities. However, the accuracy of general WiFi-based positioning methods is not accurate enough [15] to offer a typical arm span location accuracy of about 1.7 m for applications such as finding a book or item on a long library or retail outlet shelf. This can be compounded by coverage of an insufficient number of effective APs in some areas [16].

There are also several kinds of algorithms that can be used to process the transmitter and receiver data in order to determine the location, users, e.g., Gansemer et al. [17] present a fingerprinting approach based on Euclidean distance (ED). The algorithm uses four threshold parameters to adapt the calculation to the specific measuring environment. Zhuang et al. [18] present an approach by combining the channel separation polynomial regression model, fingerprinting, and extended Kalman Filtering for indoor positioning. Ladd et al. [19] present an approach for positioning using a Bayesian inference algorithm. However, most current methods do not consider the impact of the WiFi/BLE RSSI variation caused by different radio RF receiver circuits [20] embedded in smartphones. As there is no standard for the RF receiver that uses different designs of antenna and RF front-end, this could lead to different RSSIs being received in the same location [21], which would decrease the positioning accuracy. There is some existing work concerning how to mitigate the hardware variance problem as follows. Another system proposed in [22], applies unsupervised learning for mitigating against heterogeneous RSSI hardware in RF-based fingerprinting, which can also improve the location accuracy. However, it needs an additional data pre-processing procedure using the Expectation–Maximization (EM)

algorithm [23] to optimise the estimated locations when the radio map is updated. Yaqi et al. [24] also looked into the hardware heterogeneity issue and proposed to use the Spearman Correlation Coefficient to improve the positioning accuracy. Although this improved the positioning accuracy, the validation results were from a simple simulation experiment.

Moreover, with deep learning and reinforcement learning gaining popularity, an increasing number of indoor position methods using deep learning have been proposed recently. Wang et al. [25] proposed a deep learning based DeepFi positioning method using Channel State Information (CSI), which can achieve a 1.8 m average positioning accuracy. However, a CSI supported specific network card Intel 5300[4] is required, which cannot be used by smartphones. Zhang [26], also used deep learning, pre-trained using a stacked denoising autoencoder to localise users, and claims that it can lead to substantial improvement on localisation accuracy in coping with turbulent wireless signals. However, it may still be affected by the hardware heterogeneity issue. [27] proposes to use semi-supervised deep reinforcement learning in support of IoT services – positioning for instance, which can use unlabelled data to train the model. However, different measurements from different smartphones may wrongly be labelled when using semi-supervised learning.

2.2.2 Location Fingerprinting using MF measurements

Unlike RF-based methods, MF measurements location fingerprinting methods are not influenced by RF multipath effects yet still use sensors integrated into a typical smartphone. [28] used the Nearest Neighbour (NN) for localisation by matching

[4] For more details: https://www.intel.com/content/dam/www/public/us/en/documents/product-briefs/ultimate-n-wifi-link-5300-brief.pdf. Last accessed in Sep/2018

measurements collected from a wearable badge which consists of four magnetometers. This method does not need to use Pedestrian Dead Reckoning (PDR) to estimate the walking distance and direction. However, a large amount of MF measurements needs to be collected, and it uses four MF sensors. [29] proposed an IPS using a Particle Filter (PF) algorithm, which demonstrates that this is a feasible scheme for indoor positioning. [4] proposed an improved PF algorithm to reduce the computational cost using fewer particles with similar intensities of terrestrial magnetism rather than multiple particles. However, the estimated location accuracy of the first several steps is not accurate. [30, 31] presented a multi-source and multi-variate dataset consisting of multiple-sensor measurement, e.g. signal strength from WiFi, PDR, and MF measurement, which can be fused to enable more accurate positioning information. These works that have explored using MF measurements combined with inertial sensor measurements as observations for PF algorithms to improve the estimation of the user movement, provides a 1.1 - 2.0 m positioning accuracy. However, existing PF algorithms have several disadvantages: they are computationally expensive; are less suitable for use in non-networked, low resource devices when needed for near real-time location-based decision-making; measurements need to be linked to the actual ground truth location, and this needs to be trained, increasing the computational complexity; the estimated location accuracy of the first several human steps is not accurate as PF algorithms need time to converge, typically this takes about 16 steps or about 9 m [29].

2.2.3 2D Lidar Positioning

As the main purpose of 2D Lidar positioning system is to offer high accuracy location determination, which is then used for recognising activities, this will be introduced in the following Section 2.3.2.

2.2.4 The Need for Multiple IPSs

Table 4 Summary of representative examples of the accuracy of different IPSs and their drawbacks

Authors	**Techniques**	**Accuracy**	**Drawback**
Rida [12]	BLE (TOA)	1 m	Prone to interference
Faragher [32]	BLE (Fingerprinting)	4.8 m	Affected by heterogeneity
Gansemer [17]	WiFi (Fingerprinting)	3 m	Affected by heterogeneity
Kim [4]	MF (Fingerprinting)	2.8 m	High computational cost
Pratama [33]	IMU (PDR)	1.4 m	Error accumulation
Berkovich [31]	WiFi/IMU (Fusion)	1.5 m	High computational cost
Chen [34]	Ultrasonic (TOA)	1 cm	Uses specialised receivers
Tiemann [35]	UWB (Geometric)	10 cm	Uses specialised receivers
Wang [36]	RFID (Proximity)	11 cm	Uses specialised receivers
Jiao [37]	Camera (Recognition)	1.37 m	Privacy-intrusion
Kou [38]	LED (Recognition)	10 cm	High computational cost

Regarding IPSs, Table 4 summarises the accuracy and drawbacks of existing systems. BLE (TOA) has a good accuracy in free space or uncluttered areas but is prone to RF interference and attenuation from objects making its accuracy far worse. BLE or WiFi (location fingerprinting) both are affected by heterogeneity of RF receiver, e.g., in smartphones. However, WiFi can also be computationally costly to calculate the position depending on the algorithm used. IMU (PDR) can give a good accuracy, but the error accumulation increases rapidly away from a reference point at a known

location, meaning this is quite a short-range technique. Multiple sensors can be fused to increase accuracy, e.g., WiFi and an IMU but this incurs a higher computational cost. Use of ultrasonic, UWB, RFID can give a much higher accuracy. However, this uses more specialised receivers than standard ones such as mobile phones. Additionally, specialised transmitters need to be added to, and maintained in the infrastructure; such devices may be costly, e.g., for UWB. Camera systems can determine the location, but they are privacy intrusive for humans. This table also shows that most location fingerprinting systems can only achieve 2 to 3m accuracy. More detailed information about the accuracy and applications of some different IPSs, including commercial ones, can be found in Appendix A. In terms of Table 4, BLE, Wi-Fi, MF and Lidar type IPSs have the main benefit that they are not so privacy intrusive and are low cost for IPS users - either they can use a standard receiver that many users already have, e.g., in a smartphone, that is often considered indispensable in the current information age, or they are device free in that they don't require humans to have a receiver. Hence, these were selected for further study in the next chapters to consider how their location accuracy can be further improved.

Because no single standard ideal global Indoor localisation and navigation system exists, users must cope with different and varying localisation techniques and infrastructures. In addition, different built-up environments have different physical constraints support, different modes of locomotion and activities, and thematic or logical restrictions like security zones have to be considered. Hence, thus far, a range of models for structuring indoor space and localisation methods have been proposed. Often localisation technology and sensor characteristics are mixed within these models which has the disadvantage that changes to the building structure or sensor configurations may affect the entire model. Hence, [39] conclude the following minimum requirements for a flexible data model supporting indoor navigation: Support for different and multiple localisation methods/infrastructures; Support for different navigation contexts; 3D topographic representation of the interior built environment (this 3rd requirement is left for future work as the experimental studies for this work were undertaken in smaller 2D spaces). [40] ascertain that Indoor Positioning Systems (IPSs) will be indispensable in healthcare systems. They also

highlight that of the many IPSs that have been proposed in literature, most of these have been evaluated in non-representative environments such as office buildings rather than in types of physical spaces where health is monitored such as hospitals (and home) that have a differnet physical space topology that affects the location accuracy.

2.3 Human Activity Recognition Methods

A second major complementary focus of this thesis is on ADL recognition, which is also referred to as Human Activity (HAR). The specific focus is on location-driven ADL recognition as the target indoors locations are application-driven.

2.3.1 ADL Recognition using WiFi

There are a variety of methods to recognise human activities. However, each of them has its limitations. Vision-based methods including video [41] and camera [42] have achieved much progress yet face problems of being computationally intensive are privacy invasive and are affected by external environmental conditions such as light and line of sight conditions. Recognition methods that use wearable sensors [43, 44], e.g., accelerometer, are widely applied for fine-grained activities recognition. However, the weakness is that they cannot accurately determine the location for location-driven activities. RF-based methods such as CSI can capture the changes in the radio environment caused by activities. However, they are easily affected by other interference sources. Compared to these methods, RF location fingerprinting is less affected by NLOS constraints and are less privacy-invasive. Due to the mass use of smart devices and densely distributed WiFi routers, WiFi-based location positioning and human activity recognition methods are also receiving more research attention in recent years. Several WiFi-based activity recognition methods have been proposed as follows, including WiFi CSI [45], Doppler Shift [46] and high-frequency RSSI [47]. However, little work employs using WiFi location fingerprinting to recognise ADLs.

The use of WiFi CSI is one such technique that can be used for ADL recognition, e.g., E-eyes [48], CARM [49], WiKey [50] and WiFinger [51]. The principle of CSI-based

sensing is to make use of channel information in the time and frequency domain, e.g. amplitude and phase of each subcarrier at each timestamp and leverage how these features change, caused by human activities within the range of transceivers. By collecting and extracting features at a training stage, researchers are able to match features during testing with those in the training database to infer human motion. However, CSI-based methods rely heavily on a relatively stable RF environment (e.g. single occupant and no furniture movement). Each environment change would trigger an activity profile updating procedure, or it may fail to work. There are also some efforts to use detailed physical layer measurements such as Doppler shifts to detect human activities such as Wi-Vi [52] for coarser movements and WiSee [53] and WiTrack [46] for fine-grained gestures. Because human motion can lead to a pattern of Doppler shifts at the wireless receiver, more specifically, a positive Doppler shift while moving towards the receiver and a negative Doppler shift while moving away from the receiver. Doppler shifts can be mapped to human activities using Doppler shift extraction, segmentation and activity classification. However, specialised software and hardware are needed to extract Doppler features which results in an extra cost and is not suitable for off-the-shelf devices. [47], [54] investigated the feasibility of recognising activities by employing WiFi RSSI. The main idea of this work is to increase the RSSI sampling rate of a device to approximate the continuous changes of the signal affected by human movements. There are many requirements for using this kind of solution. Firstly, it requires modified WiFi firmware to obtain a sufficient RSSI sampling frequency which, however, is not applicable to most mobile devices. The second requirement is to set WiFi transmitters (or routers) in a known location where the WiFi signal can be interfered with by human activities. Also, the height of WiFi transmitters should be lower than a person's height. These requirements limit its application in practical scenarios.

Those continuous signal changes-based activity recognition methods share some fundamental limitations: they are easily affected by ambient conditions (e.g., multiple occupants) and require the use of specialised hardware (e.g., wireless card) which is not suitable for off-the-shelf smart receiver devices.

2.3.2 Other Location-driven ADL Recognition Choices

The most popular IPS is either WiFi or BLE-based IPS. The BLE-based system can also be deployed in an inverted manner, where the subject wears a beacon with, e.g., an accelerometer and magnetometer, and fixed devices in the home receive the beacon signal strength and other sensor data from the person. Both WiFi and BLE estimate locations using forms of trilateration or by constructing a radio map before the location estimation and then matching the current signals to a set of locations in the radio map index by, e.g., the RSSI at the receivers. Inside a small home, trilateration does not provide good accuracy because of non-line-of-sight issues. Radio maps mitigate these inaccuracies, but due to the variations in the signal strength for both WiFi and BLE, the estimates still limit the accuracy, typically from 2 to 3 m which is too inaccurate and typically needs to be 1 to 2 orders of magnitude lower to differentiate the use of physical items such as sink, fridge or kettle in a small house. There is also the issue that the use of WiFi and BLE requires the user to carry an on-body device – they are not device-free for the mobile host. Some studies have shown that some target users such as seniors are more disinclined to use eHealth wearables [55]. There is also an issue that such wearables require a degree of maintenance such as recharging batteries to keep wearables operational and the need to remember to wear them or carry them continually, e.g., leaving on body receiver devices off body with others or in places whilst undertaking ADLs, generates false negatives.

There has been much research investigating how to improve the ADL recognition accuracy. For example, the works of [56, 57] demonstrate the benefits of using a hybrid approach. [56] deploys BLE in the home using inverted RSSI fingerprinting, step counting, magnetometers and focuses on detection of moving path segments (using Dynamic Time Warping - DTW) or stationary waits or stays, often referred to as Stay Points, or Landmark Places. This has achieved a high accuracy of recognition for elementary actions (simple trajectories which can infer actions). Their work also suggests that an activity-centric trajectory-based prediction model is a practical solution for location estimation in homes that can be extended to design a suitable user-friendly IoT application. This is achieved by populating the radio map using

sequential RSSI data collected along a pathway (e.g., whilst moving from couch to the dining area) or stationary positions (e.g., sleeping on the bed). The location is associated with an ADL. However, such a multi-sensor hybrid LBS still suffers from the same limitations as the WiFi and BLE methods in terms of insufficient location accuracy and require the use of wearables.

Another ADL recognition choice is to use UWB, which has a high positioning accuracy of a few centimetres. Recent reductions in price and size of the transceivers make such a deployment, increasingly, a good choice at this time. UWB devices use a very large bandwidth and can transmit high data rates over short distances at very low power levels. It is not affected by the existence of other communication devices or external noise [58]. Although, it can be affected by other wide spectrum devices if misconfigured, e.g., WiMAX and digital TV [5]. Like Lidar, distance is estimated based upon time. For UWB, location estimation is based on Time difference of arrival (TDOA)-based algorithms or Time of arrival or flight (TOA)-based algorithms. The use of narrow pulses makes UWB very tolerant to multipath effects. Reflected pulses do not overlap in general, hence will not interfere. The systems use 'RAKE' receivers to capture energy from multiple paths in the same way as conventional direct-sequence spread spectrum receivers. However, despite the high positioning accuracy, it still requires the subject to wear a transmitter.

The final type of off-body sensor that can be used to accurately determine location-based ADL indoors is light-based: various cameras or a light detection and ranging (Lidar) system, which uses pulsed laser light and measures the TOA of the reflected pulses with a sensor, can be used. A major weakness with the use of cameras is that they are highly privacy-invasive. Until recently, Lidar devices were quite costly to purchase. There is also a range of Lidar devices that could be used for ADL such as flash Lidars that only face in a single direction [1D], line scanning sensors that swept a beam across a scene, taking measurements along a single [2D] plane and 3D Lidar [59]. Both 2D and 3D Lidar device can be designed to rotate 360 degrees. The major application of Lidar is for mobile unmanned vehicles and robots to track objects around them as they move [59] and to support collisions avoidance. *To the best of my*

knowledge, no work has looked at using off-body Lidar devices to recognise ADLs derived from accurate location determination, that can be used indoors as well as outdoors, and that uses Lidar devices that are 2D rather than 3D.

In addition, selecting and deploying sensors to accurately measure object locations including people, and understanding how to analyse those activities associated with those locations, need to be considered. Understanding the activities of a person inside a home requires contextual and useful information related to their inherent surroundings, which can be mapped to an activity recognition framework. One approach to modelling ADLs is based on a task-specific and intention-oriented plan representation language such as Asbru [60]. It stems from the modelling of medical protocols and monitoring, the application of such protocols [61] and [62] have developed a recognition engine to detect ADLs that were modelled using Asbru from sensor events, principally RFID tags. The engine generated a range of possible compliant ADL task sequences from a stream of sensor data to determine the ADL being conducted along with an assessment of their possibility. Another way of representing and modelling high tier behaviour is workflows, such as using an augmented Petri Net [63]. However, workflows are too prescriptive in their ordering. If workflows are applied in dynamically changing environments, they require a large number of permutations to be explicitly enumerated. Workflows can scale poorly to cases where there are many possibilities, and this is often the case for goals performed by people [64]. In addition to scalability issues, it can be tough to manage the representation of priorities and ordering. Thus, more flexibility is required when modelling hierarchal ADLs. The Asbru language is a process representation language which has similarities to workflow modelling but has been designed to provide more flexibility than workflows. Asbru allows flexibility in how it can represent temporal events, namely their duration and sequence. ADLs have some attributes and characteristics which make them challenging to represent in a logical framework. These characteristics include the variable duration of the same task, variable ordering of the tasks, and overlaps with other ADLs. Techniques which attempt to map these as a flat structure are problematic because they are unable to model flexible scenarios,

such as interweaving ADLs. The ability to monitor interweaving ADLs is a crucial advantage over existing ADL modelling methods [65].

Table 5 Summary of representative examples of the accuracy of different ADL recognition and their drawbacks

Authors	**Measurements**	**Scenarios**	**Drawback**
Sigg [47]	WiFi RSSI	Office room	Not scalable to large areas Requires carrying a receiver
Wang [66]	WiFi CSI	Living room	Prone to interference
Nguyen [67]	MF	Office room	Not scalable to large areas Requires carrying a receiver
Kwapisz [44]	IMU	Indoor/Outdoor	Requires carrying a receiver
Naeem [61]	RFID	Living room	Not scalable to large areas Requires carrying a receiver
Tao [41]	Camera	Living room	Privacy-intrusion

For location-driven ADL recognition methods, most researchers only focus on how to improve the location-driven accuracy. However, such estimated locations could be used for more than just positioning – for ADL recognition. Hence, WiFi location fingerprinting, as an infrastructure-free method was chosen to explore coarse-grained ADL recognition, as it can use many more measurements (as there are many more APs), than MF measurements. 2D Lidar Positioning as a highly accurate positioning solution, which does not require the user to carry a sensor was also chosen to explore more fine-grained ADL recognition.

2.4 Summary

This chapter presented literature reviews of indoor positioning and human activity recognition methods. The next chapter will introduce the first of the novel ranking-based location fingerprinting methods.

3 BLE Location Fingerprinting

3.1 Introduction

The use of a more straightforward BLE RSSI path loss model is first discussed before the novel, more accurate, fingerprinting method, in Study 1 based upon KTCC, is described in more detail. The main reason for the path loss study experiments (Study 0) was to study these effects in a simple free-space, in isolation from the more complex compound effects when these experiments are performed in a real cluttered space. The use of a path loss model for location determination was studied to more clearly highlight effects, such as the effect of RSSI loss with distance (which is well-known, see Section 3.2), the effect of smartphone or RF receiver orientation with respect to the receiver and the effect of objects in between the receiver and transmitter and the type of RF receiver hardware (this effect is less well-known).

In wireless AP-based IPSs, BLE or WiFi RSSI location fingerprinting method is one of the most popular positioning methods, as the spreading use of smartphones (RF receivers, users do not need to carry additional devices) and the use of BLE or WiFi RSSI is ubiquitous in wireless systems, which is the main reason why BLE or WiFi RSSI was explored to determine the user location.

The first wireless location fingerprinting study is to support finding an item, e.g., a book, location, navigation and retrieval type activity or service. This requires a location accuracy of about an arm-span. It was carried out in the QMUL Main Library, where at one time there were only a few WiFi APs that could be scanned (7 APs). So, the WiFi RSSIs in receivers was patchy in the area of study – this has since been rectified, but there was no time to repeat WiFi measurements in this space. Hence, the iBeacon device as a low-energy, low-cost and easy-to-deploy solution was adopted as the wireless AP to investigate RF RSSI measurement for location determination as the iBeacon topology and placement could be controlled. Moreover, considering that traditional WKNN using ED will be affected by the heterogeneity issue, a novel WKNN using KTCC with RSSI ranking was investigated.

3.2 Location Determination Using a Signal Path Loss Model

3.2.1 BLE RSSI Path Loss Model Theory

Power attenuation of an electromagnetic wave occurs when a signal propagates through space. This is also known as path loss. In this thesis, the relation between path loss and transmission distance have been analysed, based on a commonly used logarithmic model [68]:

$$\mathrm{PL} = P_{Tx} - P_{Rx} = PL_0 + 10\,\mathrm{nlog}_{10}\frac{d}{d_0} + X_e \tag{3.1}$$

where

- PL is the signal strength after total path loss measured in Decibels at a distance d away from the transmitting end-device;
- P_{Tx} and P_{Rx} represent the transmitting power and the received power;
- PL_0 is the signal strength after path loss at the reference distance d_0,
- d is the distance of the path;
- n is the attenuation factor;
- X_e is the normal random variable whose mean is zero.

The expression can also be expressed as follows:

$$P_{Rx}(d) = P_{Tx} - PL_0 - 10\,\mathrm{nlog}_{10}\frac{d}{d_0} - X_e \tag{3.2}$$

$$P_{Rx}(d) = P_{Rx}(d_0) - 10\,\mathrm{nlog}_{10}\frac{d}{d_0} - X_e \tag{3.3}$$

where

- $P_{Rx}(d)$ is the received signal strength at a distance d away from the transmitting end-device;
- $P_{Rx}(d_0)$ is the received signal strength at a reference distance d_0.

Based on the above expression, a linear least squares algorithm could be used to derive the expected parameters from the collected data of a test area (a free space-like indoor place). Based on [69], d_0 is usually set to 1 m.

Instead of training the path loss models for every type of different types of RF receiver, e.g., smartphone, which could result in different RSSI values in different types of receivers at the same location, using the above equations, a ready-trained distance measuring model can be adopted. Based on the empirical coefficient values for iBeacon devices from Android Beacon Library[5], the distance d can also be expressed as [70], which was adopted by us to measure the distance between the AP and the smartphone:

$$d = coefficient_1(\frac{P_{RX}(d)}{txPower})^{coefficient_2} + coefficient_3 \quad (3.4)$$

where $txpower$ is the measured signal strength when d_0 is set to 1 meter by the manufacturer (the txpower of the beacon is -51 dBm).

$coefficient_1$, $coefficient_2$ and $coefficient_3$ are different and depend on which type of smartphones are being used. For example, the coefficients and equation for Nexus 5 are 0.4203, 6.9476 and 0.54992:

$$d = 0.42093(\frac{P_{RX}(d)}{-51})^{6.9476} + 0.54992 \quad (3.5)$$

[5] For more details: https://altbeacon.github.io/android-beacon-library/. Last accessed in Sep/2018

3.3 Study 0 Evaluation: Investigation of Path Loss Effects Caused by Distance, Body Orientation to Receiver and Attenuation on RSSI Location Determination

3.3.1 BLE RSSI Path Loss due to Distance of Receiver

A BLE-based signal path loss model was first tested before the location fingerprinting study was carried out, as it is a simple model which can be quickly implemented. This pre-experiment was carried out in a hall in QMUL campus (where it is empty). Hence, it is considered that this as a free space-like place. An iBeacon device was deployed in a fixed point, and RSSI measurements were collected 3 meters away from this beacon.

Figure 3-1 The Bluebar iBeacon device (7.5 cm * 5 cm)

Figure 3-1 shows the Bluebar[6] iBeacon devices which was deployed in the library.

[6] Available from bluesensenetworks.com in 2015-06

For BLE signals transmitted using three advertising channels (hopping in channel 37, 38, 39) [16], the RSSI collected by a given device (Nexus 5) can vary up to 9.4 dB as shown in Table 6.

Table 6 shows the estimated distance and error in the pre-experiment.

Table 6 Estimated distance and error

Sampling Times	**Averaged 30 s RSSI (dBm)**	**Estimated Distance (m)**	**Error (m)**
1	-70.2	4.425	1.425
2	-74.2	6.245	3.245
3	-68.1	3.688	0.688
4	-64.8	2.772	0.228
5	-67.6	3.531	0.531
6	-73.1	5.684	2.684
7	-70.4	4.502	1.502
8	-67.9	3.624	0.624
9	-67.3	3.441	0.441
10	-71.1	4.784	1.784
Data from the Nexus 5		Average Error	1.315 (m)
		Standard Deviation	1.016 (m)

Based on the above results, 3 meters away (it is considered that users are usually 3 meters away from deployed devices) from a beacon can lead to 1.315 m averaged distance estimation error, which for the library book searching system may mislead users to the wrong bookshelf.

Furthermore, this pre-experiment was just carried in a free space-like area without considering the signal attenuation caused by human body absorption, the movement of people in real time, and the complicated layout of the space in the library with walls and metal bookshelves. Hence, using the signal path loss model to estimate locations in real-world locations and spaces was abandoned. Instead, the free space path loss model was used to first investigate, isolate and highlight the effect of RF receiver and the effect of human body orientation and attenuation on location determination.

3.3.2 BLE RSSI Variation due to Different RF Receiver Types

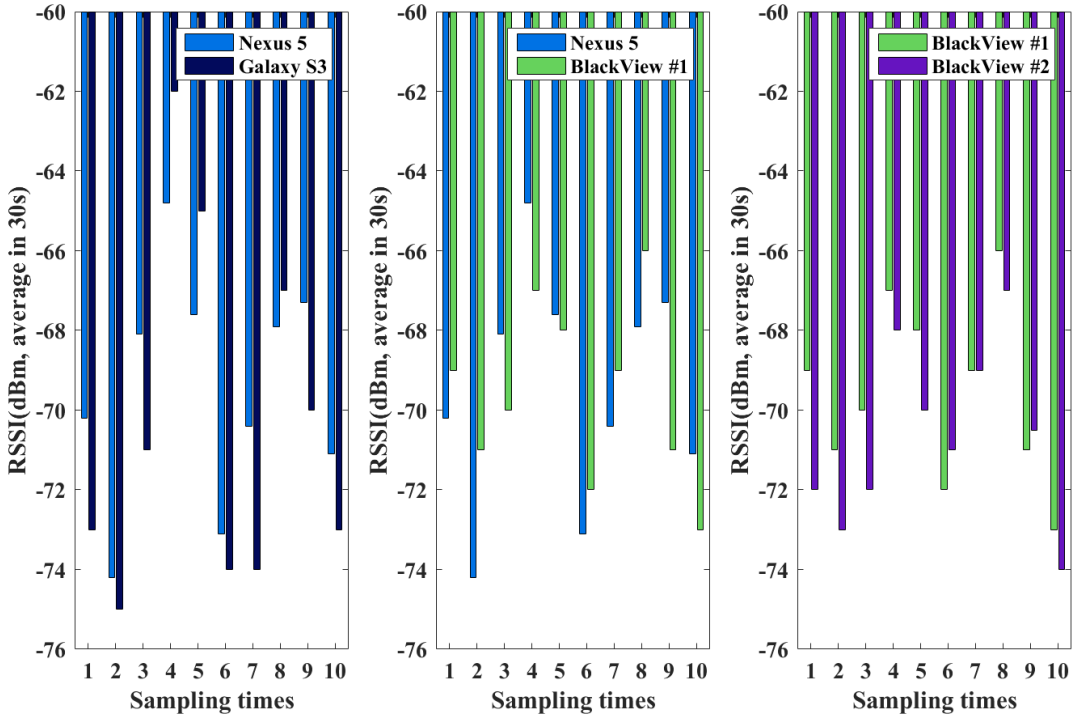

Figure 3-2 Comparison of BLE RSSI values for different smartphones at the same position and orientation

WiFi RSSI fluctuations can be caused by specific attributes of the hardware and by spatiotemporal properties. This also occurs with BLE RSSI [16, 20, 71]. As the BLE-based RSSI location determination was used, the stability of its RSSI needs to be tested. To test the RSSI variation, some measurements were collected out in a free

space area (same place where the Section 3.3.1 path loss model pre-experiment was carried out) by different RF receivers. The signal strength was simultaneously measured by different pairs of mobile devices, 3 meters away from the stationary (transmitter) beacon. According to a related study [16], 10 Hz beaconing rates and using a mean filter to process the batch data at a normal walking pace can produce good RSSI profiles. Thus, the same setting was used in the following experiments. All the smartphones were put in the same position and orientation and equipped with the Android 5.0 OS. For each pair of devices, the respective RSSI values are shown in Figure 3-2.

In Figure 3-2, the x-axis shows the sampling time (each time 30 s); the y-axis shows the RSSI averaged over 30 s. It also indicates that the RSSI measured by different types of mobile phones are different (up to 6 dB) at the same position and orientation. There are even differences between different smartphones (same type) from the same vendor (see right graph in Figure 3-2). This is caused by variations in the RSSI RF hardware in different smartphones. Therefore, it is proposed to use the RSSI ranking as the fingerprint instead of the raw RSSI measurements as from the Figure 3-2, these can be seen that they vary and follow a similar trend.

3.3.3 BLE Human Body Signal Attenuation and RF Receiver Orientation

The human body is a good absorber for 2.4 GHz radio signals; Figure 3-3 shows that the measured signal strength absorbed by the human body results in an average of 9 dB reduction in a free space area. This also demonstrates that the path loss model will be affected by human body signal absorption, which decreases its location accuracy.

The issue is also faced by using other fingerprinting methods at the same frequency, e.g., WiFi. When RSSI is measured when a human body and the RF receiver held in front of it, are facing the RF transmitter, the signal is greater than when the human is facing directly away from that transmitter, with his or her back to the transmitter. Considering multiple iBeacon devices were deployed in the library. Hence, [72] proposed to use RF fingerprint collected four times in four orientations (N, E, S, W)

at each location RP in the radio map to mitigate the distortion caused by the human body to increase the location accuracy. This technique was adopted by the Study 1 experiment, the detailed radio map design and validation is proposed in future work (see Section 7.2.1.1) as it could mitigate the distortion caused by the human body, in turn, increasing the location determination accuracy.

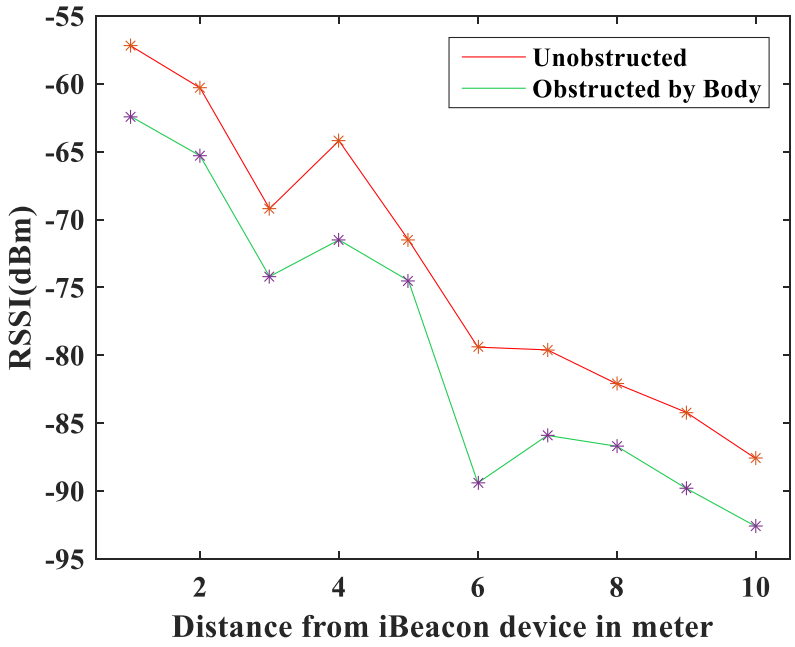

Figure 3-3 Human body reduces the BLE RSSI because it attenuates the RF signal

3.4 Wireless Location Fingerprinting Methods

The geometric-based BLE or WiFi positioning methods above rely on simply measuring the distance between Mobile Station (MS) and Base Station (BS) using RSSI. Because of multipath effects and attenuation of physical objects in the transmitter to receiver path, such measured distances are usually inaccurate (see Section 3.3.1) in real cluttered spaces, e.g., in a retail-like space. Hence, next the use of wireless RSSI location fingerprinting was investigated to support a more accurate positioning system compared with the use of a simple path loss model, as the complicated indoor spaces will seriously jeopardise the accuracy of such geometric-based methods. Also, considering the signal strength received by the wireless radio

controller embedded in different smartphones could be different, the proposed method seeks to improve the positioning accuracy, by being independent of the RSSI hardware in smartphones. One novelty of the method is that it is based upon KTCC and uses Weighted K-Nearest Neighbours Algorithm (WKNN) to correlate the position with a signal strength ranking of multiple low-power iBeacon devices.

The basic idea of location fingerprinting method is by matching a measurement value vector of an unknown place to the pre-recorded fingerprint measurements database, namely, the fingerprint map. Moreover, such fingerprints implicitly are affected by the multipath effect, which makes it reliable in complicated spaces and could offer a higher positioning accuracy than a path loss model.

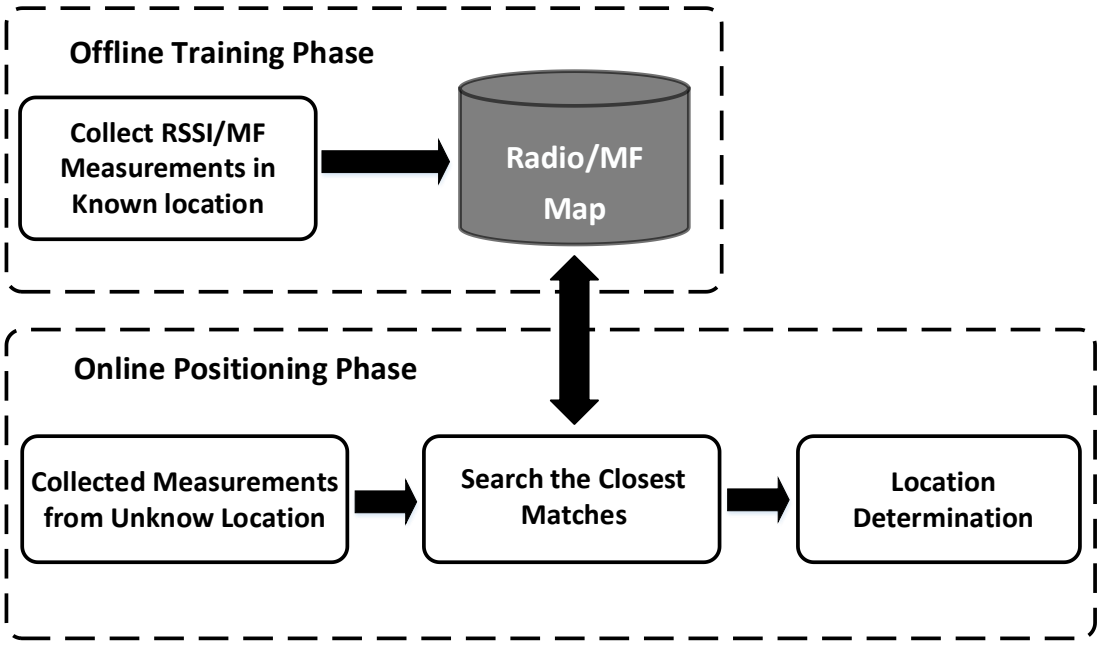

Figure 3-4 Two phases of the location fingerprinting method

Figure 3-4 illustrates two phases of general location fingerprinting methods. The arrows mean the flow direction of each step in this figure.

Generally, there are two phases in location fingerprinting. In the training phase, fingerprints (BLE or WiFi RSSI from APs, or MF measurements) are collected in pre-defined locations (RPs), which are used to create a pattern database in the target area.

Such fingerprint databases are also named as an RSSI radio map or MF map depending on the type of the collected measurements.

3.4.1 Wireless Location Fingerprinting using ED (WKNN)

In the online positioning phase, as the baseline positioning method, location fingerprinting using ED is first introduced here. The ED is usually used to determine and match the closest RPs in the radio map to estimate the location. It can be expressed using the following equation:

$$\mathrm{ED_i} = \sqrt{\sum_{\mathrm{j=1}}^{\mathrm{N}} \left(AVG\_RSSI_i^j - AVG\_RSSI_m^j \right)^2} \tag{3.6}$$

where $\mathrm{E}D_i$ is the Euclidean distance, the distance between a Measured/Test Point (MP/TP) and a RP. $\mathrm{AVG\_RSSI_i}$ is the averaged $\mathrm{RP_i's}$ RSSI vector in the pre-recorded radio map database. $\mathrm{AVG\_RSSI_m}$ is the averaged RSSI vector of a measured point, and N is the number of observed APs.

Then, the following equation (3.7) is used to estimate the coordinates of the TP (estimated location) based on WKNN [73], as a shorter ED should have a higher weight. K was set to 3 in Study 1, but it can be iterated to find the optimal one (see Section 5.4.1.2). (x, y) are the Cartesian coordinates of the selected RP:

$$(\bar{\mathrm{x}}, \bar{\mathrm{y}}) = \frac{\tau_1}{\sum_1^{\mathrm{k}} \tau}(\mathrm{x}_1, \mathrm{y}_1) + \frac{\tau_2}{\sum_1^{\mathrm{k}} \tau}(\mathrm{x}_2, \mathrm{y}_2) + \ldots + \frac{\tau_{\mathrm{k}}}{\sum_1^{\mathrm{k}} \tau}(\mathrm{x}_{\mathrm{k}}, \mathrm{y}_{\mathrm{k}}) \tag{3.7}$$

where k is a user-defined constant to pick the nearest RPs based on ED, τ is the corresponding reciprocal of the ED between a MP and a RP.

3.4.2 Wireless Location Fingerprinting using KTCC (WKNN)

3.4.2.1 KTCC

WKNN using ED distance measurement is a common algorithm to find the closest matching RPs. However, the type of the smartphone used to produce the radio map may not be the same one a user uses later for location determination, leading to RSSI differences at the same position and orientation. *To mitigate against this hardware heterogeneity issue, RSSI ranking of multiple beacons is used as they follow a similar ranking trend irrespective of the smartphone type*.

The proposed ranking-based method follows the phases shown in Figure 3-4. The main difference is that I use KTCC [74] to measure the distance, as it can measure the ordinal association between two measured quantities (two RSSI ranking vectors).

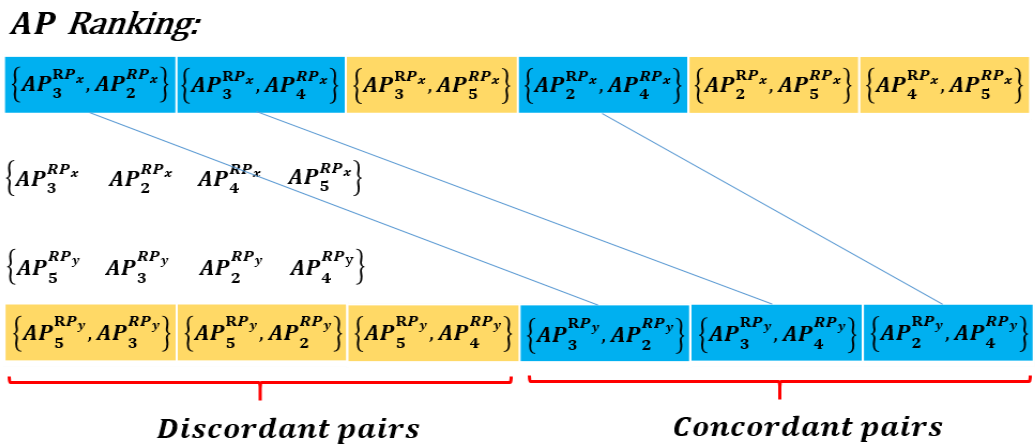

Figure 3-5 Concordant and Discordant pairs in the KTCC procedure

The definition of KTCC is expressed as equation (3.8) or (3.9):

$$\tau_1 = \frac{(\text{number of concordant pairs}) - (\text{number of discordant pairs})}{n(n-1)/2} \tag{3.8}$$

$$\tau_2 = 1 - \frac{2(\text{number of discordant pairs})}{n(n-1)} \tag{3.9}$$

where n is the number of APs, and the higher τ is, the higher ordinal association between two quantities, which means the closer they are.

The Pseudocode to Calculate the KTCC

Algorithm 3.1: How to calculate KTCC τ_2

Requires:

A = {$RSSI_{m,j}$…$RSSI_{m,n}$}, B = {$RSSI_{i,j}$…$RSSI_{i,n}$}

Return: τ

Procedure 1:

Sort Algorithm(A**):**

Sort the measured RSSI values in descending order

if A[j] > A[j-1]

or using probability comparison (mentioned in Section 3.4.2.2)

exchange A[j] and A[j-1]

Procedure 2:

binarySet(A**):**

Acquire the binary sets of A and B

Set set = new **Set**

Collections of unique elements

for i = 0 to length(A) – 1

for j = i+1 to length(A)

set add Beacons' serial number of A[i] and A[j]

return set

Procedure 3:

reversions (set A**, set** B**)):**

Get the number of discordant pairs

reversions = 0

for element c in **set** A:

if (B do not contain c)

reversions ++

return reversions

Procedure 4:

T(reversions**):**

Get the result of KTCC

return τ = 1 - 2.0 * reversions / (length(A) * (length(A) - 1))

Then, the rest of procedures of estimating a location are the same as for the ED one, using WKNN. The only difference is that the weights are calculated by using equation (3.7). There is no need to calculate the reciprocals of using ED, as the higher τ (KTCC), the closer they are.

3.4.2.2 Probability Comparison

As RSSI ranking is used as the training input rather than using the raw RSSI measurements, instead of using ED with RSSI measurements to compare which is stronger in the pairwise APs, a joint distribution is used. Let A represents the random variable for the RSSI values of AP A in the chosen time frame, and B the corresponding random variable for AP B. Assuming the APs are independent, if P($RSSI_A$>$RSSI_B$)>0.5, then AP A is chosen. More specifically if S1 is the set of RSSI measurements of AP A and S2 the set of RSSI measurements of AP B in the time frame sampled.

$$\mathrm{P}(RSSI_A > RSSI_B) = \sum_{i=-\infty}^{\infty}\left(\sum_{j=-\infty}^{i} P(RSSI_A = j\right) * P(RSSI_A = i) \qquad (3.10)$$

As RSSI values fluctuate over time, it is better to use a probabilistic approach [75].

3.5 Study 1 Evaluation: BLE Location Fingerprinting

3.5.1 Library Testbed Setup

Figure 3-6 shows the ground floor of the QMUL Main Library. The yellow area is the target area. Different IPSs could be used with different levels of effectiveness in different areas. For example, in the lobby (area A), it could use a path loss model, as it is like a free space area, people can easily find the target. In the teaching collection room (area B), the layout of this space mimics the layout found in many physical retail spaces that store products in shelving with aisles between them. A vital issue for

customer navigation is to enter the correct aisle to locate a product; else a longer detour can result.

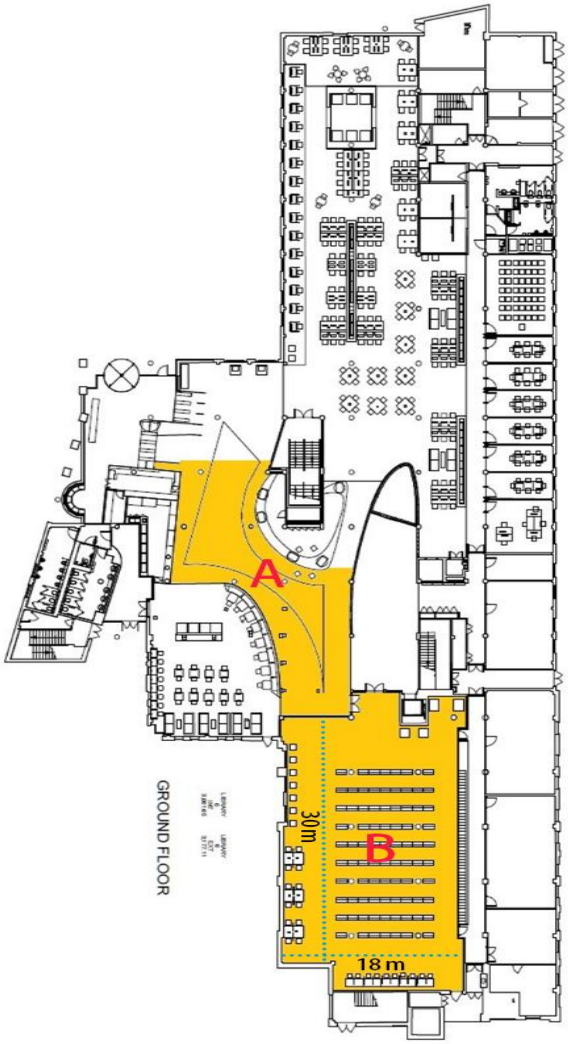

Figure 3-6 The ground floor of the QMUL Main Library

This study focused on using a BLE location fingerprinting method to localise a user in area B, which is an 18.0 m × 30.0 m teaching short-term loan book collection room of the QMUL Main Library.

The training dataset of measured Reference Points (RPs) was collected using smartphone1 (LG Nexus5). Test Point datasets (the positioning results of walking around the target area, each sample with a 2 s scanning period) were collected for

smartphone1, smartphone2 (Galaxy S3), and smartphone3 (BlackView #1). It was assummed that if scanned period is less than 2 s, the collected measurements may not have the similar data distribution as for the pre-collected RPs and that people cannot move too far in 2 s.

The single ADL in this study is a book searching and navigation, so a RSSI ranking-based KTCC IPS was implemented with multiple low-energy, low-cost iBeacons to create a flexible distribution of transmitters that could be controlled. All (BlueBar) iBeacon devices were set to use a 10 Hz advertising rate with the default low power setting. Hence, multiple deployed beacons can be detected to get sufficient and strong signals for the optimal positioning accuracy [16]. This low power setting also saves the battery life of the beacons and reduces the maintenance cost to replace run down batteries.

There are 182 RPs (each RP with 100 samples were manually collected for each orientation), which are 0.8 m apart on the x-axis and 1.2 m apart in the y-axis, which is shown in Figure 3-7. 200 TPs were also randomly collected in this area. This is to keep the RPs in the middle of the gap between two bookshelves. The regular layout of setting RPs in the library teaching collection room can also save the fingerprint collecting time for finding the coordinates for each RP in the target area. RPs were collected at a 1 m height.

Figure 3-7 also shows the layout of the target Teaching Collection Area and the positions where the iBeacon devices are. For the book finding service, because of the layout of the aisles along the x-axis, the accuracy in the y-axis is more important than x-axis, as this is needed so that the system indicates the right aisle. This can narrow the search area and make it easier for users to find their target books combined with the indoor map. So, more iBeacon devices were deployed in the y-axis to achieve a higher positioning accuracy. All estimated locations will be represented using (x, y) coordinates.

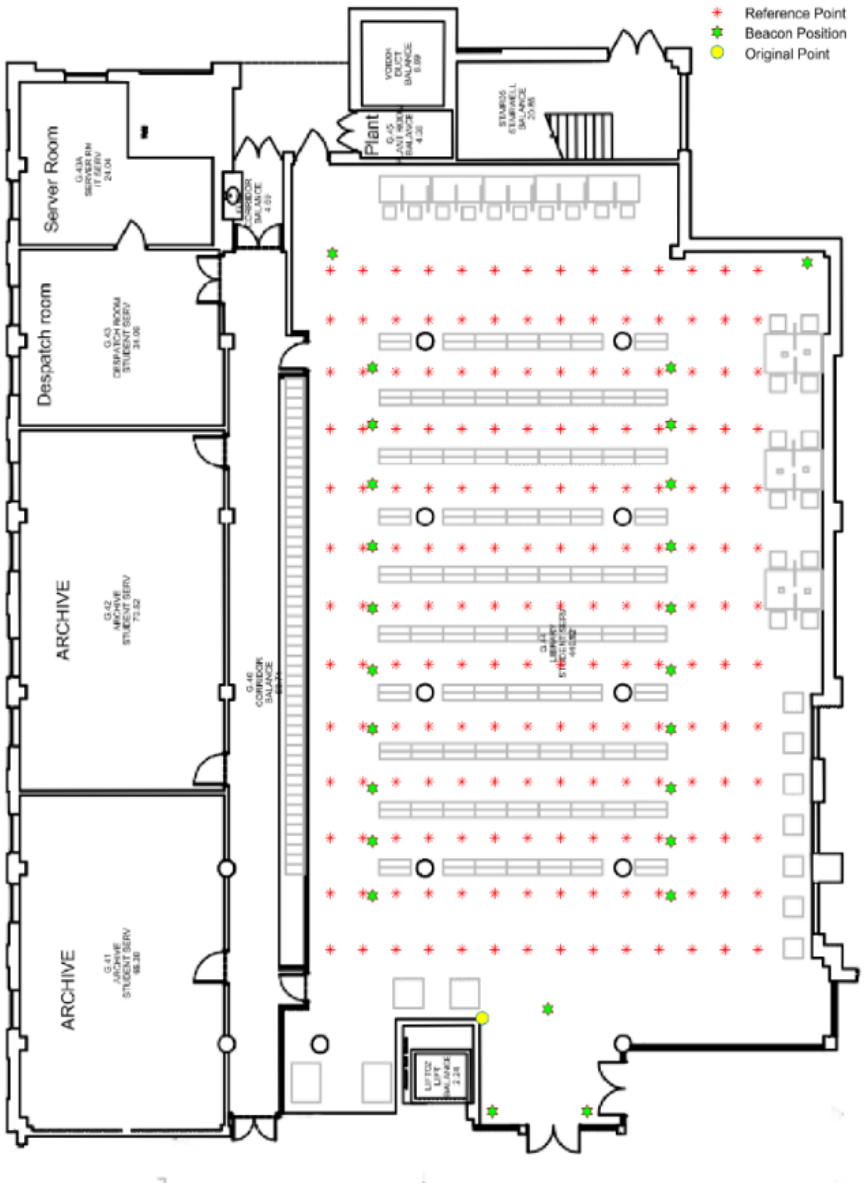

Figure 3-7 RPs and layout of Teaching Collection Area

Laser tapes or Laser distance measuring meters (distance measurement range: 10 m) were used to acquire the ground truth positions when we manually collected the fingerprints in the Library testbed as shown in Figure 3-8 (BOSCH PLR[7]).

[7] For more details: https://www.bosch-do-it.com/ae/en/diy/tools/plr-15-3165140765541-199929.jsp. Last accessed in Sep/2018

Figure 3-8 Laser tapes are used to determine the location ground truth

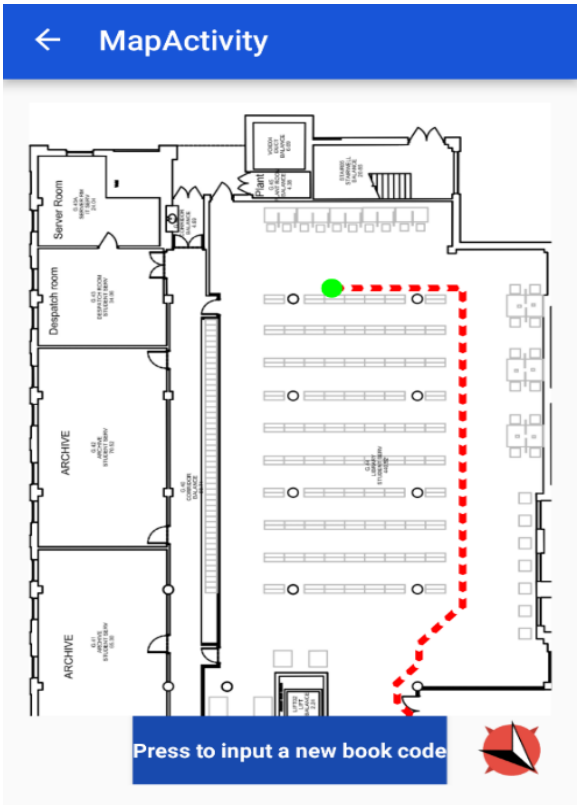

Figure 3-9 Indoor navigation display of the book finding system

Figure 3-9 shows the user interface for the indoor navigation of the book finding ADL system which was developed for Android phones.

3.5.2 BLE Location Fingerprinting Positioning Performance

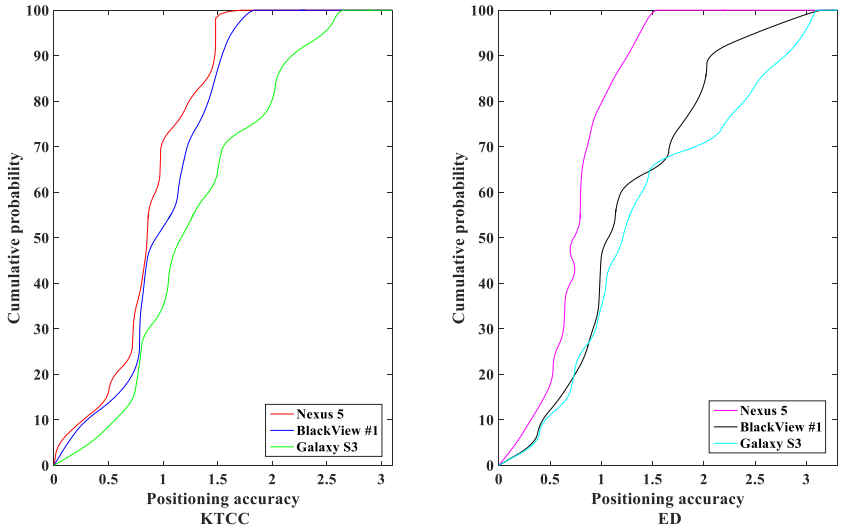

Figure 3-10 Cumulative Distribution Function (CDF) of the error distance of KTCC and ED using different smartphones

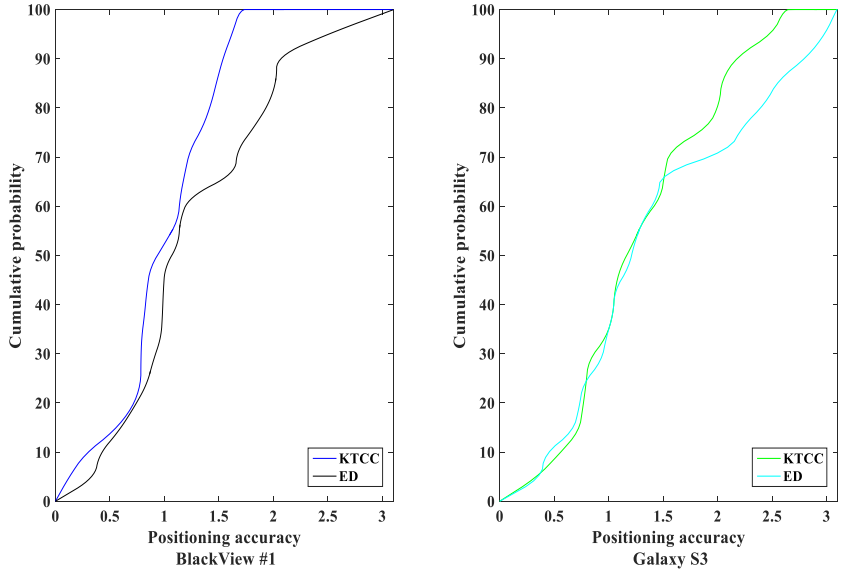

Figure 3-11 CDF of the error distance of KTCC and ED using smartphone BlackView #1 and Galaxy S3

Table 7 BLE location fingerprinting positioning performance of ED versus KTCC algorithms (Study 1)

Smartphone	Averaged Accuracy		Accuracy (90%)	
Type	ED	KTCC	ED	KTCC
Nexus 5	0.78 m	0.87 m	1.37 m	1.45 m
Galaxy S3	1.32 m	0.98 m	2.82 m	2.19 m
BlackView #1	1.45 m	1.12 m	2.12 m	1.49 m

Based on the above results, WKNN using ED determines a slightly better positioning result compared to (WKNN using KTCC) for Nexus 5, which collected the radio map, with an average positioning accuracy of 0.78 meters. However, Figure 3-10 and Table 7 shows that KTCC provides a similar higher precision with 0.98 meters accuracy (1.12 meters using BlackView #1) compared to a precision of 1.32 meters (1.45 meters BlackView #1) using ED for the Galaxy S3 phone. Similar differences were also observed for the BlackView #1 phone.

From Figure 3-11, it is also seen that when using RSSI ranking with KTCC, there is a higher accuracy for BlackView #1 (the averaged positioning accuracy increases by 22.8%) phone and the Galaxy S3 (increases by 25.8%) in comparison to the ED-based method. Therefore, it is concluded that ED can perform well when the same type of smartphone used to acquire the radio map is also used later for in-situ location determination but not as well when different phones are used. This is caused by differences in radio circuits embedded in smartphones, and such RSSI differences can be mitigated by using KTCC. This means that KTCC using RSSI ranking is more smartphone independent than ED using RSSI. This, in turn, promotes a higher indoor positioning accuracy in a more realistic complicated indoor environment.

3.6 Summary

This chapter first presents a study 0, about the use of simple RSSI path loss models in order to more clearly study the effect of increasing distance, RF receiver type and body and RF receiver orientation with respect to the transmitter. Some of the outcomes were used to improve Study 1, that investigated more accurate (than path loss models) fingerprinting methods. Instead of using traditional WKNN using ED, a novel BLE RSSI ranking-based KTCC location fingerprinting method was proposed. The validation results show that this method can mitigate against the diversity of RF receivers' hardware issue.

Note, Study 1 and its experiments took place in the QMUL Library, from 2015 to 2017, it has some critical limitations in where and how BLE beacons as transmitters could be positioned and fixed in relation to the furnishings and fixtures, as permitted by the space owners (QMUL). Apart from the decorating work in the library, which stopped the studies, batteries in the beacons needed to be replaced periodically, else these became non-operational. Each of these causes the set of fingerprints that are used to determine the location to become less effective and to reduce the location accuracy.

Hence, a location fingerprinting method that uses MF measurement will be introduced in the following chapter to mitigate against these challenges.

4 MF Location Fingerprinting

4.1 Introduction

IPSs that use wireless RSSI measurements tend not to use just a type of geometric model, such as a path loss model but are supplemented by a so-called radio map of fingerprints of actual measurements at known locations, in order to gain an increased positioning accuracy. However, even this supplemented method for an RSSI IPS is problematic as RF transmissions at low GHz frequencies are strongly affected by RF attenuation due to the changing orientation, the number of moving humans, and other static solid objects such as metal furniture between RF receivers and transmitters.

Furthermore, such RF methods depend on a deployed infrastructure of a fixed topology of RF transmitters, whose RF coverage may be variable, creating black spots where there are only weak or no RF signals, thus limiting the location accuracy. Accordingly, a more RF invariant technique using MF, combined with inertial sensor measurements is proposed, which are barely influenced by humans. Its other benefits are that no specific IPS infrastructure (low maintenance) needs to be pre-deployed and positions can be determined using a readily available receiver found in a smartphone.

In this chapter, MF Location Fingerprinting methods using a Particle Filter (PF), as this is the most adopted way to localise users using MF, so it was adopted as the baseline IPS using MF. Next, a new Fast Path Matching algorithm for MF and Inertial sensor measurements (FPM-MI) is introduced in the next Section 4.2. The evaluation results and a summary are given in Section 4.3 and 4.4 respectively.

4.2 MF Location Fingerprinting Methods

4.2.1 MF Location Fingerprinting using the PF

Particle filters are also called Monte Carlo Localisation (MCL) can be applied to indoor navigation using MF measurements. This technique was first introduced by

[76] and then utilised for robotic target-tracking applications [77]. The central idea of MCL is to use the Bayesian theorem to represent the posterior distribution of the moving targets. When a target moves, Sequential Importance Resampling (SIR) is used to approximate the posterior distribution [77]. Since MCL is based on the sample representation, the particles are resampled based on recursive Bayesian estimation, i.e., how well the actual sensed data correlates with the predicted state so that the posterior distribution of the particles converges to the true position. Therefore, it can help to better determine the track of a moving target.

Particle filter

Algorithm 4.1:

Initialization:

Particles x_0^i with uniform $\omega_0^i = \frac{1}{length(particles)}$

for each step $n = 1, 2, 3 \ldots$:

for $i = 0\ to\ length(particles) - 1$:

Measurement:

Measure magnetic signature $S_n = \|M_n\|$

//Collected from 3-axis magnetometer and S_n is the norm value

Prediction:

$x_n^i \sim P(x_n | x_{n-1}^i))$

Weight Updating (Gaussian density):

$\omega_n^i = P(S_n |\ x_n^i)$:

Resampling:

Make Cumulative Distribution Function (SIR)

Obtain new particles x_n^{i*}

Return: $\sum_{n=0}^{t-1} x_n^{i*} \times \omega_{n0}^i$

Many algorithms for sensing steps have been developed, e.g., [78], which need to be implemented in smartphones, but more recently this is supported by the smartphone

OS itself as a virtual sensor (step counter). Hence, it[8] is used to count steps, which is also used in the prediction part in algorithm 4.1 to update the particle states.

In Algorithm 4.1, the data from the virtual sensors (using a step counter to count steps and digital compass to predict headings) is used to predict the relation between each particle x_{n-1}^{i} and x_{n}^{i} in the same track (for MF measurements). This can be seen in procedure 1 of Algorithm 4.2 (in Section 4.2.2). After detecting each step, the weight of each particle needs to be updated, and the weight ω_n is calculated using the Gaussian density function as equation (4.1).

$$\omega_n = P(S_n|x_n) = \frac{1}{\sigma_r\sqrt{2\pi}} e^{-(S_n - \|f(x_n)\|)^2/2\sigma_r^2} \tag{4.1}$$

where $P(S_n|x_n)$ is the posterior distribution of the latent variable S_n, $f(x_n)$ is the estimated model of the location x_n and measurements (MF strength in the north orientation) S_n, the particle number and the standard deviation σ_r are set to 5,000 and to 2, respectively. They are set the same as define in [4].

However, even though MCL is effective at tracking moving targets, there are still limitations that can be improved. First, the computational cost of Monte Carlo localisation can be enhanced. Second, most current existing resampling algorithms are inherently inefficient. This occurs when the samples and posterior distribution do not fit each other [79].

Moreover, an accurate model of S_n and location x_n also needs to be built for an MF location fingerprinting system, which means the systems using the PF require expensive arithmetic operations and a long processing time. Hence, it's unsuitable for

[8] For more details: https://developer.android.com/guide/topics/sensors/sensors_motion.html. Last accessed in Sep/2018

low ICT resource devices and for near real-time MF location fingerprinting IPS deployment [29].

4.2.2 MF Location Fingerprinting using FPM-MI

K-Nearest Neighbours (KNN) algorithm is a widely used positioning algorithm. However, as found for the MF heat map for an area, e.g., in QMUL Main Library, there are several locations with similar MF intensities, which means using NN ($K = 1$) or KNN alone to estimate location will cause significant positioning errors.

In this algorithm, the KNN for each MF signature M_t in the fingerprints map, is selected using ED. K is assigned to be 12 in the scenario (K = 6 is chosen in the following figure to better visualize the algorithm), as this enables most (95% of) MF measurements in our training dataset, in which MF measurements were collected by continuously walking around all shelves, to match their real nearest fingerprint in the map, as in some areas, they may have a smooth MF environment with less anomalies.

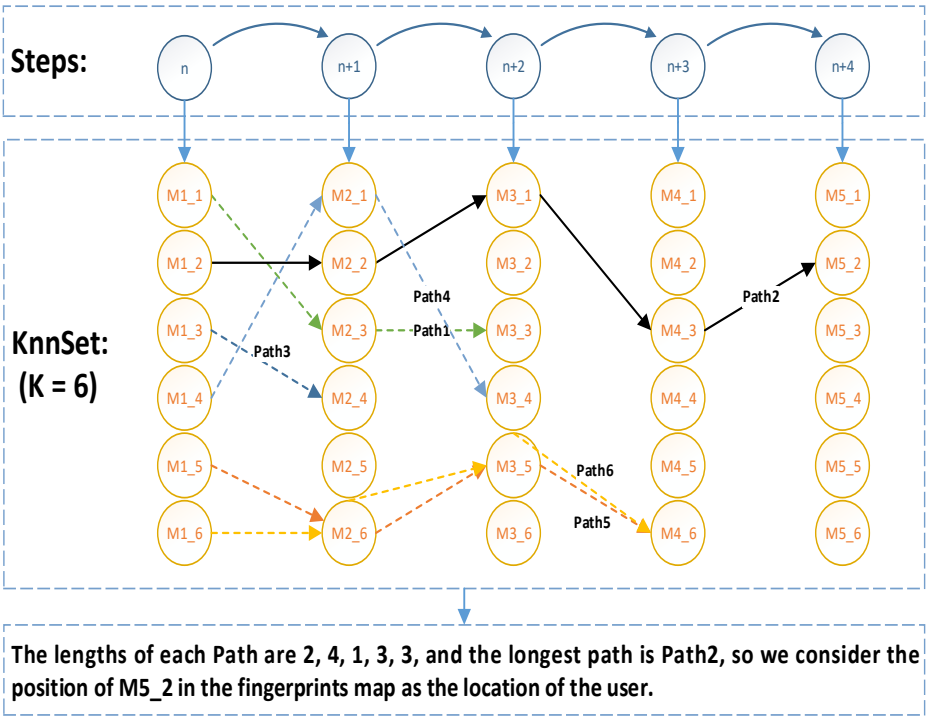

Figure 4-1 Explanations of the FPM-MI Algorithm

Next, K paths are estimated by adding points which meet the constraints of the distance and orientation between the new points, and the previously predicted one. In this process, the first neighbour point which meets the conditions (for the required distance and orientation) is selected, as the points in the first part of the $knnSet$ have a higher weight. The orientation is also measured using the Android OS virtual sensor (digital compass).

Locations will be estimated by comparing the number of satisfied points in the paths (points that satisfy the constraints, including path length as shown in Figure 4-1). The longest path means the minimal error between the two observations. Thus, it has the highest possibility of being the nearest path. So, the longest path is considered as the estimated path. The location of the last point in the path will be regarded as the estimated location.

Finally, if the number of satisfied points in the path is less than a threshold, the algorithm will expand the tFactor (in procedure 3 of Algorithm 4.2). This is used to make sure the algorithm can generate a result if for example, sensor drift happens, each time tFactor will add 0.5, as the gap between each RP is 0.5 m, and tFactor will start from 0.5), which makes the condition less restrictive. Then it will repeat procedures 3 and 4.

The new proposed MF IPS algorithm uses relatively low computation data processing in comparison to a pure PF used alone. The former requires far fewer arithmetic operations, e.g. the rough number of operations of particle filters to have an accurate estimated location is 500000 (20 (number of steps) $*$ 5000 (number of particles) $*$ 5 (1 (prediction) $+$ 1 (weights-updating) $+$ 2 (re-sampling) $+$ 1 (return))). To get a complete posterior distribution, the number of particles is usually large ($\mathrm{n} = 5000$ in the experiments). The rough number of operations of FPM-MI is 248898 (5 (number of steps) $*$ (1 (prediction) $+$ 12 (knnset)) $+ 12^4$ (match the path) $*$ 12 (number of path) $+$ 1 (return)). This is also the worst case for the algorithm, the number of path calculation operations can be further reduced by using Dynamic Programming [80].

FPM-MI Algorithm

Algorithm 4.2:

Requires:

1. Signatures $P = \{M_1 \dots M_t \dots M_n\}$

2. Fingerprints Map $M = \{M_{1,1} \dots M_{1,4} \dots M_{i,4}\}$

//j *represents the orientation* in $M_{i,j}$

3. Steps n and Orientations $O = \{o_1 \dots o_n\}$

Set $knnSet, locationSet, pathSet$ = *new* Set

Set k matched$Path = knnSet[0][i]$

for each step n=1,2,3…:

Procedure 1 - Prediction:

$X_n^i = X_{n-1}^i + \mathrm{H}_{o_n} \times$ steplength (0.5 m as default)

Procedure 2 - Find k-nearest neighbours:

$knnSet$ add $k - nearest\ neighbors\ for\ M_n$

Procedure 3 - Match the paths:

for j ***in*** $length(knnSet[i+1])$:

$point = knnSet[i+1][j]$

//loc means the location coordinates (x, y)

$dist = \|matchedpath[i].loc - point.loc\|$

//differences of distance and orientation (direction)

if $dist \leq tFactor$:

if $orientation(o_n)$: //judge the orientation

$matchedPath$ add $knnSet[i+1][j]$

$locationSet$ add $\mathrm{X}_{knnSet[i+1][j]}$

break

$pathSet$ add matchedPath

Procedure 4 - Return location:

Find the maxLength $matchedPath[i]$

if $maxLength \geq threshold$:

return the first maxLength $matchPath[i]$

else update $tFactor$ and repeat Procedure 3, 4

where $X_n^i = \begin{Bmatrix} x_n \\ y_n \end{Bmatrix}$ and $\mathrm{H}_{o_n} = \begin{Bmatrix} \cos o_n \\ \sin o_n \end{Bmatrix}$.

4.3 Study 2: MF Location Fingerprinting Evaluation

4.3.1 Stability of the MF Strength

For constructing the MF fingerprints map and linking it to the ground truth or actual locations, the same laser tape that was used in Chapter 3 (see Figure 3-8) is also used here. Geographic coordinates were determined using a data collection application, installed on a Nexus 5 phone, to collect MF fingerprints in four orientations (N, W, E, S) for each RP (240 RPs, 50 samples for each orientation), 0.5 m apart at a 1 m height.

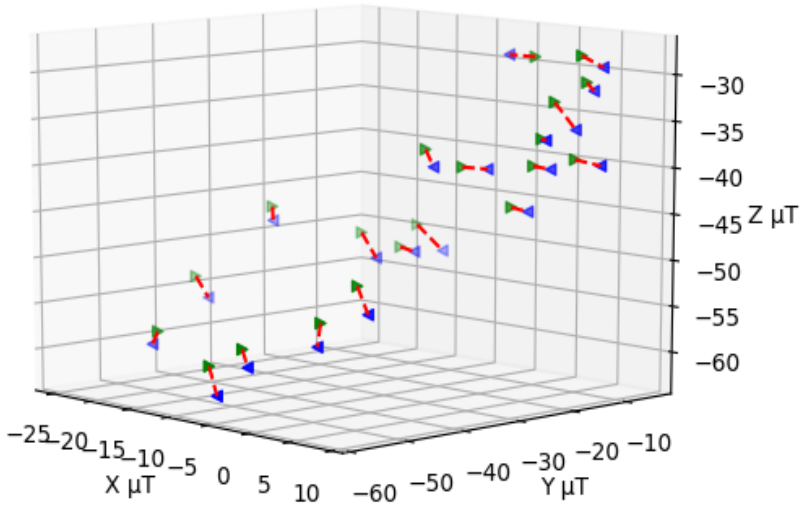

Figure 4-2 Comparison of fingerprints at a time Y and then after two months

Before testing the performance of this IPS, pre-experiments were carried inside the QMUL library to verify the stability of the MF distribution in space and over time. To ascertain this, all MF fingerprints were collected in the fingerprints map again by using the same smartphone two months after collecting the original fingerprints map. The unit of collected measurements of the MF is µT in the X, Y, and Z axes of the magnetometer on a Nexus 5, smartphone 1. To visualise the results, 20 fingerprints were randomly picked (Figure 4-2). The green arrows represent the original fingerprints, and the blue ones represent the test data collected in the same position

two months later. The red dash lines represent the ED between the two fingerprints, which acts as a similarity function to find the k-nearest neighbours of each signature in our algorithm.

The similarity of MF fingerprints was computed using the Cosine Similarity and Magnitude Difference equations from [28] as follows:

$$\text{Cos}\,\theta = \frac{1}{n}\sum_{i=1}^{n}\frac{A_i \cdot B_i}{\|A_i\|\|B_i\|} \tag{4.2}$$

$$\text{Magnitude} = \frac{\sum_{i=1}^{n}\|A_i\|}{\sum_{i=1}^{n}\|B_i\|} \tag{4.3}$$

where, A and B represent the fingerprints and test datasets, and n is the number of RPs.

The result shows that the Cosine Similarity = 0.99, and the Magnitude = 0.97, which confirms that the MF did not change much over the two month period. Further, [28], also noted that the time-invariance of the MF was even longer, at least six months. Hence, the use of MF measurements, tends to be time-invariant, assuming no MF affecting fixings in the infrastructure are changed.

The MF influence caused by electronic devices typically carried by humans such as a watch was also examined. This influence is negligible if the distance between the magnetometer and other electronic devices is more than 10 cm. This is confirmed by [28] which came to a similar conclusion. Furthermore, magnetometers are not easily influenced by furniture which contained a small amount of metal. Hence, for some user scenarios, some kinds of moved furniture or fixings will not affect the system.

4.3.2 Differences in MF strength

Based on the fingerprints collected in four orientations of the same place, the MF strength of four orientations are similar in most places, but in some spots, the MF strength from different orientations may vary drastically. The MF measurements

collected from the west, east and south directions were compared with data north used as the reference direction as shown in Figure 4-3. The drastically changed spots were close to pillars in the room, so it is believed that the variations are caused by the embedded metal in the pillars as they have a high impact within a small radius. This, in turn, means an accurate measurements model and geolocation is hard to build as it may require considering the orientation.

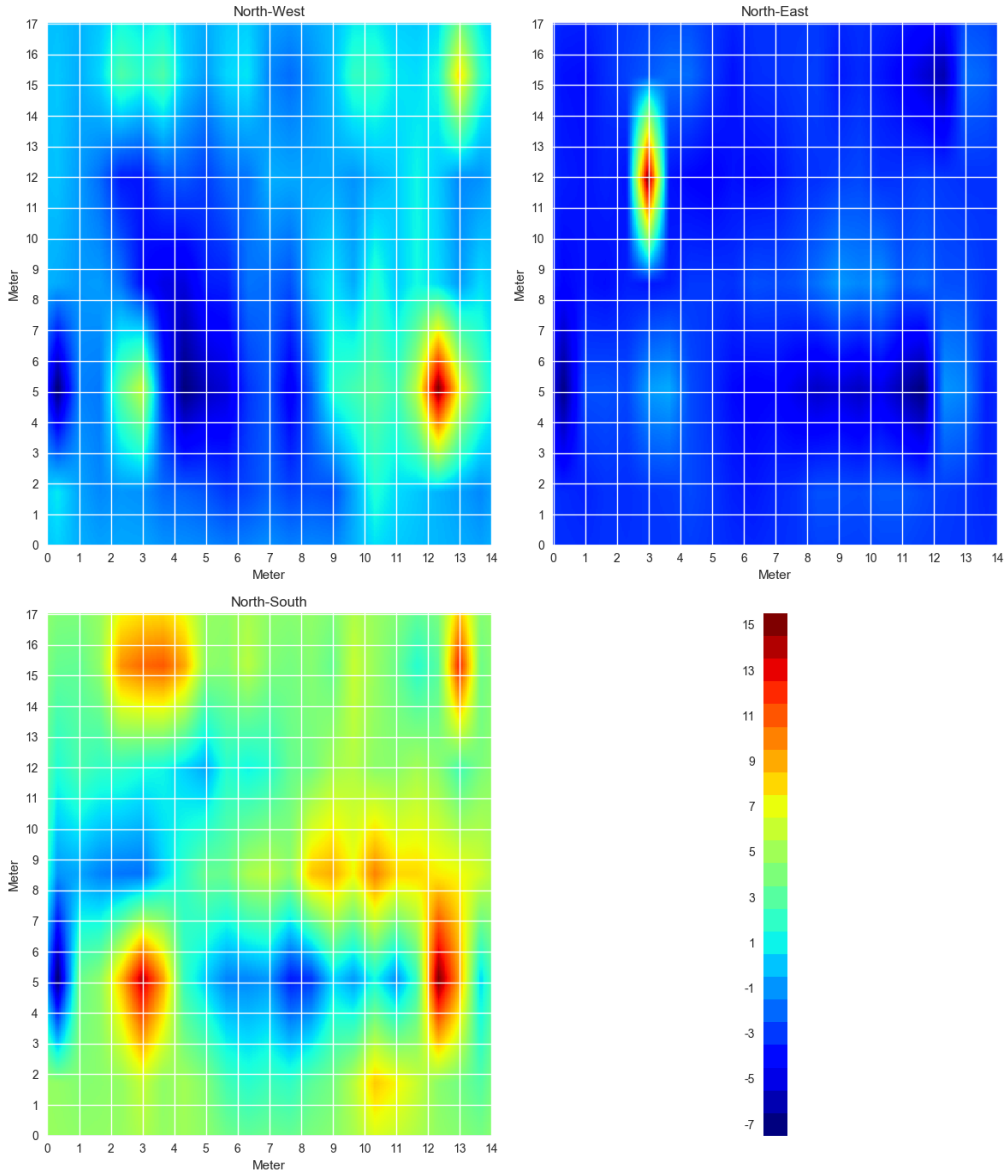

Figure 4-3 Comparison of MF intensity between North as a reference with the remaining three orientations, the bottom right graph shows the range in MF intensity differences between N and the other 3 orientations

The bottom right figure shows the intensity of the variations between them. This is also the reason why fingerprints were collected from four orientations, which would increase the data quality in the KnnSet in procedure 2 for the FPM-MI algorithm.

4.3.3 Positioning Performance

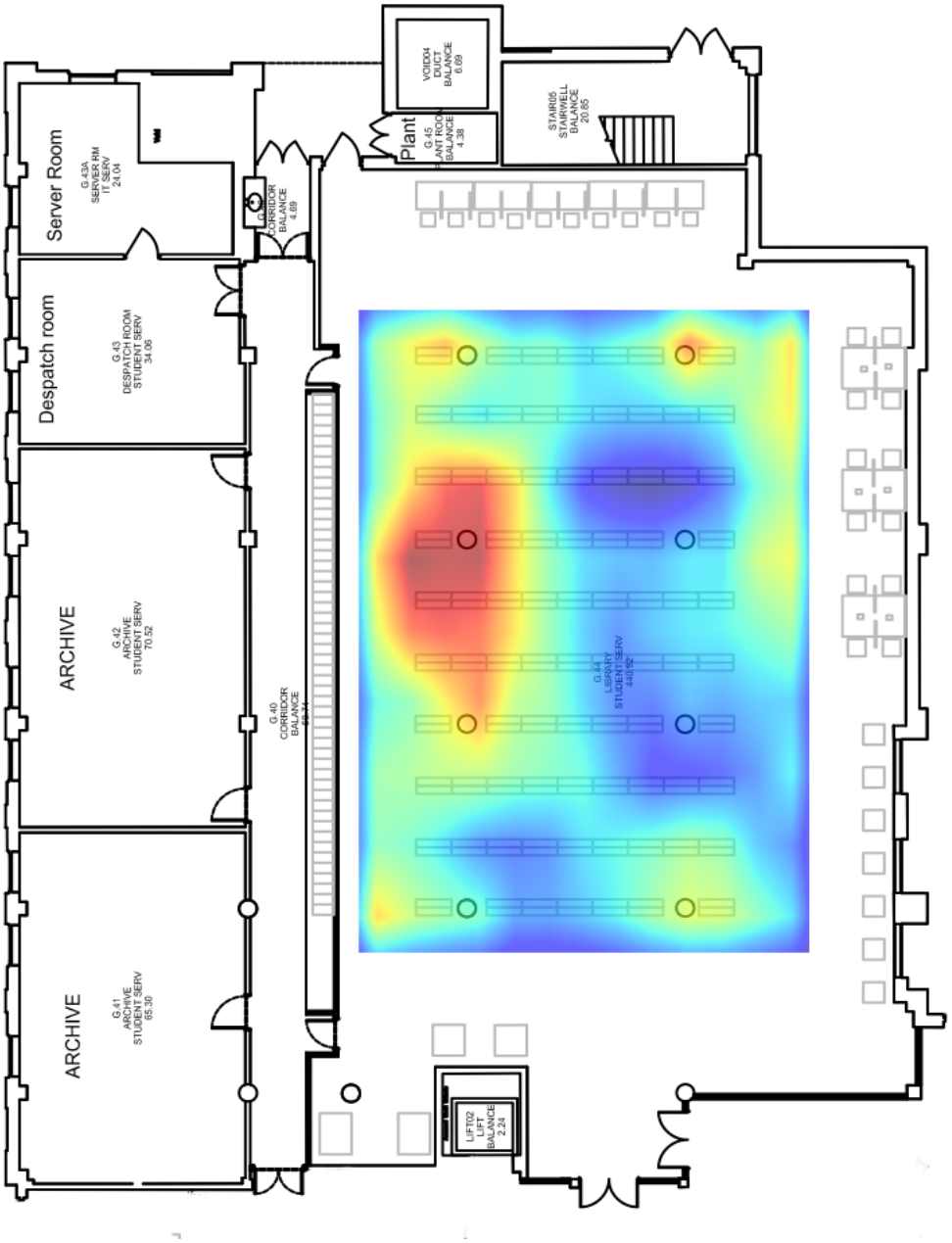

Figure 4-4 Heatmap (north orientation) of MF with respect to the floor plan

Test data was collected by continuously walking around all the shelves in the physical space shown in Figure 4-4 (the same setting as mentioned in study 1, see Section 3.5). The performance of the FPM-MI and PF algorithms is shown in Figure 4-5.

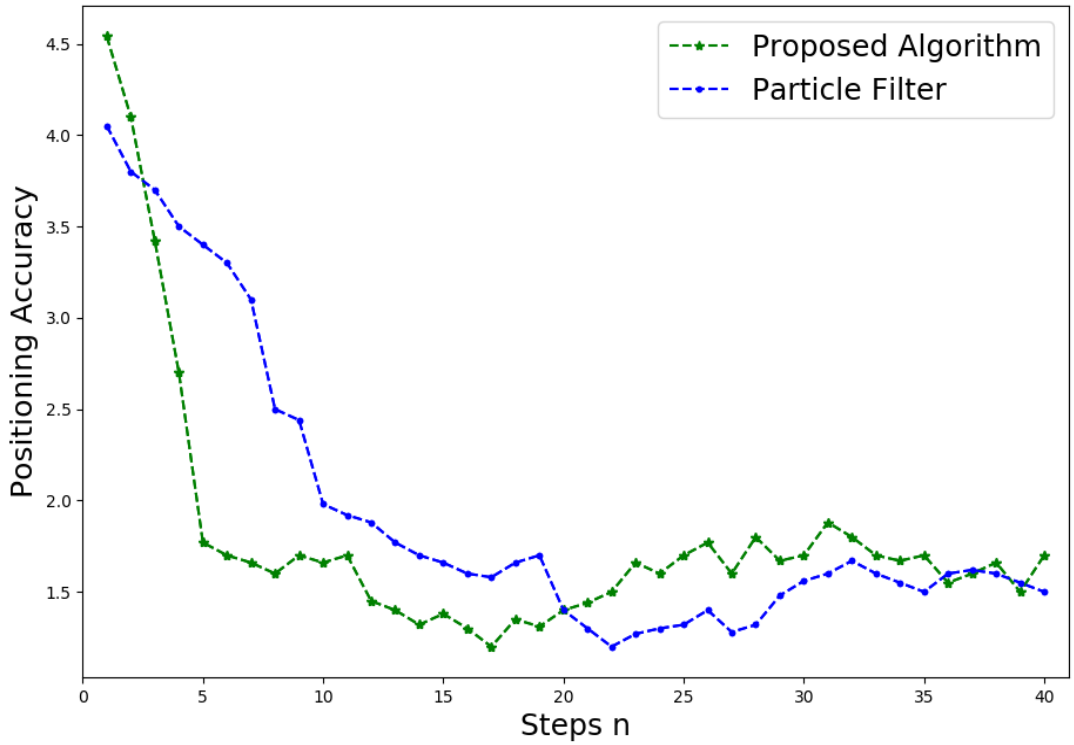

Figure 4-5 Location accuracy versus no. of steps taken for two algorithms: FPM-MI (proposed one) and PF (used as a baseline)

This indicates that the accuracy of the proposed algorithm increases faster when $n < 5$ - the change tends to be stable, which also means the proposed algorithm has a good positioning accuracy (Average Error is 1.72 m, Error Standard Deviation is 0.5 m, Error within 1.89 m with a 90% confidence, when $n = 5$) when walking a fewer steps, in contrast to using a PF. $n = 5$ is chosen as the differences between 5 to 17 is not much, and the accuracy is decreased when $n > 17$. This may be caused by error accumulation by the android inertial sensors as the number of steps increases. The MF-based system, unlike using BLE, requires no extra AP infrastructure setup. However, it also shows that after 20 (human) steps, the PF algorithm performs slightly better than the proposed FMP-MI algorithm. However, as a trade-off between computational cost and positional accuracy, the performance of the FPM-MI algorithm is sufficient.

4.4 Summary

This chapter explored the use of MF as a sensor input for another type of location fingerprinting. A novel path matching algorithm that uses MF and IMU measurements was proposed. However, the limitations of this method are as follows. First, its accuracy is not as high as RF-based location fingerprinting. Second, it does not scale well in terms of space size as there it becomes more likely that several locations with similar MF intensities will occur making the mapping of MF signature to a location more complex. Third, it is time-consuming to construct the MF measurement map. Fourth, the positioning accuracy highly relies on the performance of inertial sensors (the robustness is not tested, error accumulation may happen). Hence, this was not implemented as an algorithm for the library book finding ADL service. MF measurements will be treated as additional RF invariant input data to help increase the positioning accuracy in future work (see Section 7.2.1.4).

As the most popular IPS is a WiFi location fingerprinting system, this type of IPS was also explored in a testbed where there was a good WiFi AP coverage and density – see the next Chapter 5.

5 WiFi Location Fingerprinting and ADL Recognition

5.1 Introduction

The basic IPS for WiFi-based upon location fingerprinting is similar to that of BLE, see Chapter 3. However, further algorithms are implemented to increase the positioning accuracy.

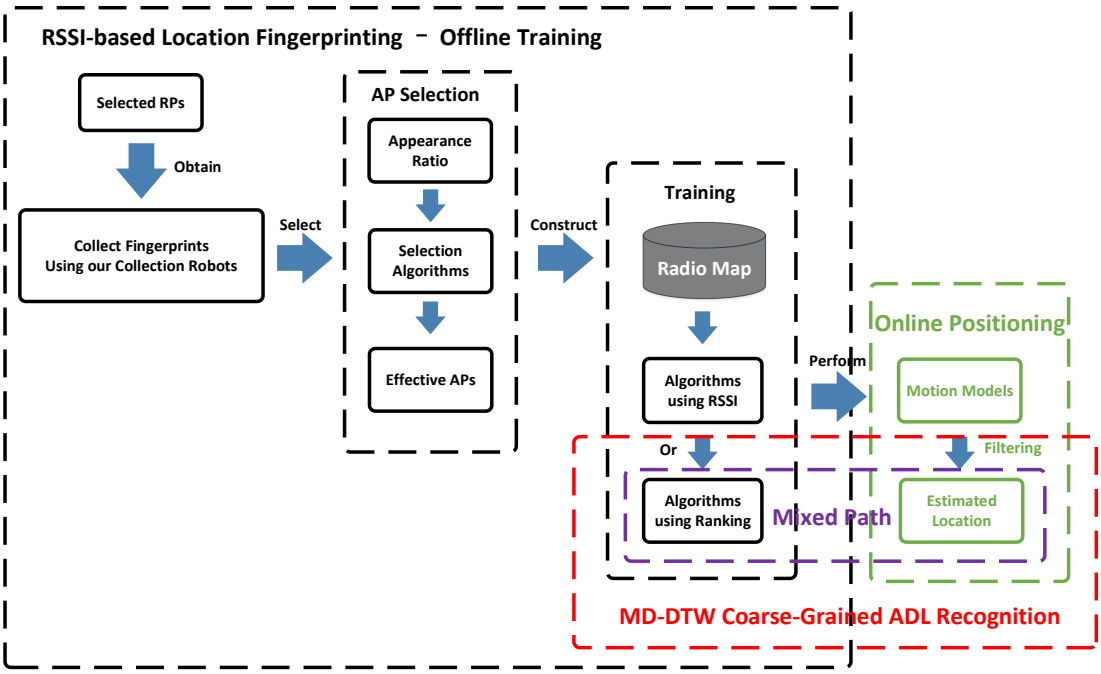

Figure 5-1 The key processes involved in RSSI fingerprinting and ADL recognition

So far, several improved IPSs have been researched, developed and validated in this research to determine the locations of physical assets that users wish to access. A default, single, associated ADL is linked to the destination location, in order to access or retrieve a physical asset. There is little focus here on the navigation algorithm to do this as it is assumed that a standard navigation algorithm can be used such as A* [81] or Dijkstra's algorithm [82]. The more accurately we can determine the location, the more accurately we trigger the default ADL. However, during daily life, many different locations can be associated with different ADLs, hence determining users' different locations could also be used for recognising different ADLs. Hence, an ADL

recognition method that uses MD-DTW is also introduced in this chapter. An overview of the key processes involved in RSSI location fingerprinting and ADL recognition is given in Figure 5-1.

In this chapter a Deep Neural Network (DNN) classification algorithm namely, a CNN ranking-based location fingerprinting method is next introduced in Section 5.2. Section 5.3 will describe a WiFi-based activity recognition method using MD-DTW. Lastly, Sections 5.4 and 5.5 will describe the evaluation results and present the chapter summary, respectively.

5.2 Algorithms to Increase WiFi Positioning Accuracy

5.2.1 WiFi AP Selection

Due to the increasing availability and high density of heterogeneous wireless APs in indoor environments, more networks and APs are becoming available that can be detected by users' mobile wireless access devices. This, however, increases the computational cost to estimate locations of the user based upon received signals from more and more APs. Because a wireless receiver can receive information, this implies that it is within range of a transmitter and gives it a positioning fix in relation to this transmitter.

Using more APs can improve the positioning accuracy due to more RSSI signal comparisons by receivers to determine the location. When discovering the transmitters or receivers, that are available, the more there are, the more computation and power is required to differentiate these locations. Note that some APs are affected more than others by interference such that their RSSI values fluctuate more at some locations within range of these APs at the frequencies used. This is caused by people moving or because of the proximity to other RF sources that are intermittently active in the same unlicensed RF frequency spectrum as WiFi, such as BLE devices being used by users and by microwave ovens. These effects affect the location determination accuracy. Appropriate AP selection not only helps to remove the APs with a more inferior or

variable location determination accuracy but also helps to minimise noise levels and to improve the computation efficiency. It is a critical challenge of how to choose the optimum number of APs for location determination in an AP sufficient scenario. This is also related to feature selection or extraction.

5.2.1.1 AP Selection Based on RSSI Interval Overlap Degree Determination

As AP selection is of significance in wireless location fingerprinting systems, an Interval Overlap Degree (IOD) algorithm is proposed to select APs. There are several key characteristics of this proposed method. Firstly, IOD uses the numerical interval as a measure to analyse the characteristics of RSSI sample values from APs and to reduce the redundancy. Secondly, IOD preserves the original features of samples instead of extracting one statistical criterion, e.g., mean or median for AP selection. Lastly, IOD achieves a higher location determination accuracy whilst improving the computational efficiency.

The concept of the overlap degree has been used for localisation in [83]. It is used to represent the overlapping area of different regions. The overlap areas with maximum overlap degrees are the estimated location, and it is postulated that it could also be used to discriminate APs.

Assume $RSSI_{1i} = \{RSSI_1^{1i}, RSSI_2^{1i}, \dots, RSSI_k^{1i}\}$ denotes k possible measurements from the i-th AP at the first RP. The numerical interval of $RSSI_{1i}$ can be defined as: $[min(RSSI_{1i}), max(RSSI_{1i})]$. this numerical interval can be visualised as the x, number, axis (the blue stripes) in Figure 5-2. The RSSI values of AP_i at each RP can all be displayed as numerical intervals. The issue is how to discriminate RPs from each other using AP_i.

IOD can be employed as a criterion to discriminate numerical intervals effectively as shown in Figure 5-2. $IOD(NI_1, NI_2)$ can be calculated as

$$IOD(NI_1, NI_2) = \frac{1}{2}\left(\frac{OI(NI_1, NI_2)}{length(NI_1)} + \frac{OI(NI_1, NI_2)}{length(NI_2)}\right) \quad (5.1)$$

In this example, there are four overlap relationships between two numerical intervals. Figure 5-2 also shows how to compute the $OI(NI_1, NI_2)$ in these four cases. The value of $OI(NI_1, NI_2)$ will be zero when there is no overlap.

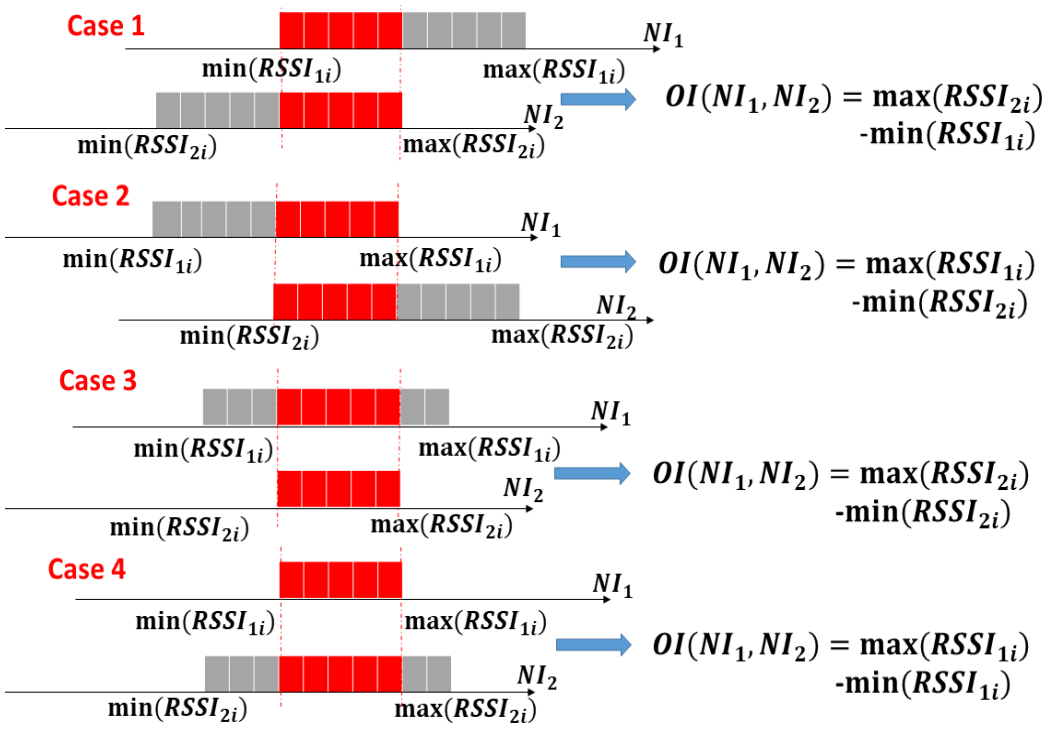

Figure 5-2 Schematic of the Interval Overlap Degree (IOD) proposed to select efficient APs. The red part denotes the Overlap Interval (OI), and the grey part is the non-overlap interval.

IOD is defined as the mean of the proportion of the overlap interval between two numerical intervals accounts in each of these two numerical intervals (see equation 5.2). The lower the IOD, the more significant is the difference between two numerical intervals, which means these RPs are more accessible to differentiate.

The RSSI samples from the same AP are different for different RPs. If $RSSI_{ia} = \{RSSI_1^{ia}, RSSI_2^{ia}, \dots, RSSI_k^{ia}\}$ denotes the RSSI sample values collected at i-th RP from AP_a and $RSSI_{ja} = \{RSSI_1^{ja}, RSSI_2^{ja}, \dots, RSSI_k^{ja}\}$ represents the RSSI samples collected at j-th RP from AP_a. IOD_{ij}^a stands for the IOD between $RSSI_{ia}$ and $RSSI_{ja}$. The higher IOD_{ij}^a is, the smaller the difference between

$RSSI_{ia}$ and $RSSI_{ja}$. This means it is more difficult to discriminate i-th RP and j-th RP using AP_a. So our target is to select APs with the lowest IOD. If N is the total number of RPs, then there are $\frac{1}{2} * N(N-1)$RP combinations in all. Let IOD_{f-a} represent the final IOD of AP_a. It can be calculated as follows:

$$IOD_{f-a} = \sum_{i}^{N-1} \sum_{j=i+1}^{N} IOD_{ij}^{a} \tag{5.2}$$

After figuring out the final IOD of all APs, them will be ranked in ascending order and select the top k APs with the lowest IOD.

5.2.1.2 Design Choices for AP Selection

1) AP Selection based on Standard Deviation

[84] introduced a Standard Deviation (SD) based AP selection algorithm. This used the SD of the collected RSSIs of a TP to analyse the signal stability of APs. The theory is that a lower SD value indicates that the mean of RSSIs transmitted from the AP is more stable and suitable to process pattern matching. Assuming $RSSI_i^j$ denotes the j-th RSSI value of AP_i and $\overline{RSSI_\iota}$ is the mean value of RSSIs from AP_i. SD_i denotes the SD of AP_i which can be calculated as follows:

$$SD_i = \sqrt{\frac{1}{n-1} \sum_{j=1}^{n} (RSSI_i^j - \overline{RSSI_\iota})^2} \tag{5.3}$$

Then, these values of each AP's SD are sorted in ascending order and selecting the top k APs with the smallest SD as a lower SD value – leads to a RSSI series from the AP that is more stable. SD is a criterion to reflect the amount of variation of a set of data values relative to the mean value. However, SD is not suitable for a situation where outliers exist. Moreover, this method requires online selection of APs for all the TPs, which needs an extra computational cost.

2) AP Selection Based on Information Gain

In information theory and machine learning, Information Gain (IG) is often used as a criterion for feature selection. For fingerprint-based positioning, AP selection is also regarded as feature selection. [85] proposed an AP selection strategy based on IG. The idea of selecting AP using IG is as follows:

If N_t is the number of APs ($AP_j, 1 \leq j \leq N_t$) that can be detected at each RP ($R_i, 1 \leq i \leq S$) in an indoor space. The IG of AP_j can be described by

$$IG(AP_j) = H(R) - H(R|AP_j) \tag{5.4}$$

where $H(R)$ is the entropy of a RP and can be demonstrated by

$$H(R) = -\sum_{i=1}^{S} P(R_i) log P(R_i) \tag{5.5}$$

where $P(R_i)$ is the prior probability of R_i. There are S RPs in total, $P(R_i) = 1/S$ was set for each RP since the probability of each RP is viewed within a uniform distribution. $H(R|AP_j)$ is the conditional entropy of a RP given the RSSI of AP_j. It can be calculated accordingly as follows:

$$H\left(R|AP_j\right) = -\sum_{V} \sum_{i=1}^{S} P(R_i|AP_j = v) log P(R_i|AP_j = v) \tag{5.6}$$

where v denotes one possible RSSI value from AP_j and V are all the possible values from AP_j. Then the conditional probability can be shown as follows:

$$P\left(R_i \middle| AP_j = v, v \in V\right) = \frac{p(AP_j = v|R_i)\, p(R_i)}{P(AP_j = v)} \tag{5.7}$$

The discriminative ability means the ability that an AP can distinguish RPs from each other. For decision tree classifiers, the higher the IG value, the better the classification ability of this feature. Therefore, a higher IG value for the AP means a strong discriminative ability towards RPs. If IG values of all APs are sorted in descending order, the top k APs with highest IG values will be chosen.

The main merits of IG are that IG makes good use of the diversity of the data samples and takes the discriminative ability of each AP into consideration. Nevertheless, IG is more likely to choose the AP with more collected sample values, some of which are unstable and more physically environmentally sensitive, leading to a degradation of positioning accuracy.

3) AP selection based on Mutual Information (MI)

Another information theory-based method is Mutual Information (MI), which is used by [86] for selecting APs. The MI of two random variables is a measure of the mutual dependence between the two variables. The higher the MI, the more information these variables share which also means redundant information. Redundant information does not bring any useful information but increases the amount of computation. Thus, the primary target of this MI-based AP selection method, which is also the difference with using IG is that MI picks out the APs with the least amount of redundant information.

If $MI(AP_a, AP_b)$ denotes the MI of AP_a and AP_b and it can be described by

$$MI(AP_a, AP_b) = H(AP_a) + H(AP_b) - H(AP_a, AP_b) \tag{5.8}$$

where $H(AP_a)$ and $H(AP_b)$ are the information entropies of AP_a and AP_b respectively. $H(AP_a, AP_b)$ expresses the joint entropy of AP_a and AP_b.

$$H(AP_a, AP_b) = -\sum_{V_2}\sum_{V_1}[P(R|v_1 \in V_1, v_2 \in V_2)logP(R)] \tag{5.9}$$

where R represents $(RSSI_a = v_1, RSSI_b = v_2)$.

The first step is to identify the AP pairs with the least MI. If N_t is the number of APs in the space, there exists $N_t(N_t - 1)/2$ AP pairs. Assuming (AP_a, AP_b) is the choice, then add another AP_c to compute the MI of AP_c and (AP_a, AP_b). In this case, (AP_a, AP_b, AP_c) with the least MI will be chosen. The process can be described by

$$arg\min_{AP_z} MI(AP_a, AP_b, \dots, AP_k) \tag{5.10}$$

where $MI(AP_a, AP_b, \dots AP_k)$ is calculated by

$$MI(AP_a, AP_b, \dots AP_z) = H(AP_a, AP_b, \dots) + H(AP_k) - H(AP_a, AP_b, \dots AP_k) \quad (5.11)$$

Following the above procedures, a group including k APs with the smallest $MI(AP_1, AP_2, \dots AP_k)$ will be chosen. The MI method can efficiently reduce RSSI redundant information.

4) Dimensionality reduction based upon Principal Component Analysis (PCA)

Instead of choosing a subset of APs, [87] replaces the elements with a subset of Principal Components (PCs), which are obtained by a transformation of the measured RSSI. The theory of the paper is based on the use of PCA to find an effective transformation such that the retained information in the chosen PCs can be maximised.

$$\begin{pmatrix} y_1 \\ \vdots \\ y_L \end{pmatrix}_{L*1} = \begin{pmatrix} a_{11} & a_{12} & \dots & a_{1D} \\ a_{21} & a_{22} & \dots & a_{2D} \\ \vdots & \vdots & \vdots & \vdots \\ a_{L1} & a_{L2} & \dots & a_{LD} \end{pmatrix}_{L*D} \begin{pmatrix} x_1 \\ \vdots \\ x_D \end{pmatrix}_{D*1} \quad (5.12)$$

The concept of using PCA, which is a statistical procedure that uses an orthogonal transformation to convert a set of observations of possibly correlated variables into a set of values of linearly uncorrelated variables called principal components. This is used to reduce the dimensions where combining APs. In other words, information reorganisation is adopted, rather than AP selection. As shown in equation (5.12), the principal components $[y_1, y_2 \dots y_L]^T$ are produced by a transformation with real numbers. With appropriate weightings (transformation matrix A), the RSSI information transmitted into Y from X can be maximised. Matrix A is determined by using PCA, as it has the ability to present data through minimising the least squares error (see equation 5.13) [87], i.e., $Y = AX$, $\hat{X}$ is the reconstruction of X from Y, $\hat{X} = A^T Y$, PCA seeks to minimise the mean square reconstruction error

$$J_\epsilon = E\left\{\left\|X - \hat{X}\right\|^2\right\} \quad (5.13)$$

The property guarantees that it can retain the maximised information when dimensions are reduced (a test dataset can be used to choose PCs). PCA can be realised using eigenvalue decomposition of a data covariance (or correlation) matrix or singular value decomposition of a data matrix, usually after mean centring (and normalising or using Z-scores) the data matrix for each attribute.

Although RSSI-based AP selection and positioning methods can be affected by a RF receiver hardware diversity issue, it can still be used for IPSs that tend to use a single type of receiver positioning system, e.g., BLE tag-based person locating system.

5.2.1.3 Ranking-based AP Selection Based on Genetic Algorithm

The proposed IOD AP selection algorithm will be compared with IG, MI, and PCA. However, those algorithms are not designed for AP ranking-based methods. To solve this, it is proposed to use a Genetic Algorithm (GA) to select APs, which uses the value of the bit (0 or 1) to represent whether or not an object, e.g., AP, is selected, and it is fit for AP selection. Moreover, unlike those algorithms, GA can directly find the optimal AP list, instead of iterating through all APs to find the optimal APs.

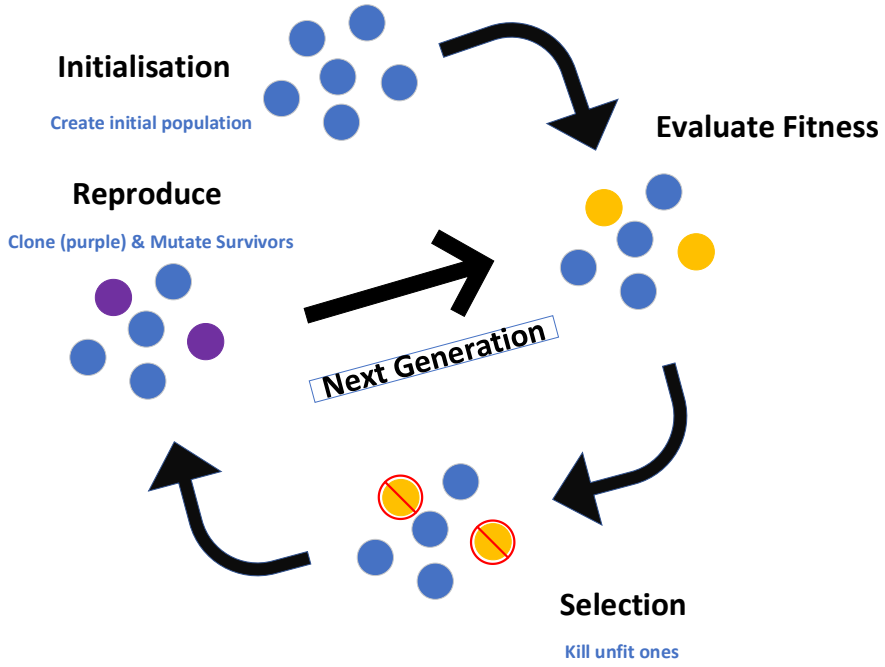

Figure 5-3 An overview of the GA algorithm

The main principle of GA is that it is based on natural selection, the process that drives biological evolution [88]. The GA repeatedly modifies a population of individual solutions. At each step, the GA selects individuals at random from the current population to be parents and uses them to produce the children for the next generation. After continuous generations, it evolves toward an optimal solution.

The main procedures of our GA are as follows:

1. **Selection**

   This procedure is to select the individuals, namely, parents, which contribute the population to the next generation (see Figure 5-3). In this case, the algorithm will randomly generate a specific number of selected APs lists, then converts them to a binary vector (see Table 8), 1 means the AP is selected, 0 means this AP is not selected. Individual solutions are selected using a fitness function (in this case, the performance when using a validation dataset), where fitter solutions will have more chance to be selected.

Table 8 An example of selected AP lists

num	AP_1	AP_2	AP_3	⋯	⋯	⋯	AP_{n-2}	AP_{n-1}	AP_n
1	0	1	1	⋯	⋯	⋯	0	0	1
2	1	1	1	⋯	…	⋯	1	1	0
⋮	⋮	⋮	⋮	⋮	⋮	⋮	⋮	⋮	⋮
m	0	0	0	⋯	⋯	⋯	0	1	1

2. **Crossover**

   This procedure combines two parents to form children for the next generation. Based on the assumption that the good performance of positioning accuracy using KTCC is correlate with the specific sub-groups of AP rankings, which also makes GA a good fit for the ranking-based AP selection, as in the

crossover procedure (part of the AP lists will be switched, the Reproduce part shown in the above figure), the parents will change sub-groups (DNA segment) to achieve a better positioning performance in the new generation.

3. **Mutation**

   In this procedure, random changes will be applied to individual parents to form children, i.e., single segment randomly changed from 1 to 0 or 0 to 1 based on the mutation rate.

The design of the fitness function is the next design issue. There are two ways to build fitness functions. The first one is to use the results of IG, MI, IOD, or combined them together as the fitness function. However, as RSSI measurements were collected at each RP and TP 20 times, there is enough data to build both a validation and a test dataset. In this case, the performance of the validation dataset can be used as the fitness function.

5.2.1.4 AP Selection Based on Appearance Ratio

In the office testbed, a total of 106 APs were detected in a pre-recorded radio map. However, if all of those APs were used, it will not only increase the computational cost to estimate locations but also reduce the location estimation accuracy as some may be in places that are more susceptible to RF. For example, fingerprints are collected at each RP for 20 times (2 seconds active scanning each time，the same reason as mentioned in Section 3.5.1), not all APs can be detected at each time. If AP_a is detected once, this measurement is recorded, if not, a value, e.g., -100 will be filled (this is to keep the input uniform to the CNN model). In this case, if AP selection algorithms are directly used, those AP selection algorithms would select the missing APs identified with -100 values (dBm), which will decrease the accuracy.

To solve this, it is proposed to select the APs using the appearance ratio first (when this ratio is set to 90%, 67 APs are selected), then using the proposed AP selection algorithms on those selected APs. The idea of appearance ratio is simple, at each RP,

several scans are recorded, then based on appearance ratio (appearance times divided by total scanned times) to select APs at each RP, then all selected APs are combined, which is in order to mitigate the filling values.

5.2.2 RSSI Ranking based Location Fingerprinting using CNN

DNN models are usually categorised as supervised ML algorithms because the network approximates (classification) a target function (but it can be unsupervised, e.g., using autoencoder [89]). This algorithm optimise a loss function representing the difference between the network's outcome and the label of each sample. An activation function is used to define the output of each node that is fed further in the network. Different types of activation functions (e.g., relu, tanh [90]) and DNN model (e.g., CNN, Recurrent Neural Network - RNN) exist, with different performance results, according to the application domain. Figure 5-4 gives an example of deep neural network architecture.

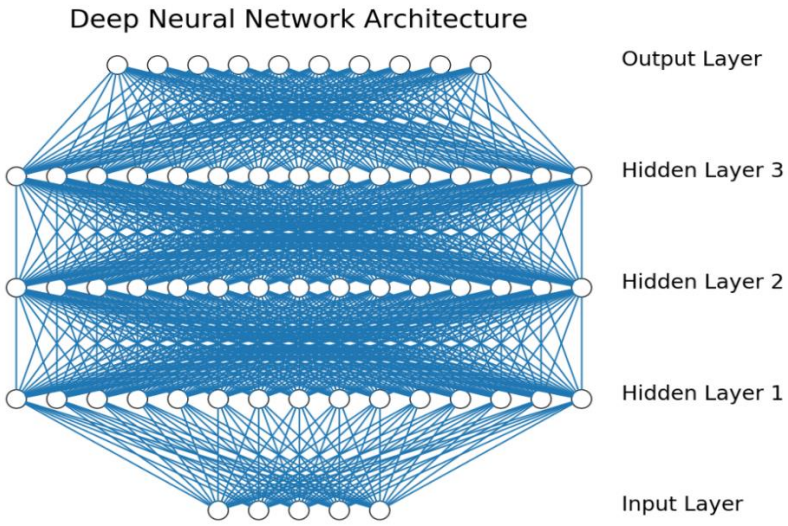

Figure 5-4 An example of a Deep Neural Network Architecture (The input layer with 5 inputs, 15 neurons in each hidden layer, 10 outputs in the output layer)

DNN models have been applied successfully to solve complicated issues, e.g., facial recognition, financial trading, driverless car, virtual personal assistants, and machine translation. CNN is one of the most successful models of DNN [89] – it is good at feature extraction. It has already been shown that the RSSI ranking-based location fingerprinting can mitigate against the RF receiver heterogeneity issue (see Section 3.4.2), which means the RSSI ranking relation between different APs could also help to match the data pattern, which means CNN can also be used to extract such a ranking feature. Hence, CNN was adopted to estimate locations in this thesis instead of using a simple deep neural network. Also, the use of regression with CNN could be used to estimated location (where outputs are directly estimated coordinates).

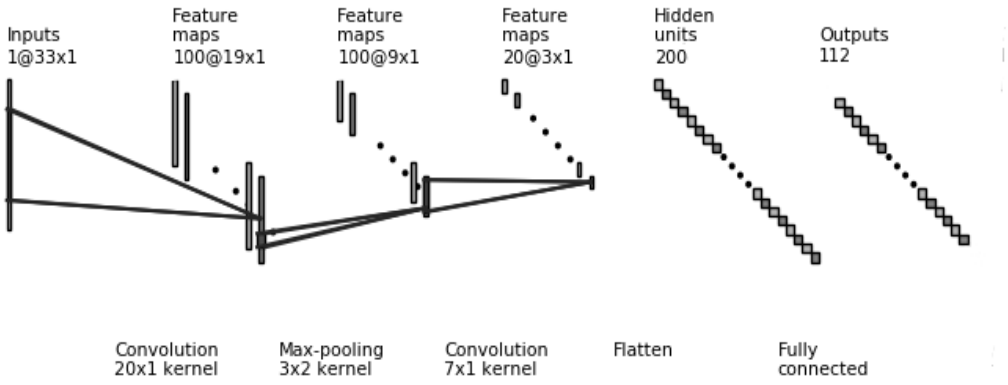

Figure 5-5 The architecture of our CNN Model (one example of using 33 RSSI ranking inputs, and 112 outputs (RPs))

Several IPS employ deep learning algorithms to estimate user location [91]. However, most of those methods just use raw RSSI measurements as the input data to train their positioning models, which does not consider the RF heterogeneity receiver impact and the consequent need to collect data from different smartphones. To mitigate against this hardware heterogeneity issue, RSSI ranking is used as our input.

For classification problems using deep neural network models, it is common to use a so called softmax layer at the top of the network. For example, given 3 possible classes,

the softmax layer has 3 nodes denoted by p_i, where $i = 1, 2, 3$. p_i specifies a discrete probability distribution, therefore, $\sum_i^3 p_i = 1$. Let h be the activation of the penultimate layer nodes (k), W is the weight connecting the penultimate layer to the softmax layer, the total input into a softmax layer, given by a, is

$$a_i = \sum_k h_k W_{ki} \tag{5.14}$$

$$p_i = \frac{\exp(a_i)}{\sum_{j=1}^{3} \exp(a_j)} \tag{5.15}$$

Then, the outputs of softmax layer p_i will be treated as the weight in WKNN to estimate the user location.

Figure 5-5 shows the architecture of the CNN model. Keras[9] (Tensorflow as a backend) was used to implement the CNN model. The model consisted of two 1D convolutional layers and one max-pooling layer. After the convolutional layer, the model has a fully connected layer that is used to connect to the Softmax layer. The outputs of the Softmax layer become the weights in the location determining phase.

For example, after using the GA-based AP selection algorithm, 33 APs are selected. Then, the model inputs are a ranking of these APs. After the hyper-parameters (e.g., layer number, learning rate), were tuned, the following structure was found to be effective. The first convolutional layer has a depth of 100 and a filter size of 15. The filter size of the pooling layer is 3 with a stride of 2, which will mitigate against the overfitting issue [92] of the model. The filter size of the convolution layer is 7, and the depth is 20. Next, the fully connected layer has 200 neurons, and tanh [90], as a popular activation choice, is used as the non-linearity function. Adam [93] as an adaptive optimisation algorithm was used as it does not need to set a fixed learning rate. In the end, the softmax layer is used to classify the test points.

[9] For more details: https://keras.io/. Last accessed in Sep/2018

5.2.3 Using Kalman Filters to Further Improve the Accuracy

Since the locations can be estimated using the already proposed location determination methods, a fusion algorithm (Kalman Filter/Extended Kalman Filter) can also be applied to further improve the positioning accuracy.

5.2.3.1 Kalman Filter

Kalman filter is an algorithm that uses a serial observed measurements over time, containing statistical noise and other inaccuracies, and produces estimates of unknown variables that tend to be more accurate than those based on a single measurement alone, by estimating a joint probability distribution over the variables for each timeframe [94], which is usually applied in control system and robot navigation. As in this research, a motion model and estimated locations could also be fused using such a filter to further increase the positioning accuracy, it was investigated.

There are two phases when applying a Kalman filter. Firstly, the Kalman filter produces estimates of the current state variables, along with their uncertainties. Once the outcome of the next measurement (necessarily corrupted with some amount of error, including random noise) is observed, these estimates are updated using a Kalman gain (weighted average), with more weight being given to estimates with a higher certainty. The algorithm is recursive, which only uses the present input measurements and the previously calculated state and its uncertainty matrix, no additional past information is required. Hence, the Kalman filter was adopted to increase the real-time positioning accuracy. In order to use the Kalman filter, a state vector needs to be defined for the moving target (user or robot) at time t as

$$\mathrm{o(t)} = \begin{bmatrix} p(t) \\ v(t) \end{bmatrix} \tag{5.16}$$

where $p(t) = [x, y]^T$ and $v(t) = \left[v_x(t), v_y(t), \right]^T$ in our scenario, which is also based on the assumption that the movement of the moving target is smooth, no abrupt changes happen, and the movement is approximately a uniform linear motion.

As the states of the user in a discrete-time way (sampling interval), the time interval between consecutive measurements is defined as δt. The notation of time t will change to k, indicating that $t = k * \delta t$. Thus, according to [94], to predict the position and velocity, the following five equations need to be calculated:

$$\hat{x}_k^- = A\hat{x}_{k-1} + Bu_{k-1} \tag{5.17}$$

$$P_k^- = AP_{k-1}A^T + Q \tag{5.18}$$

$$K_k = P_k^- H^T (HP_k^- H^T + R)^{-1} \tag{5.19}$$

$$\hat{x}_k = \hat{x}_k^- + K_k(z_k - H\hat{x}_k^-) \tag{5.20}$$

$$P_k = (1 - K_k H)P_k^- \tag{5.21}$$

where

- $\hat{x}_k^-$ is the state estimate, and $\hat{x}_k$ is the updated state estimate.
- A is the transfer matrix between states at consecutive time steps, which can be expressed as

$$A = \begin{bmatrix} 1 & 0 & \delta t & 0 \\ 0 & 1 & 0 & \delta t \\ 0 & 0 & 1 & 0 \\ 0 & 0 & 0 & 1 \end{bmatrix} \tag{5.22}$$

- B is the control-input model which is applied to the control vector u_k, since there is no control-input, $u_k = 0$.
- P_k^- is the estimated covariance matrix of time step k based on the output of time step k-1.
- Q is the covariance matrix of the Gaussian noise for the process of getting the a priori estimation from the transfer matrix A and R is the covariance matrix of the Gaussian noise in the measurements of the moving target's states. In

practice, Q and R might change with each time step or measurement, but it is just assumed that they are constant [95].

- K_k is the Kalman gain which describes the influence of the measurement on the final posterior estimation.
- z_k is the measurement of the moving target's position, H is the observation matrix, in practice, H might also change with each time step or measurement, but it is assumed that they are constant. H in this case is defined as:

$$\mathrm{H} = \begin{bmatrix} 1 & 0 & 0 & 0 \\ 0 & 1 & 0 & 0 \end{bmatrix} \tag{5.23}$$

5.2.3.2 Extended Kalman Filter

Although Kalman Filtering has been applied in a wide range of areas and has achieved significant success, its implementation has a constraint that the dynamic system must be linear. However, this condition is hard to satisfy since some dynamic systems in the real world may be more complicated and hence cannot be summarised with a linear function. Hence, the Extended Kalman Filter (EKF) as an extension of the Kalman Filter has been developed for such a nonlinear system [96].

EKF is able to estimate and update the states of a nonlinear system by linearising it with the help of a first-order Taylor-expansion. In other words, when predicting the state in the next time step using a state transition function, instead of finding the transfer matrix, it is found that the partial derivatives of the state transition function and observation function, represented by a Jacobian matrix. In contrast to KF, the state o(t) for EKF is defined as

$$\mathrm{o(t)} = \begin{bmatrix} p(t) \\ vel(t) \\ \theta(t) \end{bmatrix} \tag{5.24}$$

where $p(t)$ is the same as for KF, $vel(t)$ differs from KF's $v(t)$; in equation (5.24), it's a scalar indicating the speed of the moving target; $\theta(t)$ represents the

heading orientation of the moving target. So, the new state transition equations for each parameter in the state $\mathrm{o(t)}$ in the 2D scenario will be (update location):

$$\mathrm{x(t)} = \mathrm{x(t-1)} + \mathrm{vel(t-1)} * \sin(\theta(\mathrm{t-1}))* \delta\mathrm{t} \tag{5.25}$$

$$\mathrm{y(t)} = \mathrm{y(t-1)} + \mathrm{vel(t-1)} * \cos(\theta(\mathrm{t-1}))* \delta\mathrm{t} \tag{5.26}$$

$$vel(t) = vel(t-1) \tag{5.27}$$

$$\theta(t) = \theta(t-1) \tag{5.28}$$

which make the system non-linear. By finding a matrix of partial derivatives of the four above equations, the linearised model of the system can be derived [96] to estimate or update the states of the moving target.

5.3 WiFi Location Fingerprinting-based ADL Recognition

Location fingerprinting for WiFi, just as for BLE, typically works in two phases, which is shown in Figure 3-4. A radio map is established in an offline phase where the RSSI signals from multiple APs are collected and mapped to known locations. Then a matching process against the radio map is conducted in an on-line phase. The accuracy of traditional location fingerprinting methods which employ a single-point to match with the radio map is about 2 – 3 m. In contrast, the research in [97] proposed a path-based (or profile-based) method assisted with using sequential MF measurements to improve navigation accuracy increases by up to 11.5-21.6% compared to using single-point matching. Khuong, et al, [67] proposed to use sequential MF measurements to predict daily routes to increase the positioning accuracy. However, most researchers tend to overlook the use of the sequential WiFi measurements, which could offer more data than using MF measurements. Hence, one objective of this thesis is to investigate the feasibility of using sequential WiFi RSSI measurements for location-driven ADL recognition.

5.3.1 Activity Recognition using Path Fingerprints

In this research, the aim is to recognise coarse-grained ADLs using a WiFi fingerprint matching method (as it can offer more measurements compare to MF measurements) to determine a location that is mapped to, or linked to an ADL. Since trajectories of human mobility contain the cue to infer ADLs, path matching can help us to find the closest trained path as well as its corresponding activity. Unlike using location fingerprinting methods to localise a single-point location, which is mentioned in Section 3.4, the path-based matching method uses RSSI ranking vectors from multiple historical points to match the routine database. Assume L is a path with a set of locations, $L = \{l_1, l_2, \cdots, l_i, \cdots, l_n\}$, used as a trajectory of human mobility, where n points are used to represent the path. At the training stage, RSSI ranking vectors (represented by using the MAC address), i.e., $R_i = \{MAC_1, MAC_2, \cdots, MAC_m\}$ will be collected at each point l_i along the predefined path L, where m is the number of detected APs. Then the coordinates of these points $l_i \in L$ as well as their RSSI ranking vectors will be sorted by a set order (i.e., heading direction) and will be saved as a path fingerprint (i.e.,$L_j = \{[pos_1,\ R_1], [pos_2, R_2], \cdots, [pos_i, R_i], \cdots, [pos_n, R_n]\}$, where pos_i is the corresponding ground truth or estimated coordinates). Many path fingerprints such as this constitute the path database. For the online or operational stage, suppose a user has already walked several steps, therefore, the new trajectory can be represented by $L_{new} = \{l'_1, l'_2, \cdots, l'_k\}$ with a k length, and l'_k stands for the current (last) location. The corresponding RSSI ranking vectors of L_{new} are $\{R'_1, R'_2, \cdots, R'_K\}$. The matching process is to find the closest paths in the route database. Since the lengths of different paths are usually different, MD-DTW [98] is employed to calculate the distance (in this case, ED or KTCC) between them. Then, the closest predefined path will be considered as the corresponding activity.

5.3.2 Multi-Dimensional Dynamic Time Warping

Dynamic Time Warping (DTW) is a well-known algorithm to evaluate the comparison between two-time series with different lengths [99]. This is used to help recognise

specific defined ADLs. Suppose two time-series P and Q, ($P = p_1, p_2, \dots p_i, \dots p_n, Q = q_1, q_2, \dots, q_j, q_m$). To align these, a matrix can be established. Each element of the matrix stands for the distance (typically the ED, but in this case, KTCC is used) between $p_i \; and \; q_j$. The main target of DTW is to find the warping path W ($W = w_1, w_2, \dots w_k, \dots w_K$). As shown in Figure 5-6, W starts from w_1 and ends at w_K ($\max(n, m) < K < m + n - 1$). Then the path direction only has three cases at each w_k. The step length is restricted to the warping path to adjacent cells. The distance between P and Q is $\frac{1}{K}\sum_1^K W_k$.

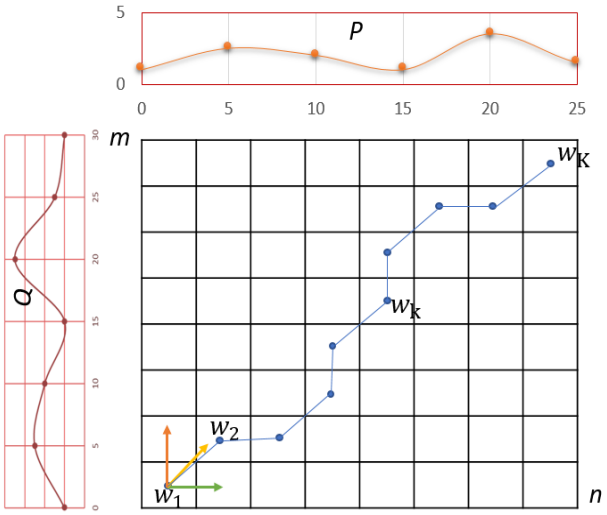

Figure 5-6 An example of the warping path

This ordinary DTW can effectively classify two time-series from a single source. However, in many cases, signals have multi-dimensions and will be employed at the same time, which can be used to better align two time-series for a single measurement dimension. Therefore, [98] proposed an improved MD-DTW method which was used in gesture recognition by a camera. Assume P^S and Q^S are two time-series S-dimension features, i.e., $P^S = p_1^S, p_2^S, \dots p_i^S, \dots, p_n^S$, $Q^S = q_1^S, q_2^S, \dots q_j^S, \dots, q_m^S$. Then the elements of distance matrix turn $Dis_{n,m} = \sum_{s=1}^{S}(p_i^S - q_j^S)^2$. Considering the range difference of S-dimension feature values, normalising each dimension of feature values can effectively remove the difference. Usually, each dimension of feature values are separately standardised to a zero mean and unit variance.

Compared to the location path (the path of the ground truth or the estimated locations using location fingerprinting methods) matching scheme, ranking-based matching adds a process of RSSI to rank MAC address vectors from multiple points. Hence, fused matching can be implemented by using two different variables, locations and sorted RSSI ranking MAC address vectors.

Their feature matrix F_{Pos} and F_R are denoted as below.

$$F_{Pos} = \begin{bmatrix} x_{l_1} & y_{l_1} \\ x_{l_2} & x_{l_2} \\ \vdots & \vdots \\ x_{l_q} & x_{l_q} \end{bmatrix} F_R = \begin{bmatrix} MAC_{l_1}^1 & MAC_{l_1}^2 & \cdots & MAC_{l_1}^N \\ MAC_{l_2}^1 & MAC_{l_2}^2 & \cdots & MAC_{l_2}^N \\ \vdots & \vdots & \vdots & \vdots \\ MAC_{l_q}^1 & MAC_{l_q}^2 & \dots & MAC_{l_q}^N \end{bmatrix} \tag{5.29}$$

The x_l and y_l are the estimated locations, instead of the ground truth locations. Based upon a pre-experiment, by using estimated locations, a higher recognition accuracy (increased by about 20%) can be achieved with respect to using the ground truth locations. It is postulated that the bias of estimated location could also help to increase the recognition accuracy, namely, the designed path matching accuracy.

A single feature sequence has been used for path matching [97, 100]. However, there is no work that fuses these two feature sequences for path matching, since multiple feature sequence fusion could provide more information compared to a single feature to increase the accuracy of path matching. What's more, the fusion method can also be extended into scenarios with multi-source information. For example, smartphones can collect signals not only from WiFi, but other sensors such as magnetic field F_{MF} and BLE. Therefore, the multi-source fusion feature matrix can be denoted by F_F (5.30). In this case, by only fusing F_{Pos} and F_R can be viewed as a good test for path matching by using multi-source features.

$$F_F = \begin{bmatrix} F_{Pos}^1 & F_R^1 & F_{MF}^1 & \dots \\ F_{Pos}^2 & F_R^2 & F_{MF}^2 & \cdots \\ \vdots & \vdots & \vdots & \\ F_{Pos}^q & F_R^q & F_{MF}^q & \cdots \end{bmatrix} \tag{5.30}$$

The fusion process is as follows. Firstly, as the range of KTCC results is from 0 to 1, instead of standardising each type measurement, I normalised the distance between the estimated coordinates, which min-max normalisation can map the distance values to the range of 0 to 1 to and make each type of result be within the same scale. Equation (5.31) shows the normalised the distance $(\tilde{z})$. Then, in the phase of path matching, MD-DTW (uses sum of the distances of each type measurements as a new distance) is utilised to find the best match. In this case, to recognise the trajectory of human mobility, it needs to find the path which minimises the distance between the current path and the pre-trained path (i.e., $\mathrm{MD-DTW} = \mathrm{argmin}\{\frac{1}{K}\sum_1^K \mathrm{W}_k^S\}$).

$$\tilde{z} = \frac{z - \min(z)}{\max(z) - \min(z)} \tag{5.31}$$

where z equals to $sqrt\left(\left(x_i - x_j\right)^2 + \left(y_i - y_j\right)^2\right)$, this is the ED of two-dimensional coordinates. i and j represent different index of estimated coordinates.

5.4 Study 3-a and 3-b: WiFi Location Fingerprinting and ADL Recognition Evaluation

5.4.1 WiFi Location Fingerprinting Positioning Performance

5.4.1.1 PhD Office Testbed Setup

A field experiment was conducted in a 13.0 m × 30.0 m QMUL PhD office. The training dataset was collected using smartphone1 (LG Nexus5)[10]; validation and test datasets were collected from both smartphone1 and smartphone3 (BlackView #1)[11].

[10] For more details: http://www.lg.com/uk/mobile-phones/lg-D821. Last accessed in Sep/2018

[11] For more details: http://www.blackview.hk/blackview-78/. Last accessed in Sep/2018

Figure 5-7 The 3D layout of the PhD office

Over 106 APs (106 different MAC addresses) were detected during the training data collection procedure. it is postulated some of them are dummy ones, as they have similar signal strength, and only three physical WiFi routers can be seen in this office. Hence, this is also another reason why the use AP selection algorithms is beneficial. Figure 5-7 shows the layout of the office; Figure 5-8 shows the coverage of the WiFi APs of the PhD office. The colour bar in the right part means the number of APs and its corresponding colour.

Figure 5-8 The coverage of the WiFi APs of the PhD office

At each RP, the varying RSSI measurements (and hence varying AP ranking) was collected for 20 times, with a 2 second scanning period each time using an active scanning mode. It should be noticed that it is true that the more time that is spent to collect measurements, the more accurate the data distribution that is acquired in turn, leading to a more accurate positioning accuracy. However, as a trade-off to promote more rapid radio map construction, measurements for 40 seconds at each RP was collected.

Then these 2 seconds scan measurements were integrated into a RSSI or its ranking vector by using averaging or a total probability comparison, which can maximally avoid the filling values, as if one AP was not detected, a value -100 will be filled in the experiment, as our methods require a uniform input (as shown in Figure 5-8, not every AP can be scanned at each RP or TP). Hence at each RP, it has 20 RSSIs or its ranking vectors.

The 112 blue RPs shown in Figure 5-9 are the training dataset, which is used to train our positioning models; positioning accuracy of validation and test dataset is evaluated by using the rest 70 red TPs. RSSI measurements were collected at TPs at different times, a total 20 times. The RSSI of each AP or the moving pattern of persons in the office may be slightly different so the robustness of the system needs to be tested. Half of the collected TP measurements will be treated as a positioning validation dataset, and the rest dataset will be treated as a positioning test dataset for the GA-based AP selection algorithm.

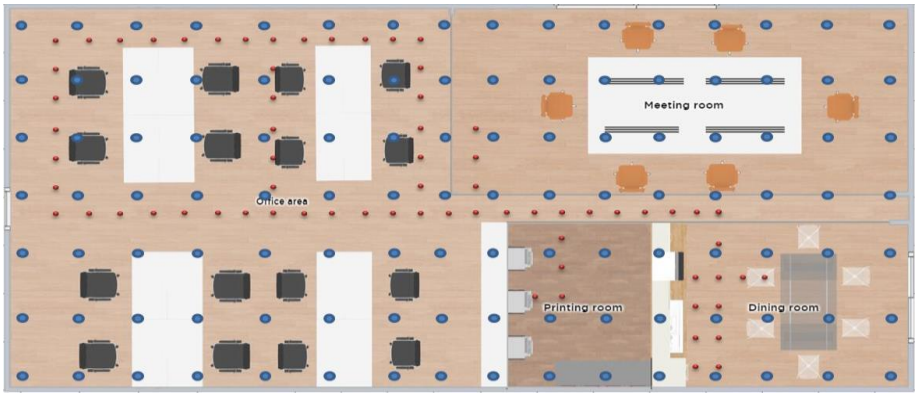

Figure 5-9 The office testbed and its RPs and TPs layout

Figure 5-9 also shows the 2D layout of the office. The blue dots are RPs, which are 1m apart. The red dots are TPs, the distance between each TP is 0.5m. This training dataset (RP) was collected over the night with no people around using our fingerprints collection UAV with a 1m hovering height, which is shown in Figure 5-10. Validation and test datasets are collected by the author manually holding the phone at a 1m height.

Figure 5-10 The office WiFi fingerprint collection drone (UAV)

Figure 5-10 shows the fingerprint collection UAV. As yet, it is still a prototype, which cannot be used to collect and update the radio map automatically. The data was collected point by point by manually controlled the UAV. A fully automatic UAV will be part of future work to help collect and update the radio map (see Section 7.2.1.1).

5.4.1.2 WiFi Location Fingerprinting Positioning Performance

In the office testbed pre-experiment, two different types of radio map were used; one used averaged RSSI at each RP, which makes a relatively stable feature of each RP, another type used multiple scan measurements, which maintains the data diversity

(distribution). Then, repeated estimating locations were undertaken by changing the parameter K in WKNN. Figure 5-11 shows that the accuracy (averaged positioning accuracy, the unit is m) is related to the k. So, k with the best performance of using validation dataset can be investigated to increase the positioning accuracy. However, k = 4 is chosen for the rest experiments, as it is a huge computational burden to iterate all the k numbers. The best performances of KTCC, KTCC (using a total probability comparison, see Section 3.4.2.2), ED, and ED (using averaged RSSI measurements) are 2.57 m (k = 8), 3.74 m (k = 84), 2.44 m (k = 23), and 2.18 m (k = 32), respectively. This also shows ED with averaged RSSI performs better than using multiple scan measurements. KTCC using ranking fingerprints based on a total probability comparison, performs worse than KTCC using multiple scan measurements. This may cause KTCC to became sensitive to a varying RSSI, which causes a varying RSSI ranking. The focus here is on ranking-based RSSI AP selection algorithms. So, in the following experiments, the multiple measurements radio map will be used for our proposed ranking methods. Moreover, it can offer more training data to train our CNN models.

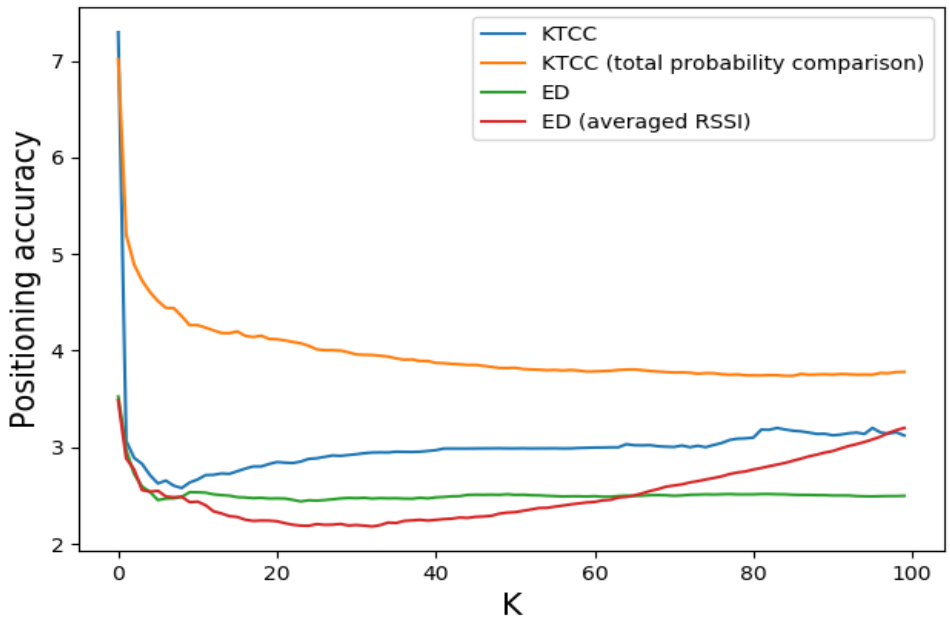

Figure 5-11 The positioning accuracy using different Ks in WKNN

Furthermore, the best positioning performances of above methods (same order) using a total of 106 APs are 2.91m, 3.84m, 2.77m, and 2.51m, which by using an appearance ratio method (67 APs are selected from all 106 APs using appearance ratio) only, the positioning accuracy increased by 11.6%, 2.6%, 11.9%, and 13.1%, respectively. By using appearance ratio 39 APs (36.8% of the total AP amount) can be deleted.

Next, three AP selection algorithms, SD, IG and MI (see Section 5.2.1) were employed to act as baseline algorithms to compare with this proposed IOD algorithm. Figure 5-12 shows the positioning accuracy of the four algorithms. IOD in the magenta colour shows the best performance compared to the other algorithms when the number of APs is 21 or more. Moreover, the best positioning accuracy is 2.13 m for the IOD appears when using 37 APs, whose positioning accuracy is 12.6%, 18.0%, and 24.1% higher than using IG, MI, and SD, respectively. Starting at 27 APs, all those algorithms tend to be stable, and the gap between them is reducing, which means they have a similar positioning accuracy.

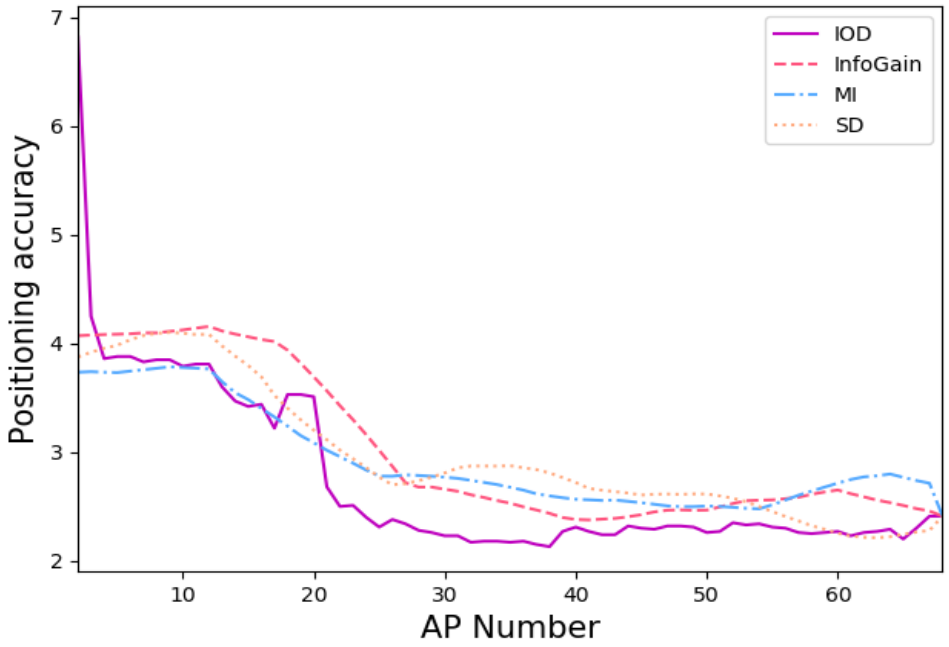

Figure 5-12 The location accuracy of four AP selection algorithms IOD, InfoGain, MI and SD with respect to the number of APs used

Based on the results, it is concluded that using an AP selection algorithm will not only reduce the computational cost but also increase the positioning accuracy. The proposed IOD AP selection algorithm performs better than using IG and MI, but PCA performs better than our IOD method based on the results shown in Figure 5-13. However, PCA is not a 'real' AP selection algorithm as it needs to calculate PCs after each scan, which has a higher computational cost than using AP selection algorithms when doing online positioning. The PCA method will be treated as the baseline positioning method to compare with our ranking-based methods. As the best positioning accuracy of PCA is 2.01 m (black dashed line), which is higher than the best positioning accuracy of our IOD algorithm (2.13 m) when using 37 APs and when using only 2-dimensional converted coordinates.

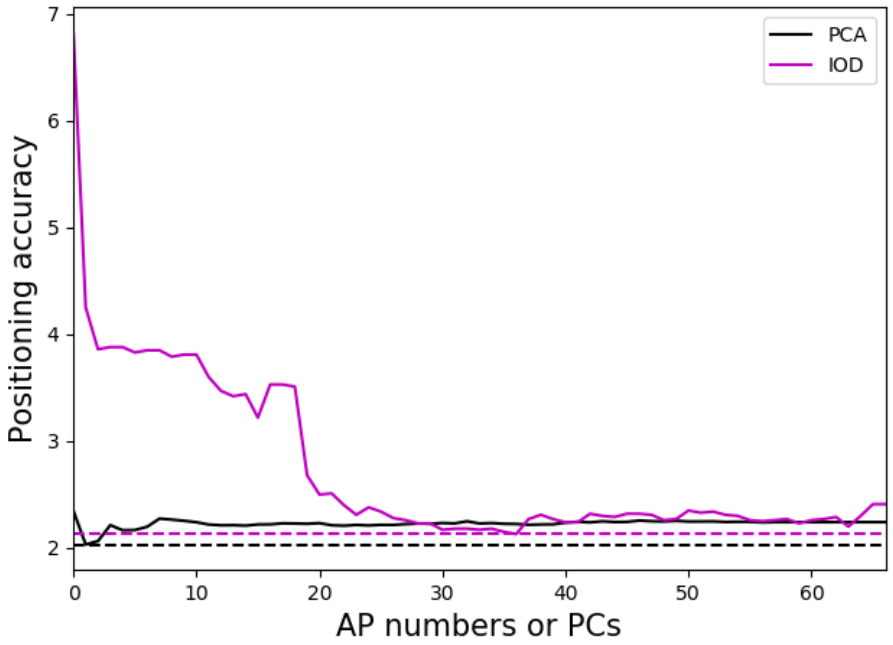

Figure 5-13 Performances of using IOD and PCA

However, those AP selection algorithms (IOD, IG, MI, PCA) are not designed for RSSI ranking-based AP selection. To solve this, the GA-based algorithm was proposed to select APs, which can directly find the optimal AP list, instead of iterating the number of all APs to find the optimal APs for each specified number. Figure 5-14 shows the performance relation between using the validation dataset and test dataset. Tthe best performance of using the validation dataset will be used to select APs. It also

shows the improved accuracy when using the proposed GA, as its positioning accuracy converges after 28 training epochs to 1.92 m. Then, the selected AP list (33 APs) will be used for the KTCC and CNN methods.

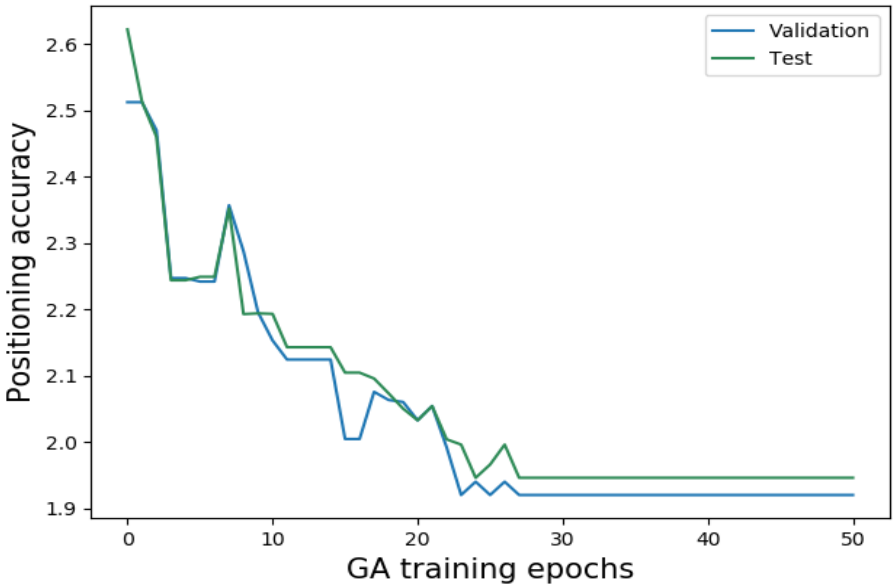

Figure 5-14 Improved positioning accuracy using GA

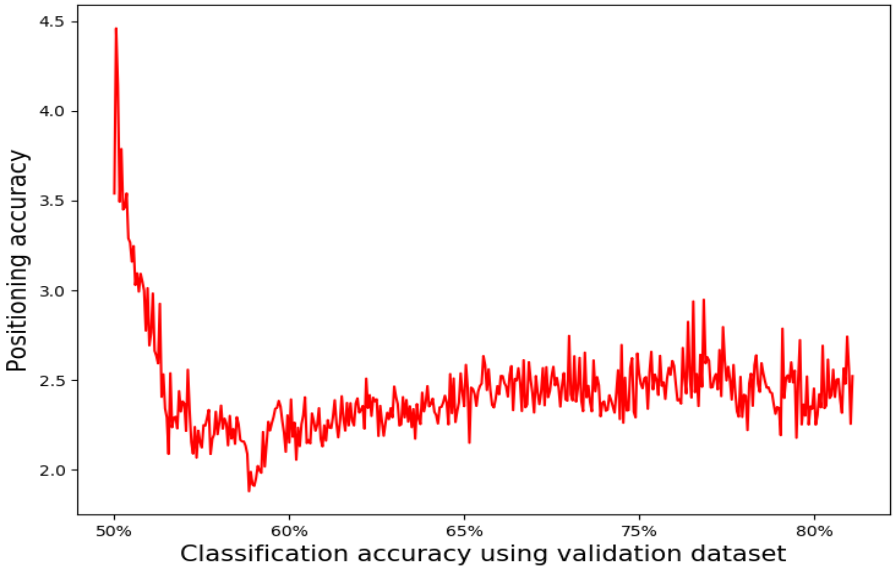

Figure 5-15 Improved positioning accuracy using CNN

Figure 5-15 shows the performance of using our CNN model with GA selected APs. It also shows with more the training, the positioning accuracy increased, then decreased, which means that this relates to how 'accurate' the model was trained. The best positioning accuracy achieved to 1.88 m, where the corresponding classification accuracy is 57%. It is not so simple that the higher classification accuracy the higher positioning accuracy becomes. This may also be caused by an insufficient collected fingerprints in radio map. An 'overtrained' model could also cause a decreased positioning accuracy, which means a balance between classification accuracy and positioning accuracy needs to be observed. This similar positioning accuracy also means that fewer hyper-parameters tuning needed traditional algorithm (e.g., using WKNN, only k is needed to be tuned) has the ability to compete with the state-of-art neural network in the field of IPS. However, it is possible to achieve a higher positioning accuracy by tuning the hyperparameters of neural networks with more training data. So, methods can be chosen based upon the requirements. In this experiment, KTCC was used to do the rest experiments, because of its simplicity.

Both KTCC and CNN-based methods perform 3.5% and 6.4% better than the PCA baseline method, whose accuracy is 2.01m.

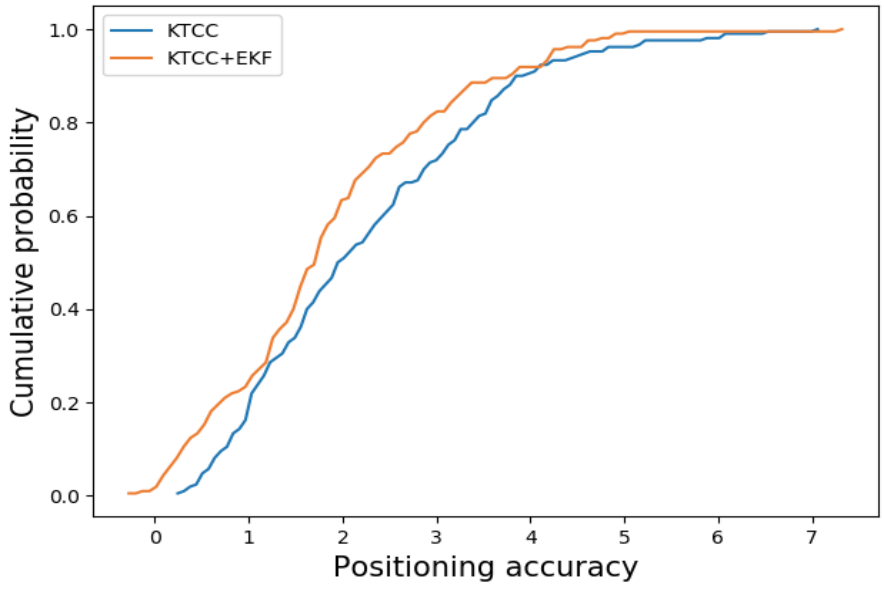

Figure 5-16 Improved positioning accuracy using EKF is combined with KTCC

As measurements are collected from several designed paths, the EKF model can be deployed to increase the positioning accuracy by using a uniform motion model. The positioning accuracy increased from 1.94 m to 1.42 m, when the EKF was applied. Figure 5-16 shows the improved positioning accuracy using EKF.

To test our proposed RSSI ranking location fingerprinting method using KTCC again (the first experiment, see Section 3.5.2), a repeat experiment was carried out in the Lab testbed. Figure 5-17 shows that for the using a different phone (BlackView #1), the proposed method (averaged positioning accuracy 2.42 m, 90% in 4.52 m) performs better than using the ED method (3.18 m, 90% in 4.51 m), which also proves that our ranking method is more robust and mitigates the RF receiver heterogeneity issue.

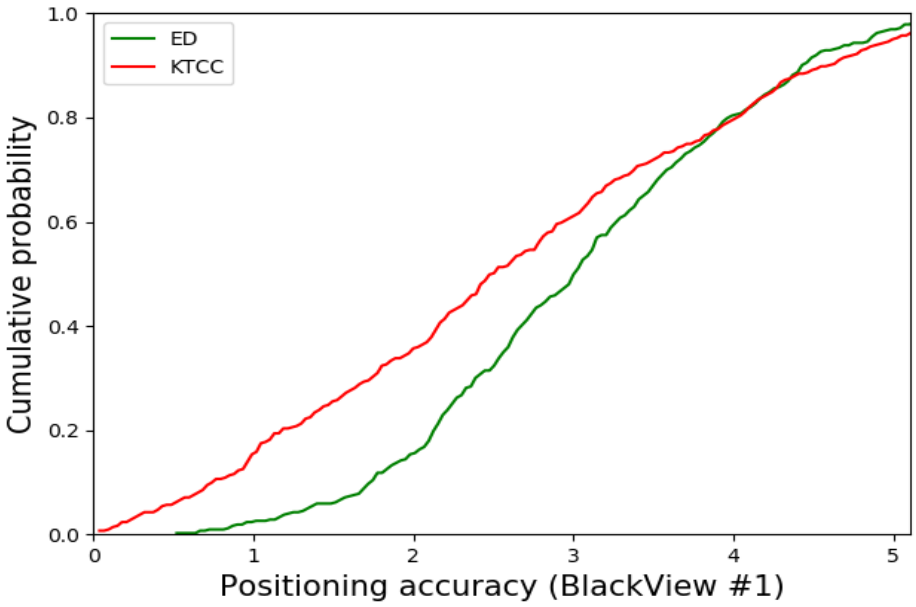

Figure 5-17 Accuracy comparison using a different phone

5.4.2 WiFi ADL Recognition Performance

9 specific activities (detailed trajectories see Appendix B)have been identified which can be inferred from analysing the moving paths of the user. The 9 activities are listed in Table 9. These activities are divided into two classes based upon the region in which the activities occur. It can also be considered that it relies on the different length of the

paths to categorise activities (it is assumed that the more different measurements, the more easily it can be matched).

Table 9 List of Class A and B activities

Classes	Task ID	Activities	Path
Class A	1-3	Leave the office	From user desk to exit
	4-6	Have a meeting	From user desk to meeting room
	7-9	Print documents	From user desk to printing room
	10-12	Go to kitchen	From user desk to kitchen
Class B	13	Eat food	From microwave to dinner table
	14	Make tea	From fridge to kettle
	15	Drink tea	From kettle to dinner table
	16	Heat food	From firdge to microwave
	17	Have a drink	From fridge to dinner table

Figure 5-18 Overview of Class A (office) ADL

Figure 5-19 Overview of Class B (kitchen) ADL

The activities within the Class A that have the longer paths mainly refer to the user mobility from the office area (detailed location is user's desk) to other areas (outside of the office, printing room, meeting room and kitchen) which are shown in Figure 5-18. The Class B activities with shorter paths (fewer steps) reflect user mobility within the kitchen which are shown in Figure 5-19.

Since the activity recognition accuracy is related to the path length (the path length can be presented by a number of sequential fixed points in that path, i.e., the number of rows, the q in F_c and F_R) and dimension of feature matrix, these two classes activities can constitute a comparative test for the effect of path length on recognition accuracy. As shown in Figure 5-18, the starting point of activities is the user desk (purple pentagram). User can walk from desk to the aisle along the green line, blue line and red line. Thus, if a user wants to move to the printing room, he can go to the aisle firstly following three different lines and then goes to the printing room from the aisle. This means the printing activity has 3 paths and so do the activities of leaving the office, having a meeting and going to the kitchen. There are 12 paths in all for Class A activities.

As for the activities in the kitchen shown in Figure 5-19, each activity refers to a line in a different colour (make tea - red line; heat food - blue line; drink tea - yellow line; eat food - pink line; have a drink - green line). Compared to the paths shown in Class A, the paths in shown in Class B (inside a kitchen) is finer. For each activity in Class B, only 1 path was chosen for each activity to test the performance of the method (as it is short and has no alternative paths). Hence, for Class B, there are 5 paths in total. During the experiment, it is repeatedly collected activities for 20 times so that there were (12+5)*20 = 340 paths.

Table 10 WiFi location-driven activity recognition accuracy (as a %)

Percent	**Single Dimension DTW**			**Fusion MD DTW**		
	C1	***C2***	***mix***	***C1***	***C2***	***mix***
Estimated location	44.6	30.0	40.3	--	--	--
Ranking Vectors	77.9	62.0	73.2	--	--	--
Fused Vectors	--	--	--	79.8	76.0	79.5

Table 10 shows the activity recognition accuracy when using a single input data dimension (it only uses sequential estimated locations or ranking vectors) method and fusion (uses both estimated locations and ranking vectors) method. C1 stands for the class A activities, C2 stands for class B activities, and mix stands for the total C1 and C2 activities. From the results, it can be seen that the recognition accuracy of C1 is better than that of C2 which indicates that the activities with shorter paths are harder to be recognised than the activities with longer paths. This can also explain the degradation of recognition accuracy for the mixed set compared to that of C1. This also means that the longer path, the higher recognition accuracy.

Moreover, the proposed fusion MD-DTW performs the best recognition accuracy compare to the single dimension-based method; the Class of C1, C2 and the mix recognition accuracy of the fusion-based method is improved 78.9 % (C1 estimated location) and 2.4 % (C1 ranking), 153.3 % (C2 estimated location) and 22.5 % (C2

ranking), and 97.3 % (mix estimated) and 8.6 % (mix ranking) compared to estimated location and ranking vector-based single dimension methods respectively. It also means ranking-based fingerprints can do more than just localisation; it can also be explored to recognise ADLs.

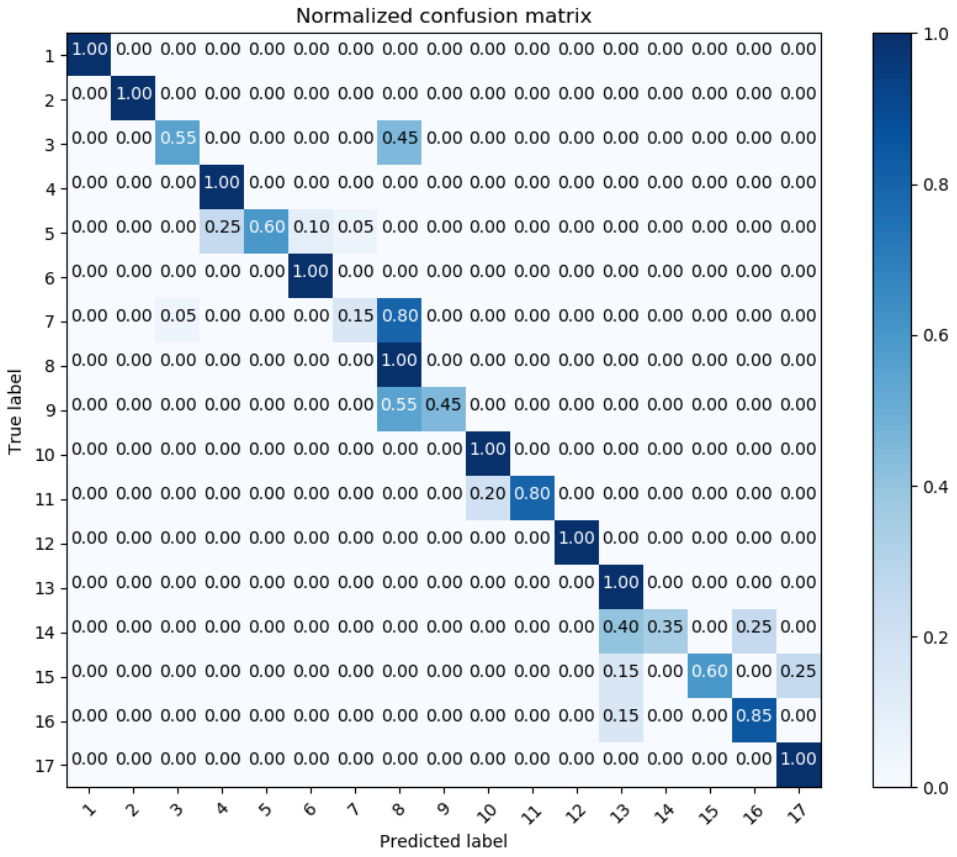

Figure 5-20 Confusion matrix of the recognition results

Figure 5-20 Confusion matrix of the recognition results give the confusion matrix for using the proposed method to recognise the designed activities. The worst performance (15%) is to recognise the print document activity (80% data are wrongly recognised to activity 8 – the same type activity as 7, but a different path). However, it is acceptable as the final output still will be the print document activity. The reason of this is the path 7 and 8 share a lot of common points (step or distance) and the same start point and end point, which make them hard to discriminate. This also happens to path 3 and path 7, path 14 and path 16, and path 15 and path 17. However, it is found that if the

paths have more than 4 different steps (2 m), the recognition accuracies of most paths become 100%, which means it has a high probability to discriminate paths with a 2 m (distance) difference.

However, it is not simply related to the distance, a more detailed relation between steps (distance) and the number of common steps and recognition accuracy will be considered in the future (see Section 7.2.1.1).

5.5 Summary

In this chapter, RSSI ranking location fingerprinting methods were repeatedly tested and validated in an office environment using WiFi RSSI along with AP selection and EKF algorithms. Such algorithms could not only reduce the computation cost but also increase the positioning accuracy.

Moreover, such RSSI ranking is also used to recognise ADLs using MD-DTW. However, the results show that this kind of recognition method faces the following challenges (they are also the reasons that I have explored the 2D Lidar-based recognition system):

1. The user needs to carry sensors (smartphone) all the time, if not, a user's movement cannot be tracked.

2. There is a need to accurately determine the start and end points for the ADL, as it affects the ADL recognition accuracy.

3. The recognition accuracy of a short ADL path seems inadequate.

Hence, the next chapter will introduce a far more accurate 2D Lidar positioning system and its ADL recognition method.

6 2D Lidar Positioning and ADL Recognition

6.1 Introduction

The final study is to investigate the use of off-body, light-based sensors to investigation determine the location of users, accurately and hence to determine location determination ADLs. Light detection and ranging, Lidar, also referred to as LiDAR, LADAR or LIDAR, uses pulsed laser light to measure the TOF reflected pulses with a sensor. Until recently, towards the end of this PhD, Lidar devices were quite costly to purchase and investigate prior to this. It is postulated that the rise of autonomous vehicles, was part a driver for a greater production and a lower cost for Lidar devices. The motivation for investigating this additional technique is twofold: first, as stated in the introduction and survey, Lidar offers greater accuracy than some common, current mainstream IPS techniques based upon RF RSSI and MF. Second, many IPS techniques require participants to carry on body devices, e.g., smartphones, - humans are not device free in order to receive IPS signals. Although in the current information age, mobile devices are on the increase, an issue is humans get older; seniors can simply forget or may not be able to attach physically and to carry their location transceiver devices (see Section 2.3.2). Hence, the final IPS is in contrast to the ones investigated so far, an off-body device-free technique – Lidar. There are a range of Lidar devices that could be used for location determination and location determination ADL recognition, such as flash Lidars that only face in a single direction (1D), line scanning sensors that sweep a beam across a scene, taking measurements along a single (2D) plane and 3D Lidar [59]. Both 2D and 3D Lidar devices can be designed to rotate 360 degrees to pulse laser light.

The primary application of Lidar is for mobile unmanned vehicles and robots to track objects around them as they move and to support collisions avoidance. *To the best of my knowledge, no work has looked at using off-body low-cost (2D rather than 3D) Lidar devices to recognise ADLs.* There are two main reasons that 3D Lidar is not used to recognise ADLs. First, the higher cost of 3D Lidar prohibits the deployment in our scenarios; Second, 3D Lidar can also offer more fine-grained 3D point cloud

information, which may also jeopardise user's privacy (the visualisation of 3D Lidar measurements are similar to camera videos). Next, an innovative method is introduced for recognising daily activities using a sequence to sequence model [101] to analyse location data from a 2D Lidar measurement.

6.2 2D Lidar Off-body Positioning

6.2.1 2D Lidar Measurement Collection based upon Hausdorff Distance

A low cost, 2D, rotating Lidar system called RPLIDAR (version A1) from Slamtech[12] was used and configured to continuously scan a physical space until the user switches it off. 2D Lidar is height sensitive to what it can detect. A good height for horizontal pulses is to hit the upper mobile host, e.g., human torso, and to have a direct line of sight to all the indoor landmarks of interest, else the ADLs at these landmarks will be missed. Lidar uses a type of laser to emit the light pulses to detect distance. This is a Category 1 laser[13], the safest category, which cannot emit levels of optical radiation above the exposure limits for the human eye under any exposure conditions.

For many location-driven ADLs, there is often no mobile host presence in a space for much of the day, e.g., for residential rooms such as a kitchen, there is often no user presence for much of the day. Hence, much of the recorded measurements contain no user activities leading to a massive, largely redundant positioning dataset. Hence, to solve this problem, a threshold based on Hausdorff distance [102] is used, which measures how far two subsets of a metric space are from each other representing two time sequential scans. Hence, it can be used to detect the presence of a user.

---

[12] Available from https://www.slamtec.com/en/Lidar/A1.

[13] IEC-60825-1: Safety of laser products International Electrotechnical Commission. Edition 1.2, August 2001

First, the raw Lidar radial distance and angle measurements will be converted to Cartesian coordinates. The position of Lidar is denoted by the origin point $(0,0)$. Then the Hausdorff distance between two different scans I and J is calculated. The Hausdorff distance between Lidar scans I and J is defined as:

$$H_d(I,J) = \max\{sup_{i\in I} inf_{j\in J} d(i,j), sup_{j\in J} inf_{i\in I} d(i,j)\} \quad (6.1)$$

where sup represents the supremum, and inf represents infimum. $d(i,j)$ means the ED between a point i in the scan I and point j in scan J.

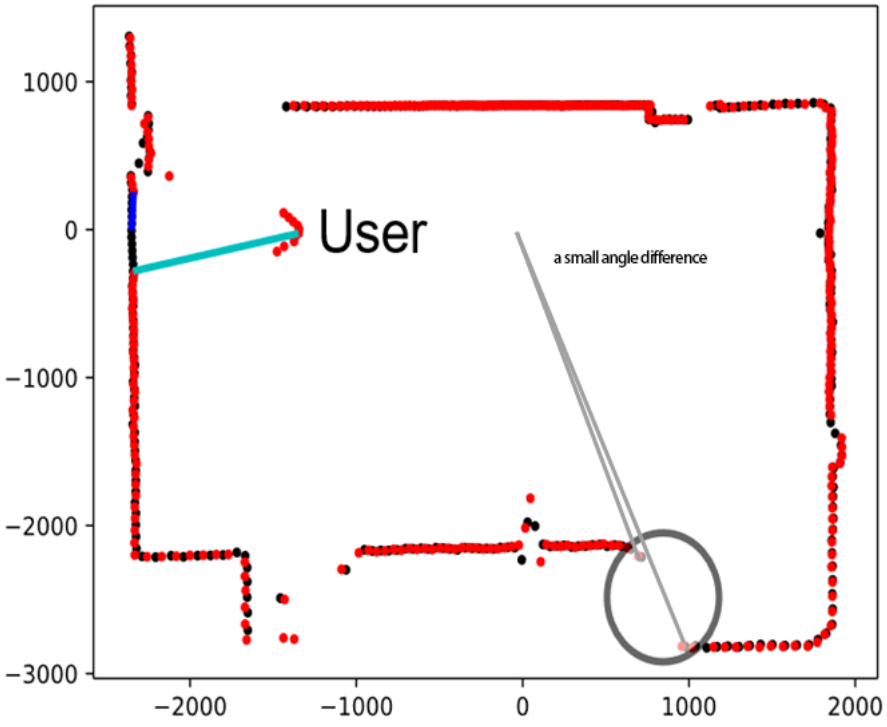

Figure 6-1 How the Hausdorff distance works (in millimeters)

The origin point (0,0) is where the Lidar is located, and the distance measurement unit is millimetres. The black points are from a scan (e.g., scan 1), without any moving objects. The red points are from a scan (scan 27) where a user walks into the kitchen. Mobile host movement causes the blue lines, which is shown in Figure 6-1. The length

of the light blue line means $sup_{x \in X} inf_{y \in Y} d(scan27, scan1)$, which is also the directed (or forward) Hausdorff distance between scan 27 and scan 1. The distance of the dark blue line equals the directed Hausdorff distance between scan 1 and scan 27 - $sup_{x \in X} inf_{y \in Y} d(scan1, scan27)$. When a mobile host moves, the kitchen boundary beyond the user from the Lidar device is not detected as the mobile host blocks the light beam. Based on this feature, Hausdoff distance with a threshold is used to determine if recording the 2D Lidar measurements.

Instead of using the Hausdorff distance, I also tried to differentiate between two scans based on comparing distances at each angle. However, a small angle difference can lead to a considerable difference in distance, which is shown in Figure 6-1 (the points in the grey circle with a small angle difference, but with a considerable distance).

6.2.2 2D Lidar Measurements Pre-processing

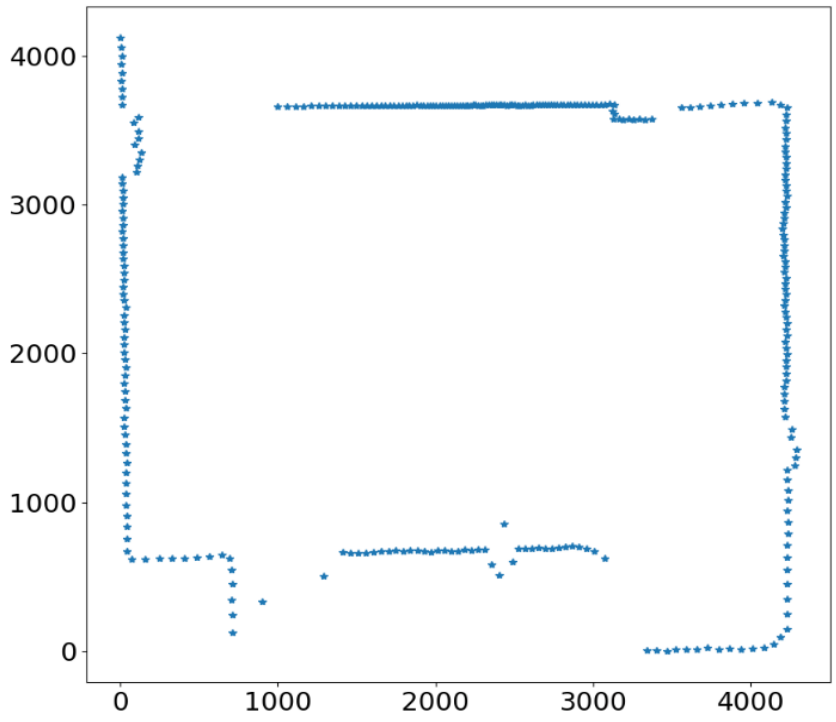

Figure 6-2 Converted 2D Lidar map (one example single scan, in millimeters)

The raw measurements were collected from the 2D Lidar chosen consists of time, distance, angle, and quality. Because of the noisy and uncertain sensor measurements, occupancy grid mapping [103] is used, an algorithm often adopted by mobile robots, to address the uncertainty of the Lidar measurements, and to construct a consistent map (floor plan).

The difference between Figure 6-2 and Figure 6-1 is that the original point was changed to make sure all coordinates of both x and y of Lidar points coordinates are above 0, which will make it easy to convert the point map to an occupancy grid map, as all the coordinates of the grid map are positive.

In our 2D Lidar-based off-body positioning system, occupancy grid map is used to address the problem of generating a consistent map from noisy and uncertainty of our 2D Lidar measurements. The principle of the grid cells is to represent the map as a field of random variables, arranged in an evenly spaced grid cell. Each variable is binary and corresponds to the occupancy of the location it covers. The occupancy grid mapping algorithms implement the approximate posterior estimation for those random variables: $\mathrm{p}(\mathrm{m}|z_{1:t}, x_{1:t})$, where m is the map, $z_{1:t}$ is the set of measurements from time 1 to t, $x_{1:t}$ is the set of the robot poses from 1 to t, however, in our case, $x_{1:t}$ is fixed, as the position of our 2D Lidar is fixed. In the map, m_i will be denoted the grid cell with index i, which is often in 2D maps. The notation $p(m_i)$ represents the probability of an occupied cell i. Thus, the posterior of a map is that

$$\mathrm{p}(\mathrm{m}|z_{1:t}, x_{1:t}) = \prod_i \mathrm{p}(m_i|z_{1:t}, x_{1:t}) \tag{6.2}$$

Due to this factorisation, a binary Bayes theorem (occupied or not) can be used to estimate the occupancy probability of each grid cell in the map. The Log odds was used to represent the probability that each grid cell is occupied, as in this case, it can merely use addition and subtraction to update the probability based on the new measurement (see equation 6.8). The $\mathrm{Odd}(\mathrm{s})$ will be

$$\mathrm{Odd}(\mathrm{s}) = \frac{p(s=1)}{p(s=0)} \tag{6.3}$$

where $p(s=1)$ means the probability of the grid cell is occupied, $p(s=0)$ means the probability of the grid cell is free (not occupied). The sum of $p(s=1)$ and $p(s=0)$ equals 1.

When there is a new measurement $z\sim\{0,1\}$, $\mathrm{Odd}(s)$ is updated as follows:

$$\mathrm{Odd}(s|z)=\frac{p(s=1|z)}{p(s=0|z)} \tag{6.4}$$

Then, based on the Bayes' theorem:

$$p(s=1|z)=\frac{p(z|s=1)p(s=1)}{p(z)} \tag{6.5}$$

$$p(s=0|z)=\frac{p(z|s=0)p(s=0)}{p(z)} \tag{6.6}$$

$$\mathrm{Odd}(s|z)=\frac{p(z|s=1)}{p(z|s=0)}\frac{p(s=1)}{p(s=0)}=\frac{p(z|s=1)}{p(z|s=0)}\mathrm{Odd}(s) \tag{6.7}$$

$$\log\mathrm{Odd}(s|z)=\log\frac{p(z|s=1)}{p(z|s=0)}+\log\mathrm{Odd}(s) \tag{6.8}$$

where the 1st part of equation (6.8) is the measurement model, where $\mathrm{looccu}=\log\frac{p(z=1|s=1)}{p(z=1|s=0)}$ and $\mathrm{lofree}=\log\frac{p(z=0|s=1)}{p(z=0|s=0)}$. Both are constant. If in the initial state, no grid should be occupied. So, $\log\mathrm{Odd}(s)=\log\frac{p(s=1)}{p(s=0)}=\log\frac{0.5}{0.5}=0$.

For example, $\mathrm{looccu}=0.8$, $\mathrm{lofree}=-0.7$, the higher the value, the higher probability that this grid cell is occupied.

To build the occupancy grid map, it needs to collect several scans, then calculate the occupied probability of each grid cell. Bresenham line generation algorithm [104] was

used to determine which grid cells are passed by the light beam, namely, which grid cells are free.

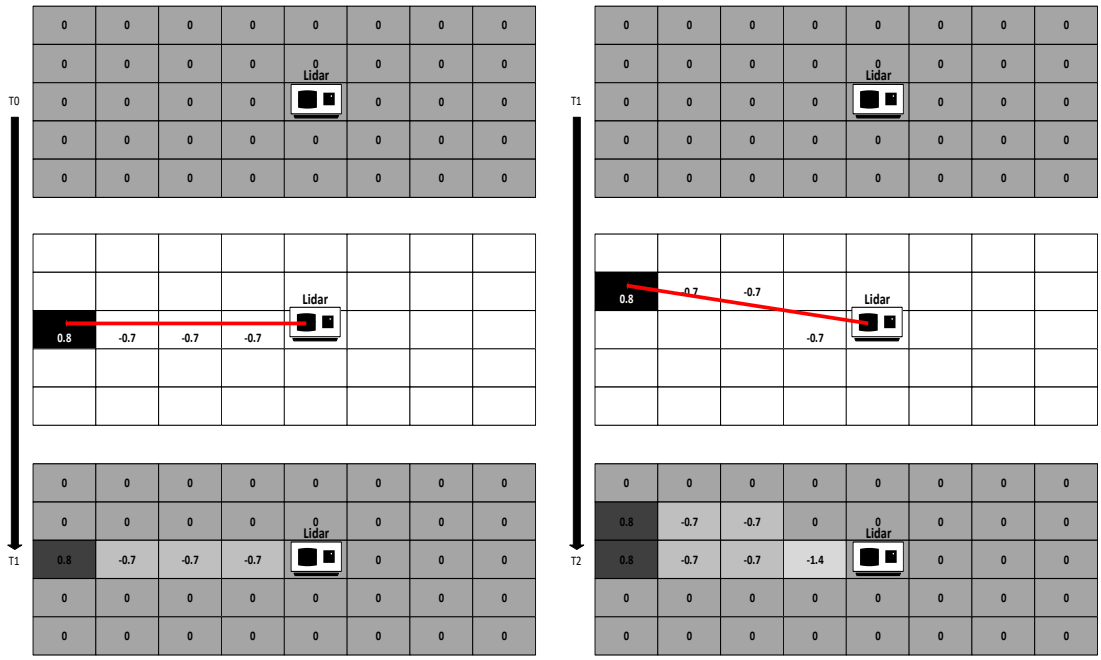

Figure 6-3 How occupancy grid mapping works

The basic rules of Bresenham line generation algorithm are that, first, transforming the equation of a line from the typical slope-intercept form into something different (see equation 6.12); next, using the new equation to draw a line based on the error accumulation.

The slope-intercept form is shown as follows:

$$f(x) = y = mx + b \tag{6.9}$$

where m is the slope and b is the intercept of the y-axis. y equals to

$$y = \frac{(\Delta y)}{(\Delta x)}x + b \tag{6.10}$$

Then,

$$(\Delta x)\mathrm{y} = (\Delta y)x + (\Delta x)b \tag{6.11}$$

$$\mathrm{f(x,y)} = 0 = \mathrm{Ax} + \mathrm{By} + \mathrm{c} = (\Delta y)x - (\Delta x)\mathrm{y} + (\Delta x)b \tag{6.12}$$

where $A = \Delta y$, $B = -\Delta x$, $C = (\Delta x)b$. For any $\mathrm{f(x,y)}$ not equals to 0, this means that $\mathrm{(x,y)}$ is not on the line; if $\mathrm{f(x,y)} > 0$, this means that $\mathrm{(x,y)}$ is above the line; if $\mathrm{f(x,y)} < 0$, this means that $\mathrm{(x,y)}$ is below the line.

I set the starting point (x_0, y_0) on the line, then $\mathrm{f}(x_0, y_0)$ equals to 0. Because of the property of the grid map, all coordinates are integers. Then, there will be several cases, for example, if the slope $k \leq 1$ (the rest cases, e.g., $k > 1$ can be converted to this form by swap x and y), the problem is to find out whether the next point should be at $(x_0 + 1, y_0)$ or $(x_0 + 1, y_0 + 1)$. To solve this problem, the midpoint between these two points can be used: $\mathrm{f}\left(x_0 + 1, y_0 + \frac{1}{2}\right)$. If the value of $\mathrm{f}\left(x_0 + 1, y_0 + \frac{1}{2}\right)$ is positive, then the ideal line is below the midpoint and closer to the point $(x_0 + 1, y_0 + 1)$. The difference is as follows:

$$\mathrm{D} = \mathrm{f}\left(x_0 + 1, y_0 + \tfrac{1}{2}\right) - \mathrm{f}(x_0, y_0) \tag{6.13}$$

$$\mathrm{D} = [\mathrm{A}x_0 + \mathrm{B}y_0 + \mathrm{C} + \mathrm{A} + \tfrac{1}{2}\mathrm{B}] - [\mathrm{A}x_0 + \mathrm{B}y_0 + \mathrm{C} + \mathrm{A}] \tag{6.14}$$

$$\mathrm{D} = \mathrm{A} + \tfrac{1}{2}\mathrm{B} \tag{6.15}$$

where $\mathrm{A} = (\Delta y)$, $\mathrm{B} = -(\Delta x)$, $\mathrm{C} = (\Delta x)b$. If D is positive, $(x_0 + 1, y_0 + 1)$ is chosen, else, $(x_0 + 1, y_0)$ is chosen.

For the rest midpoints, (using the second midpoint as an example)

$$\mathrm{f}\left(x_0 + 2, y_0 + \tfrac{1}{2}\right) = \mathrm{f}\left(x_0 + 1, y_0 + \tfrac{1}{2}\right) + \mathrm{A} = \mathrm{D} + \mathrm{A} \tag{6.16}$$

$$\text{or } \mathrm{f}\left(x_0 + 2, y_0 + \tfrac{3}{2}\right) = \mathrm{f}\left(x_0 + 1, y_0 + \tfrac{1}{2}\right) + \mathrm{A} + \mathrm{B} = \mathrm{D} + \mathrm{A} + \mathrm{B} \tag{6.17}$$

So, it can accumulate error, then, $D_{new} = D_{old} + A\ (D_{old} < 0)\ or\ D_{old} + A + B\ (D_{old} > 0)$. The point is chosen based on the value of D, if D is positive, $(x_{previous} + 1, y_{previous} + 1)$ is chosen, else, $(x_{previous} + 1, y_{previous})$ is chosen. It can also multiply 2 to everything with no consequence, e.g. $2\mathrm{D} = 2\mathrm{A} + \mathrm{B}$, $2\left(\mathrm{f}\left(x_0 + 2, y_0 + \frac{1}{2}\right)\right) = 2\mathrm{A} + 2\mathrm{f}\left(x_0 + 1, y_0 + \frac{1}{2}\right)$, which makes it easy to calculate, as all variables are integers.

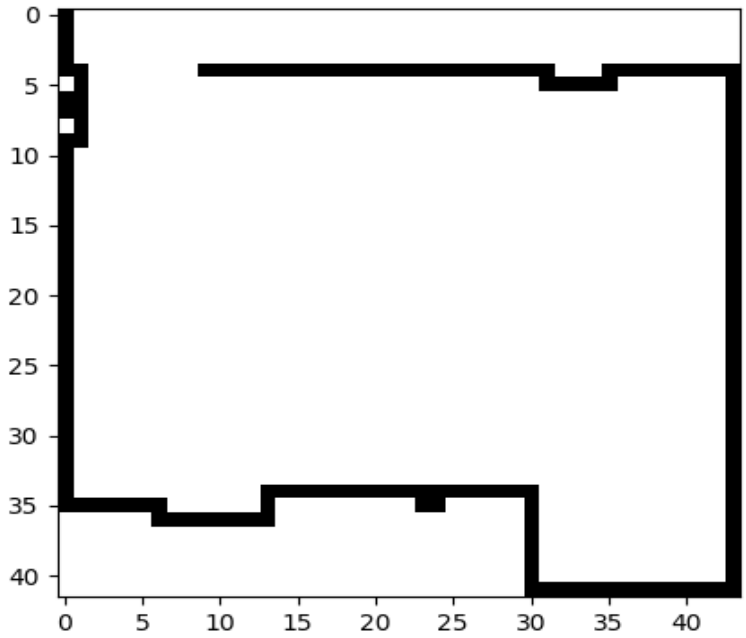

Figure 6-4 An occupancy grid map where each grid cell equals 10*10 cm^2

Figure 6-4 shows our grid map after choosing an occupancy rate (4 is chosen as the map barely changed based on the visualisation of training data). The real layout of the space is the same as shown in Figure 6-11.

6.2.3 Multiple Target (User) Tracking

On occasion, when using Lidar, a few outliers will also show up in the processed location-based 'image map'. This reduces the localisation and recognition accuracy, especially when more than one mobile user is present in the same room. So, DBSCAN

[105] is used to reduce such anomalies and to represent different mobile users as clusters.

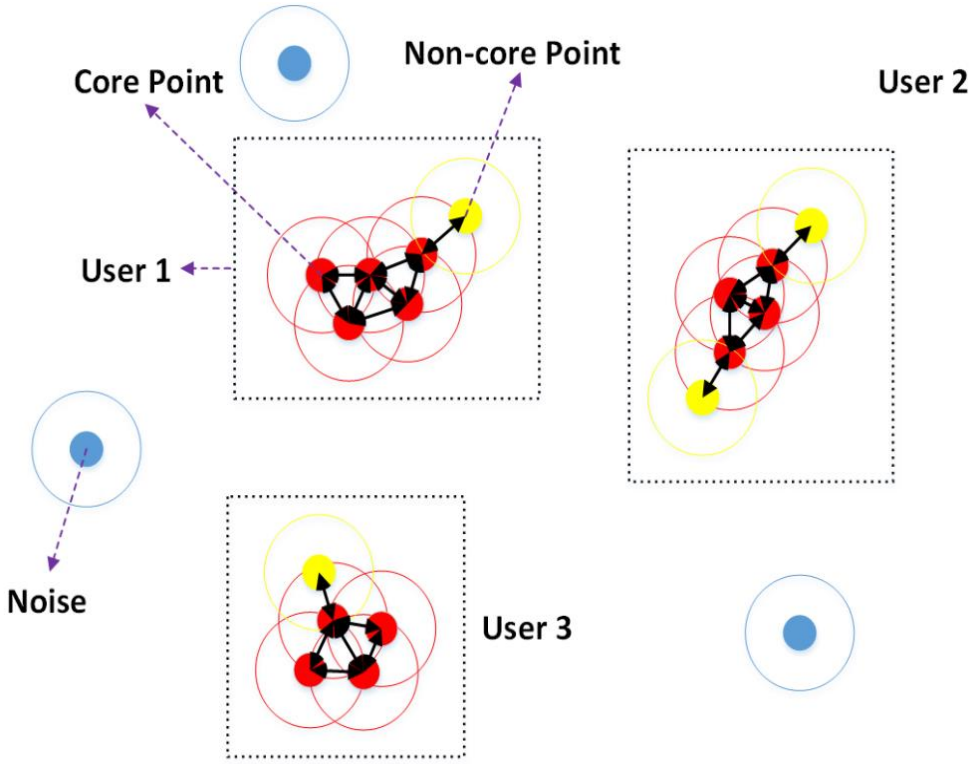

Figure 6-5 DBSCAN is used to reduce noise and to cluster users (for minPts=2)

DBSCAN is a clustering algorithm based on regional data density, which is often used for outlier detection. It also marks outliers lying in low-density regions for removal. The algorithm requires two parameters; one is a radius ε, another one is minPts. Points are classified as follows:

- A core point means at least minPts points are within a ε radius. Each cluster consists of at least one core point. In this case, I set minPts=2, ε=2 (this is considered the human width is over 20 cm) when using the converted grid map.

- A non-core point means the point that can directly reach is less than minPts core points. The non-core points can be counted into the same cluster or delete them – it does not matter. They cannot be used to reach more points.

- All points that are not reachable from any other point are considered as noise points (outliers).

Then, the nose points will be removed, and the rests clusters will be treated as users.

Then, the nose points will be removed, and the rests clusters will be treated as users. This can support to locate multiple users in the same time. However, it cannot identify who is who if there are more than one user. So, how to identify the users will be another issue which needs to be solved in the future. Note that it is presumed that not many users will appear in the same room, with one blocking the other.

6.3 2D Lidar Off-body ADL Recognition

6.3.1 Stay Point Recognition

In the 2D Lidar off-body ADL recognition experiment, the location data was segmented into fixed time periods of 30 seconds and then identify points where the host stays for at least a few seconds, so-called stay points. The 30 s was chosen as a trade-off between the time taken to move between landmarks and to allow sufficient time to link and analyse a small chain of landmarks visits that may be stay points together as simple ADLs, versus creating and having to analyse much more complex ADL chains. A stay point recognition algorithm [106] was used to identify key landmarks in this time segment, as our basic assumption is that staying at a location means that this point is significant. The subject may well pass other landmarks, but these are not necessarily relevant to the activity being performed.

The basic idea for stay point recognition is as follows:

The trajectory is represented as the set:

$$S = \{loc_k = (t_k, l_k) | k = 1,2..n\} \tag{6.18}$$

where l is the cartesian coordinates, t is the timestamp.

I transform the data into the following equations:

$$\mathrm{f}(t_k) = t_k - t_e \tag{6.19}$$

$$\mathrm{Z} = \mathrm{g}(f(t_k)) \tag{6.20}$$

$$\mathrm{Z} = \mathrm{g}(f(t_k)) = \sum_{n=2}^{k} distance(l_n, l_{n-1}) \tag{6.21}$$

where t_e is the time when the subject enters a space of interest, e.g., the kitchen, distance is the ED. The horizontal axis in Figure 6-6 represents $\mathrm{f}(t_k)$ is the time when the subject enters the kitchen and $distance(l_k, l_{k-1})$ is the ED between two points. In equation (6.20), it subtracts the time of entry because no data collection is logged when the kitchen is empty.

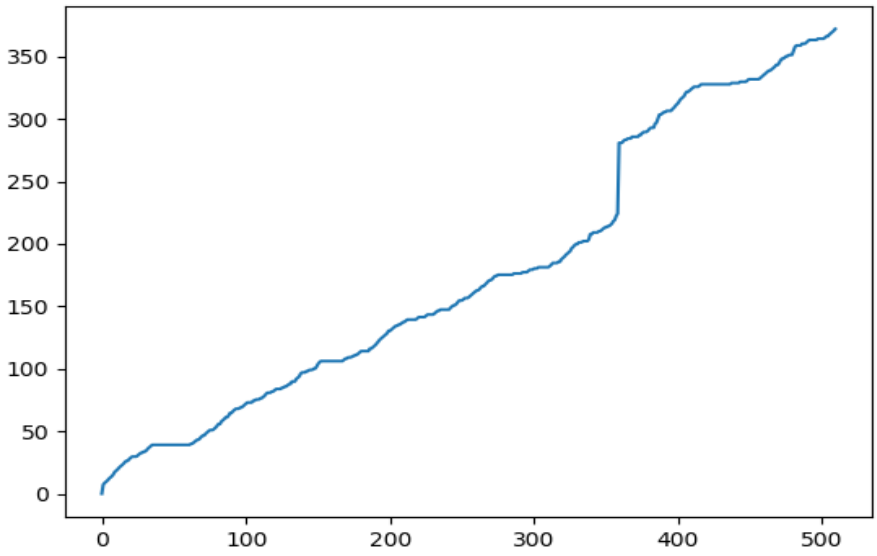

Figure 6-6 Z transformation representing when a user enters the kitchen. The horizonal axis (one example from the recognition experiment) represents $\mathbf{f}(\boldsymbol{t_k})$ and the vertical axis represents Z, which is a monatomic increasing curve.

As $g(l_k)$ increases, its first derivative will be always greater or equal to zero, which is shown in Figure 6-7. The stay-points should be where g is horizontal, i.e. the local minima of the derivative of the curve. To identify the local minima, it checks the zero-crossing of the second derivative, as the second derivative may not equal to zero as g is a discrete function. Figure 6-7 depicts the second derivative, and the red boxes means the selected regions.

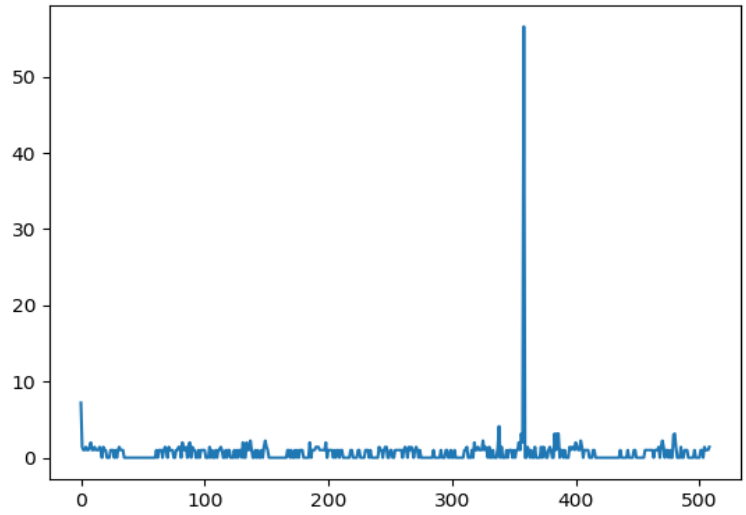

Figure 6-7 The first derivative of the z transformation curve

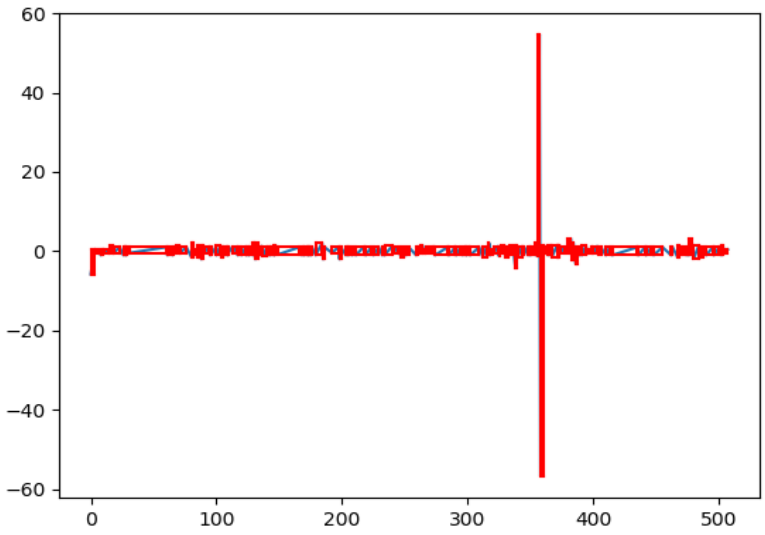

Figure 6-8 The second derivative of the curve

The red boxes not only include the stay points but also include inflections, which are caused when you walk slowly, then speedily.

To reduce the inflections, it uses a confidence value to recognise the stay point. Based on paper [106], a single confidence value of data point was used as:

$$\mathrm{C}(P_i) = 100 \text{ g}' \leq 0.01 \tag{6.22}$$

$$\text{Else: } \mathrm{C}(P_i) = 100 - \frac{\text{g}'-0.01}{0.01} \tag{6.23}$$

$$\mathrm{C}(P_k, P_w) = \frac{\sum_{i=k}^{w} \mathrm{C}(P_i)}{w-k+1} \tag{6.24}$$

where g' is the first derivative. It is set $\mathrm{C}(P_k, P_w)$ in $\mathrm{C}(P_i, P_j)$. i, j are the boundary points of zero-crossing of region k; w is the confidence level of this sub-region, above 80. The center of those points will be treated as the stay points.

6.3.2 Sequence-to-Sequence (Seq2Seq) Model

The target objective is to recognise location-driven human daily activities, the inputs are sequential estimated locations, in this case, 2D Lidar measurements. A natural choice to data analysis choice to classify sequential measurements is to use a RNN model. Long short-term memory (LSTM) with a 10 encoding space was selected as the basic algorithm of the Seq2Seq model to recognise activities.

Then the research question is how to build the corresponding output activities. Since for example, a kitchen has various landmarks, such as a table, sink, fridge, and microwave, 2D Lidar can be used to track motion between landmarks and to detect the continued presence at a landmark – a so-called stay point. One solution to define those output activities can be based on those landmarks, as most activities happen near those landmarks. However, there could be different landmarks in each user's house. So, the

aforementioned stay point recognition algorithm was used to recognise those key landmarks.

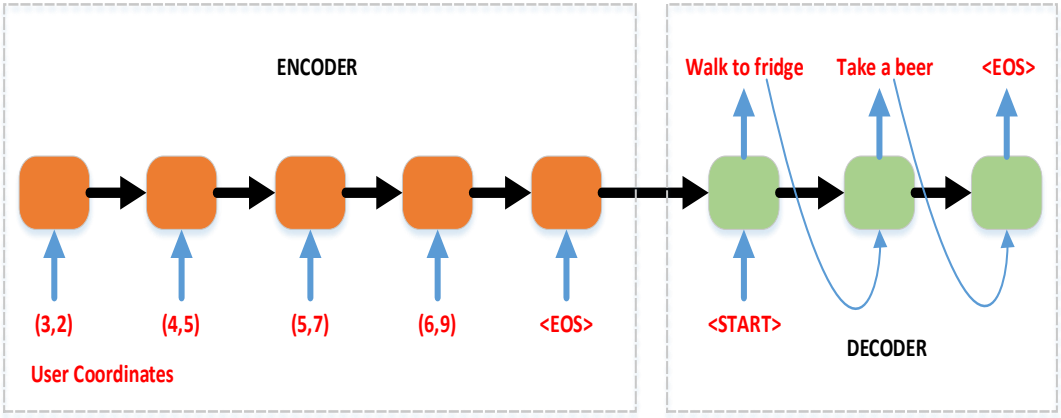

Figure 6-9 The sequential coordinates represent the encoder input; then the decoder outputs the corresponding activities, where <EOS> represents the end of the action sequence.

Seq2Seq is a general-purpose encoder-decoder model, which is initially built for machine translation [101], but has also been used for a wide variety of tasks, e.g., image captioning and text summarisation. The reason Seq2Seq model is chosen is that the sequential location information is analogous to a translation problem. Each sequential location information belongs to different corresponding activities.

Because activities can take different amounts of time, selecting fixed periods, such as 30 seconds, and then mapping each selected fixed period to one activity does not work. There can, for example, be more than one activity in 30 seconds. Hence the use of a simple neural network also does not work. To collect training data, data were segmented using stay points and then annotate the stay points and annotate the sub-sections of each segment with the elementary activities. Lidar measurements were collected in a kitchen. The user is asked to label the stay points and related activities. Then the trajectory of every 30 s will be the input data to train the Seq2Seq model. The corresponding activity will be the labelled data, e.g., in a 30 s time slot, the corresponding activities are {from table to fridge, use fridge, prepare to cook}, then these activities can be represented as {2, 3, 8} (see the list prior to Figure 6-17), then

based on the activity number, this was converted into a one-hot encoding[14], where categorical variables are converted into a 0/1 form, which then forms the input to the Seq2Seq model.

6.4 Study 4-a and 4-b: 2D Lidar Off-body Positioning and ADL Recognition Evaluation

6.4.1 2D Lidar Off-body Positioning Performance

Because of the challenges with using on-body devices such as accompanied (mobile phones), or attached (wearables) devices, which may become detached or run out of power, which may be less usable by some types of users such as the elderly and because office type indoor spaces may not be representative of living spaces which some types of users do not frequent, e.g., the elderly, a device-free or an off body positioning device was investigated – Lidar.

Figure 6-10 2D (PRLIDAR) Lidar IPS device

[14] For more details: http://scikit-learn.org/stable/modules/generated/sklearn.preprocessing.OneHotEncoder.html. Last accessed in Sep/2018

The Lidar that used was a 2D PRLIDAR, which is shown in Figure 6-10. It supports 5-10Hz Adaptive Scan Frequency and a 0.2 to 10 m distance range. The Lidar scanning rate was modified to 6 Hz, which means six positioning results can be acquired in one second. All these scans are converted into a grid map, then compared to each other. As the Lidar was deployed in a fixed position, e.g., to scan a kitchen, the detected boundary of the kitchen should be matched most grids of the last detected boundary; if not, the scan will be deleted. The rests measurements in this 1s time period can still offer high centimetre-level accuracy in confidence.

The experiment area is a kitchen shown in Figure 6-11, is about 20 m^2, which is the same layout as shown in Figure 6-4. Lidar was deployed on the table.

Figure 6-11 The 3D View of the kitchen testbed

Figure 6-12 visualises one trajectory of the user, that is the user walked from the door to the table, then walked to the fridge. Since the 2D Lidar-based off-body positioning system can offer centimetre positioning accuracy, the actual positioning results of the user would like a 'tail', instead of a single-point, which is shown in Figure 6-13, which is caused by the human body width. However, our activity recognition methods only require a series of single position result. In this case, it uses the averaged result to represent the user and use a circle to represent the user.

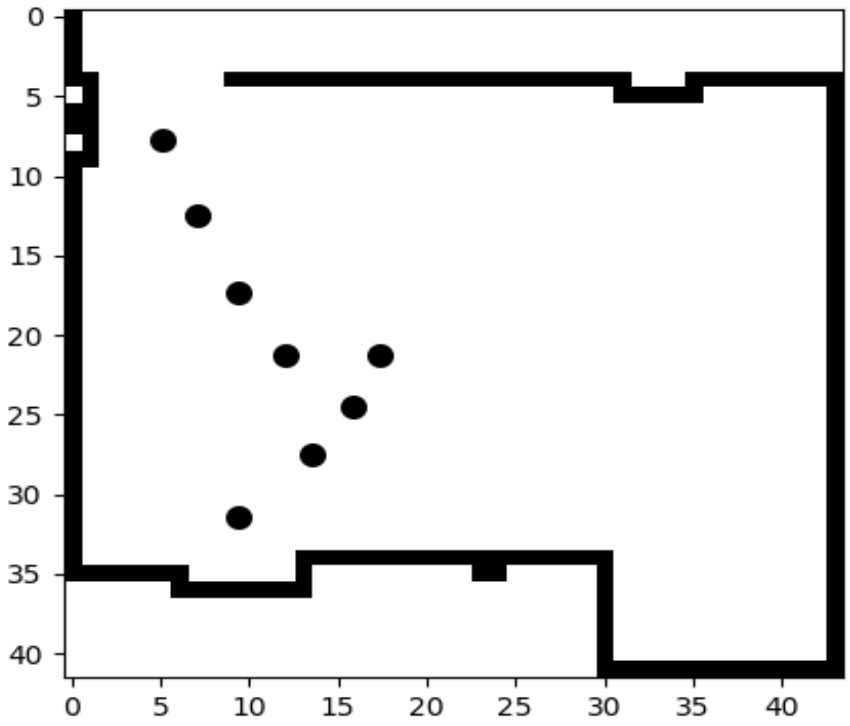

Figure 6-12 One trajectory of a user, tracked using the Lidar system

Figure 6-13 The actual shape of a user path displayed in the grid map

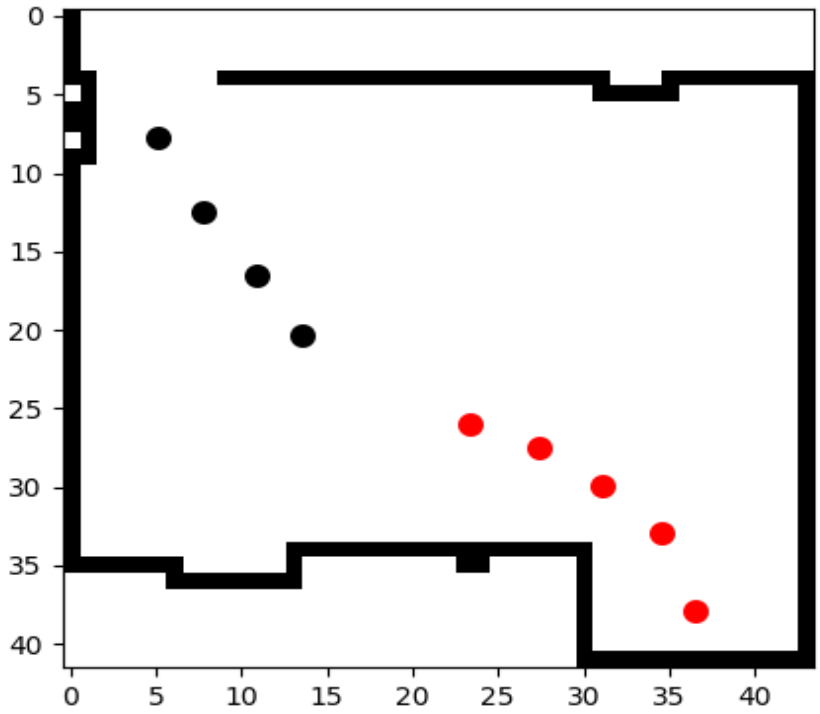

Figure 6-14 Two users are recognised in the kitchen

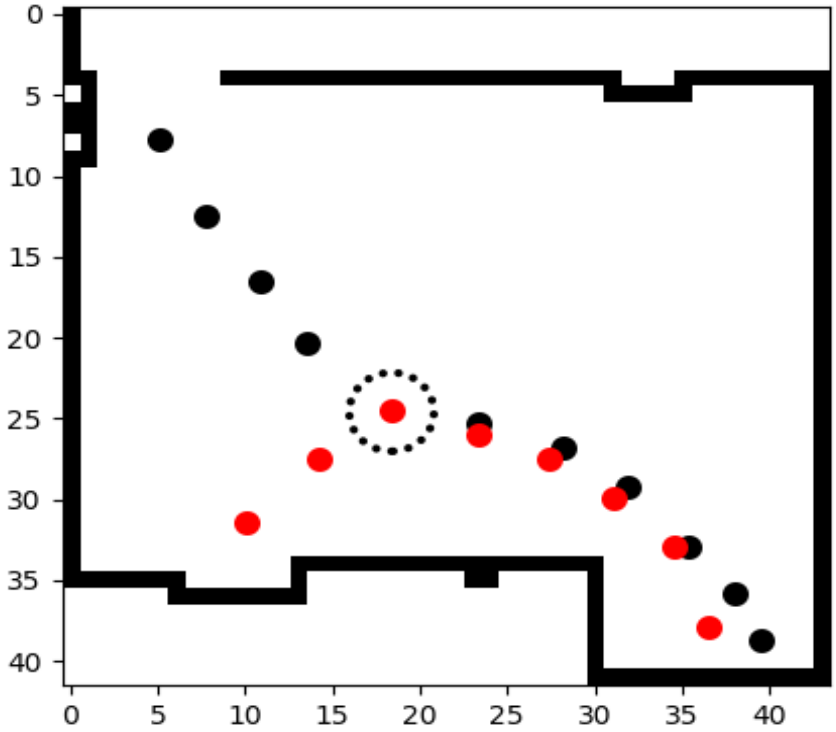

Figure 6-15 Two clusters will merge into one if two users are close enough

Figure 6-14 shows that two users are recognised and tracked using Lidar. However, if two users are close enough (within a ε radius, i.e., 20 cm), two clusters generated using DBSCAN will merge into one cluster, which is shown in Figure 6-15. If this happens, the system will use the coordinates of the merged cluster (dashed black circle) to represent the position of both users. For example, in Figure 6-15, the black dots represent user 1 walked from a 'top door' to the 'back' door, the red dots represent user 2, who walked from the back door to the fridge. These users passed each other in the position of the dashed black circle, and the two clusters merged into one.

Based on the result, the system can discriminate different users' trajectories. However, it cannot discriminate who the user he/she is. This will be discussed in the future.

6.4.2 2D Lidar Off-body ADL Recognition Performance

For the localisation part, the system works well. Based on the comparison, each data point can be classified into the real grid (grid map). However, if two users are close enough (less than 20 cm), two clusters may merge into one, but this was not a major issue. Moreover, a mobile human or host that is detected by the system could become undetected within a later period in the same sequence, that did not leave via a door stay point. It could then perhaps assume this has changed its vertical position, e.g., fallen, as the Lidar scan is set to a certain height (1.1m in our case). 1.1 m is chosen as a trade-off between being low enough to detect kitchen units that are offset from a room wall, so it can detect if the user is close to them, versus being high enough to detect an upright human. If a user becomes undetected, at the height of less than 1.1m for a period during a sequence, it could presume the mobile user or host has fallen down on the floor.

For human activity recognition, stay point was used as the reduced set of important landmarks and as an activity connector. So, the first step is to recognise a mobile host's stay points, then ask an observer to label the stay points and the activity category for the ground truth. The collected dataset consisted of a total of 536 times 30 s time slots

of acquired Lidar measurements happened in the kitchen. Of this, 100 times 30 s was used for the test set and the rest for the training set. The next step is to use the sequential location data as inputs to train the model, where the corresponding label data represents the labelled activities (see Figure 6-9).

In Figure 6-16, the grey grids represent a user's trajectory over a period. The black ones mean the recognised stay points. As an example, I only visualise part of the dataset. Here, six stay points (landmarks) are identified. I asked an observer to label those stay points and to point out the related activities to provide the ground truth. There are several ways to label ADLs. First, several elementary ADLs was set, i.e. eating, drinking or use the fridge, then ask the user to label the corresponding sequential location data. Another way is to ask the user to label personalised activities. In our experiment, there are 17 activities labelled by a mobile host based upon daily simple kitchen activities.

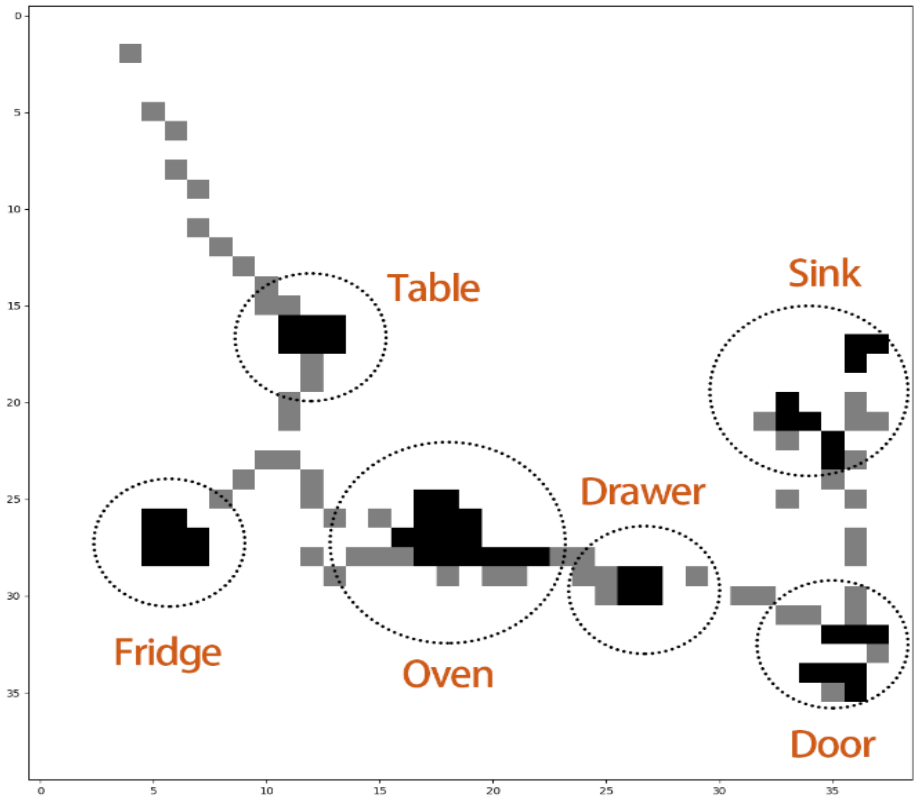

Figure 6-16 Labelled stay points in a home kitchen scenario as detected by Lidar

There are several ways to label activities; one is to set several elementary activities, i.e. eating, drinking or use the fridge, then to ask the user to label the corresponding sequential location data. Another way is to ask the user to label personalised activities. In our experiment, there are 17 activities labelled by the user based on daily data collection, which is 1) from door to table, 2) from table to fridge, 3) use fridge, 4) fridge to warehouse, 5) prepare cat food, 6) warehouse to back door, 7) go out for cat, 8) no one in the kitchen, 9) open back door, 10) back door to fridge, 11) prepare to cook, 12) oven to fridge, 13) fridge to back door, 14) use breadboard (drawer), 15) use oven, 16) go out back door, 17) washup.

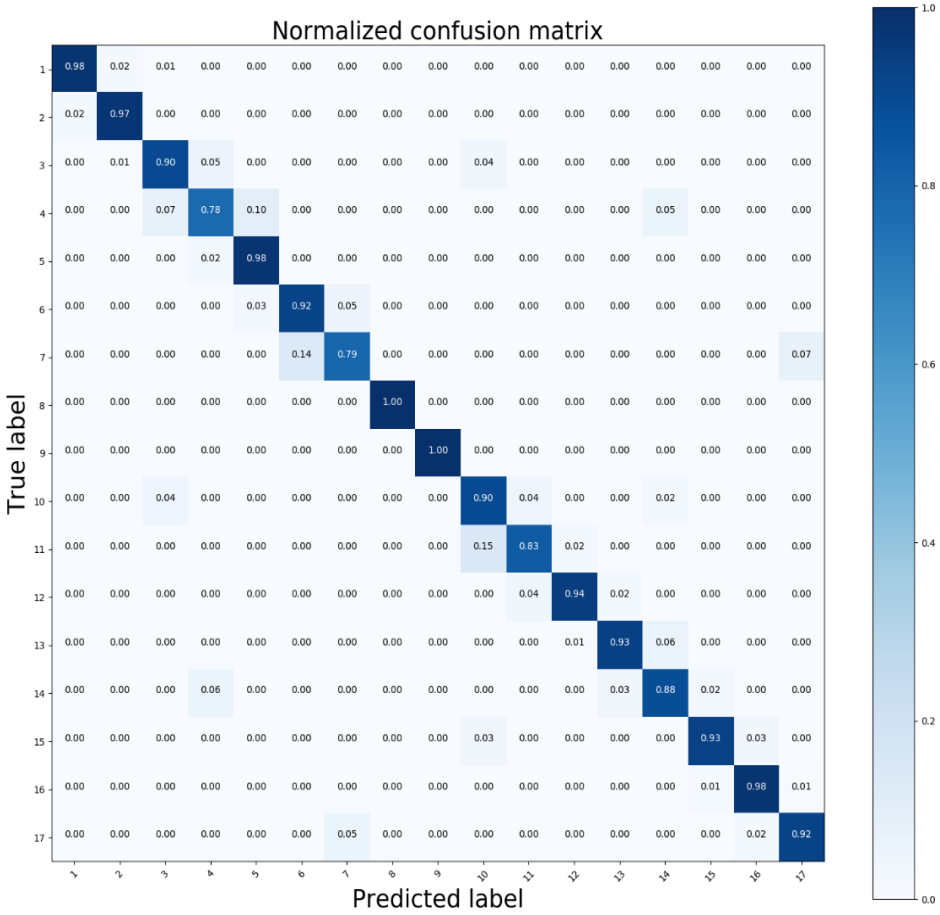

Figure 6-17 Recognition confusion matrix

Note that the labelled activities can include several different hierarchical levels. For example, ‘food pantry’ as a stay point was recognised. Within a specific 30 s, a human user can either move from the food pantry to backdoor or stay at or very near to the

food pantry. Actions can also be labelled differently. A mobile host is not only near a stay point, but ADLs are associated with a stay point, e.g., preparing cat food in the food pantry or putting something into the food pantry. Moreover, if the user is not willing to label or wrongly label the activity or there is a new activity, the system cannot correctly predict the activity.

Although the sequence recognition accuracy is reasonable at 88%, when the predicted sequences are the same as the ground truth ones, a few activities from the total activity sequence are wrongly recognised, which is shown in Figure 6-17. The darker the blue, the more accurate the recognition. 1 to 17 represent the 17 labelled activities. The hypothesis is that those activities that involve interactions with fewer, clearer to detect stay points, can achieve a better recognition accuracy than those activities with more stay points that can be linked to multiple ADLs. Interweaving ADLs like activity 7 and 11 only achieve 78% and 83% recognition accuracy, which is relatively lower than other activity recognition accuracy. This is because they are involved in more stay points, which can be classified into other activities. However, it is still acceptable and means the model has the ability to discriminate interweaving ADLs.

6.5 Summary

In summary, this chapter first introduces the 2D Lidar-based off-body positioning system, which includes three parts: 1) using a Hausdorff distance threshold to collect data to identify when there are periods of no human activity, e.g., humans who work away from home are not likely to be present in the kitchen in much of the day; 2) Lidar measurements are processed to construct a grid map, which will decrease the uncertainty of using raw measurements; 3) multiple targets can be tracked using DBSCAN, as multiple users may present in the kitchen at the same time. Then, that processed location information will be treated as the input data in the human activity recognition methods.

High positioning accuracy 2D lidar measurements of a kitchen at different times were collected to test the proposed Seq2Seq based recognition method (also to solve the

problems of using WiFi to recognise ADLs). Traditional ADL recognition usually requires mobile hosts to carry sensors to generate the data that are analysed via an enumeration of hierarchical plans. In contrast, it was proposed, developed and validated that 2D Lidar measurements could be used to accurately determine ADLs. I combined the use of Lidar with the state-of-art Seq2Seq RNN model to classify ADLs linked to the Lidar generated stay points and transitions between stay points. The validation shows that a 2D Lidar location determination method can provide an accurate localisation accuracy and a good accuracy (88%) in recognising seventeen location-driven daily activities. The next chapter gives the conclusion and future work.

7 Conclusion and Further Work

7.1 Contributions

This thesis concerns the problem of improving the location estimation accuracy of mobile targets indoor using reasonable solutions in different indoor scenarios (see Table 1). Then based on the improved estimated locations to offer high-quality LBS, in our case, high accuracy location determination ADL recognition.

The principal, novel, contributions aspects of this research are:

- A novel smartphone independent indoor positioning method using RSSI ranking from multiple low-energy iBeacon devices has been proposed, which is validated in a library room and a PhD office that contain many metal bookshelves and parallel aisles. Moreover, WiFi RSSI ranking, with KTCC and CNN was also tested in an office environment and validated. These systems could also be suitable for scenarios with the Internet of Things (IoT), as the growing number of transmitters embedded in smart objects can also be treated as wireless APs.

- RSSI location fingerprinting procedures were studied, which includes 1) how to build fingerprints database; 2) how to select APs to reduce the data dimensions; 3) how to use the state-of-art deep learning algorithms to achieve a higher positioning accuracy.

- An additional contribution to improve location fingerprinting is that I also investigated how the MF anomalies can be used to estimate accurate location information. A novel Fast Path Matching algorithm for MF measurements (FPM-MI) algorithm (see Section 4.2.2) was proposed that only requires a person to walk a much shorter distance of about 3 m in order to have an arm span location accuracy. In contrast, a conventional Particle filter (PF) algorithm requires someone to walk 9 m before it can get such a location fix. The system

was validated in the same library, with multiple metal shelves and pillars. The positioning accuracy is within 1.8 meters, with a 90% confidence and with no extra infrastructure setup to support the target IPS application.

- A novel multi-source information fusion method for ADL recognition that fuses estimated locations and RSSI ranking of the routine was proposed. It can also be extended in multi-source signal scenarios (e.g. MF measurements) to upgrade the route recognition accuracy.

- Device-free sensing methods such as 2D Lidar can also be used for recognition of location-related human activities without anyone needing to carry a single sensor in a specific area. Although a camera can also achieve similar goals, it is far more privacy-invasive. Hence, an innovative method for recognising daily activities using a Seq2Seq model, which is widely used in the field of Natural Language Processing (NLP) was proposed to deal with sequential location data from a 2D Lidar, as it is considered that recognising ADLs is analogous to a translation problem. The results obtained indicate that this method can provide an accurate positioning accuracy and good accuracy (88%) in recognising 17 targeted location-driven daily activities.

This PhD project resulted in the following publications.

1. **Z. Ma,** S. Poslad, J. Bigham, X. Zhang, and L. Men, "A BLE RSSI ranking based indoor positioning system for generic smartphones," in IEEE 16th Wireless Telecommunications Symposium (WTS), 2017, pp. 1–8.

2. **Z. Ma,** S. Poslad, S. Hu, and X. Zhang, "A fast path matching algorithm for indoor positioning systems using magnetic field measurements," in IEEE 28th Annual International Symposium on Personal, Indoor, and Mobile Radio Communications (PIMRC), 2017, pp. 1–5.

3. **Z. Ma**, J. Bigham, S. Poslad, B. Wu, and E. Bodanese, “Device-Free, Activity during Daily Life, Recognition Using a Low-Cost Lidar”. IEEE Global Communications Conference (GLOBECOM) 2018. (**Travel Grant**)

4. B. Wu, **Z. Ma,** S. Poslad, “An efficient wireless access point selection algorithm for location determination based on RSSI interval overlap degree (IOD) determination,” in IEEE 17th Wireless Telecommunications Symposium (WTS), 2018, pp. 1–8.

5. B. Wu**, Z. Ma,** S. Poslad, and Y. Dong, “Using WiFi Fingerprint Based Location Awareness for Activities of Daily Living Recognition”. In 5th International Conference on Behavioral, Economic, and Socio-Cultural Computing (BESC), 2018.

6. F. Lv, H. Yang, **Z. Ma**, and S. Poslad. “Indoor Activities Classification System Based on Android phone and Machine Learning.” Computer Programming Skills and Maintenance 2017, 02 (2017): 40-43.

7.2 Outlook / Further Work

This section will outline several potential research directions to extend the proposed indoor positioning and recognition methods further.

7.2.1 Indoor Positioning Methods

7.2.1.1 Fingerprints Collection Robot and Radio Map Design and Testing

Although a fingerprint collection robot (prototype) was developed, which was mentioned in Chapter 5, to help construct radio maps, the robots are still not ‘intelligent-enough’, as they need to manually set the designed path, which the robots can follow. However, this also faces challenges when knowing where it is in the building to label the fingerprints and how to avoid moving objectives. So, mobile robot

SLAM [107], [108] multiple sensors fusion [109], [110] and collision-free path replanning [111], [112] could be studied to achieve this goal.

Moreover, as shown in the paper [72], the human body attenuation issue exists, the orientations and places of collected fingerprints at each RP should be considered. So, how to design and sample fingerprints, e.g., collecting 4 orientations (N, W, S, E) or sequential path fingerprints will be another aspect of the future work. Such designed radio map will also be open-source to promote more indoor positioning research, the radio map of the Lab testbed is available in http://iot.eecs.qmul.ac.uk.

7.2.1.2 WiFi Round Trip Time

Google has launched the first developer preview build of Android P version in 2018. Some new features were published, which WiFi Round Trip Time (RTT) was one of them. The IEEE 802.11mc is more commonly known as RTT, which allows computing devices to measure the distance to its nearby WiFi APs and to determine the user locations. With more than three nearby WiFi APs, geometric-based algorithms methods can be applied to estimate locations, no radio map is required in free space like spaces, avoiding the radio map construction work in those places, which is time-consuming and laborious and make RSSI location determination with less maintenance work. Also, with the growing number of deployed WiFi APs, the positioning accuracy can be further increased. However, not all devices, at this time, only the Google Pixel line of smartphones have the hardware support for this feature[15].

7.2.1.3 AOA-supported BLE 5 Positioning Beacon

An iBeacon device with designed antenna array can make it possible to compute Angle of Arrival (AOA) based on phase differences, which can be used to locate users.

[15] For more details: https://en.wikipedia.org/wiki/Pixel_(smartphone). Last accessed in Sep/2018

Moreover, the BLE Special Interest Group presented the BLE 5 version[16] on 16 June 2016, which is the latest version of the BLE wireless communication standard. It is used for communication between various smart home and IoT devices as it is a high-speed (up to 2Mbps), long-range (up to 400 m), low-power consumption standard. The increased range and low-power consumption mean BLE 5 can play a crucial role in making beacons more practical and appealing. It also means that the designed AOA-supported beacons can be situated further away with increased accuracy.

7.2.1.4 Smartphone-based Sensor Fusion Indoor Positioning System

A smartphone-based sensor fusion IPS proposal[17] was submitted and accepted by Indoor Positioning and Indoor Navigation (IPIN) 2018, a world-leading indoor positioning and navigation conference. The main idea of this proposal is how to fuse the positioning methods which are mentioned in this thesis. e.g., multi-dimension location fingerprinting using both wireless selected AP ranking and MF measurements; fusing (EKF and PF) the predicted PDR result with the estimated location using the location fingerprinting.

7.2.1.5 Fusion Positioning for Augmented Reality

Google's Tango-based[18] consumer smartphone has a significant impact on many applications, especially in the area of indoor positioning, as it can offer centimetre positioning accuracy using a Tango-based smartphone. However, it can only run on just two types of smartphone. Now, Google is releasing ARCore[19], which will bring

---

[16] For more details: https://en.wikipedia.org/wiki/Bluetooth#Bluetooth_5. Last accessed in Sep/2018

[17] For more details: http://ipin2018.ifsttar.fr/. Last accessed in Sep/2018

[18] For more details: https://en.wikipedia.org/wiki/Tango_(platform). Last accessed in Sep/2018

[19] For more details: https://developers.google.com/ar/discover/. Last accessed in Sep/2018

the power of Tango to millions of more Android smartphones. This can bring a great opportunity to indoor LBS applications. Khuong and Luo [113] proposed to fuse traditional smartphone-based positioning methods with Tango, which can mitigate the Tango failure issue (e.g., insufficient light). This can also be explored with ARCore.

7.2.1.6 3D Indoor Positioning

As indoor spaces at work, leisure and for retail get more complex, there is an increasing need to address 3D positioning to identify which floor a physical asset is on that triggers a LD-AD. This also requires models and representations of 3D topographic indoor spaces [39].

7.2.2 ADL Recognition

7.2.2.1 More Advanced Machine Learning Methods

As I have considered that location-driven ADL recognition could be analogous to a translation problem, which also faces the challenge of insufficient specified labelled training measurements, as not all those ADLs can happen and are recorded for each data collection. Such a challenge could be solved by using state-of-art machine learning methods, e.g., one-shot learning [114], in which the training data will be paired with other data to expand the dataset, and then trained by a siamese network;

7.2.2.2 CSI/Radar-based methods

ADLs were thus far recognised based only on location information. More advanced data fusion can be considered, e.g., using location information with inertial sensors measurements to recognise far more fine-grained activities. Moreover, as most indoor positioning methods are using radio signals, such signals could also be parsed by using WiFi CSI [49], [45] or specialised Radar [115], [116] to recognise ADLs. Then, those measurements could also be fused to achieve a higher ADL recognition accuracy.

7.2.2.3 GPS-free outdoor positioning and ADL recognition

Low-Power Wide-Area Network (LPWAN) is a type of wireless telecommunication wide area network that is designed to enable long-range communication of low bit rate things. Among LPWAN, LoRaWAN[20] is a medium access control (MAC) protocol built on top of the LoRa technology developed by LoRa Alliance, which allows low-powered devices to communicate with the internet-connected applications via LoRaWAN gateways in a bi-directional manner. In LoRaWAN, the characteristic of periodic data uplink transmissions from the low-powered devices to the LoRaWAN in various monitoring and reporting applications provide great potential for location estimation of these devices without any hardware implementation and power consumption of positioning module. With the more deployed gateways, the more fine-grained LoRa RSSI fingerprints can be collected, which means a higher outdoor positioning results can be achieved. This could also be used to recognise outdoor activities.

[20] For more details: https://www.thethingsnetwork.org/docs/lorawan/. Last accessed in Sep/2018

8 Bibliography / References

[1] G. M. Giaglis, A. Pateli, K. Fouskas, P. Kourouthanassis, and A. Tsamakos, "On the potential use of mobile positioning technologies in indoor environments," in *the Proceedings of the 15 th Bled Electronic Commerce Conference-e-Reality: Constructing the e-Economy*, 2002, pp. 17-19.

[2] M. K. Jedrziewski, V. M.-Y. Lee, and J. Q. Trojanowski, "Physical activity and cognitive health," *Alzheimer's & Dementia*, vol. 3, pp. 98-108, 2007.

[3] K. A. Nguyen and Z. Luo, "Selective mixture of Gaussians clustering for location fingerprinting," in *Proceedings of the 11th International Conference on Mobile and Ubiquitous Systems: Computing, Networking and Services*, 2014, pp. 328-337.

[4] S.-E. Kim, Y. Kim, J. Yoon, and E. S. Kim, "Indoor positioning system using geomagnetic anomalies for smartphones," in *Indoor Positioning and Indoor Navigation (IPIN), 2012 International Conference on*, 2012, pp. 1-5.

[5] R. Aiello and A. Batra, *Ultra wideband systems: technologies and applications*: Newnes, 2006.

[6] Y. Gu, A. Lo, and I. Niemegeers, "A survey of indoor positioning systems for wireless personal networks," *IEEE Communications surveys & tutorials*, vol. 11, pp. 13-32, 2009.

[7] H. M. Khoury and V. R. Kamat, "Evaluation of position tracking technologies for user localization in indoor construction environments," *Automation in Construction*, vol. 18, pp. 444-457, 2009.

[8] B. Ozdenizci, K. Ok, V. Coskun, and M. N. Aydin, "Development of an indoor navigation system using NFC technology," in *Information and Computing (ICIC), 2011 Fourth International Conference on*, 2011, pp. 11-14.

[9] A. Harter, A. Hopper, P. Steggles, A. Ward, and P. Webster, "The anatomy of a context-aware application," *Wireless Networks*, vol. 8, pp. 187-197, 2002.

[10] J. Armstrong, Y. A. Sekercioglu, and A. Neild, "Visible light positioning: a roadmap for international standardization," *IEEE Communications Magazine*, vol. 51, pp. 68-73, 2013.

[11] P. Martin, B.-J. Ho, N. Grupen, S. Munoz, and M. Srivastava, "An ibeacon primer for indoor localization: demo abstract," in *Proceedings of the 1st ACM Conference on Embedded Systems for Energy-Efficient Buildings*, 2014, pp. 190-191.

[12] M. E. Rida, F. Liu, Y. Jadi, A. A. A. Algawhari, and A. Askourih, "Indoor location position based on bluetooth signal strength," in *Information Science and Control Engineering (ICISCE), 2015 2nd International Conference on*, 2015, pp. 769-773.

[13] P. Deepesh, R. Rath, A. Tiwary, V. N. Rao, and N. Kanakalata, "Experiences with using iBeacons for Indoor Positioning," in *Proceedings of the 9th India Software Engineering Conference*, 2016, pp. 184-189.

[14] J. Zhang, G. Han, N. Sun, and L. Shu, "Path-loss-based fingerprint localization approach for location-based services in indoor environments," *IEEE Access*, vol. 5, pp. 13756-13769, 2017.

[15] G. Jekabsons, V. Kairish, and V. Zuravlyov, "An analysis of Wi-Fi based indoor positioning accuracy," *Scientific Journal of Riga Technical University. Computer Sciences*, vol. 44, pp. 131-137, 2011.

[16] R. Faragher and R. Harle, "An analysis of the accuracy of bluetooth low energy for indoor positioning applications," in *Proceedings of the 27th International Technical Meeting of the Satellite Division of the Institute of Navigation (ION GNSS+'14)*, 2014, pp. 201-210.

[17] S. Gansemer, S. Pueschel, R. Frackowiak, S. Hakobyan, and U. Grossmann, "Improved RSSI-based euclidean distance positioning algorithm for large and dynamic WLAN environments," *International Journal of Computing*, vol. 9, pp. 37-44, 2010.

[18] Y. Zhuang, J. Yang, Y. Li, L. Qi, and N. El-Sheimy, "Smartphone-based indoor localization with bluetooth low energy beacons," *Sensors*, vol. 16, p. 596, 2016.

[19] A. M. Ladd, K. E. Bekris, A. Rudys, L. E. Kavraki, and D. S. Wallach, "Robotics-based location sensing using wireless ethernet," *Wireless Networks*, vol. 11, pp. 189-204, 2005.

[20] B. Viel and M. Asplund, "Why is fingerprint-based indoor localization still so hard?," in *Pervasive Computing and Communications Workshops (PERCOM Workshops), 2014 IEEE International Conference on*, 2014, pp. 443-448.

[21] G. Lui, T. Gallagher, B. Li, A. G. Dempster, and C. Rizos, "Differences in RSSI readings made by different Wi-Fi chipsets: A limitation of WLAN localization," in *Localization and GNSS (ICL-GNSS), 2011 International Conference on*, 2011, pp. 53-57.

[22] A. W. Tsui, Y.-H. Chuang, and H.-H. Chu, "Unsupervised learning for solving RSS hardware variance problem in WiFi localization," *Mobile Networks and Applications*, vol. 14, pp. 677-691, 2009.

[23] E. Tzoreff and A. J. Weiss, "Expectation-maximization algorithm for direct position determination," *Signal Processing*, vol. 133, pp. 32-39, 2017.

[24] Y. Xie, Y. Wang, A. Nallanathan, and L. Wang, "An Improved K-Nearest-Neighbor Indoor Localization Method Based on Spearman Distance," *IEEE Signal Process. Lett.*, vol. 23, pp. 351-355, 2016.

[25] X. Wang, L. Gao, S. Mao, and S. Pandey, "CSI-based fingerprinting for indoor localization: A deep learning approach," *IEEE Transactions on Vehicular Technology*, vol. 66, pp. 763-776, 2017.

[26] W. Zhang, K. Liu, W. Zhang, Y. Zhang, and J. Gu, "Deep neural networks for wireless localization in indoor and outdoor environments," *Neurocomputing*, vol. 194, pp. 279-287, 2016.

[27] M. Mohammadi, A. Al-Fuqaha, M. Guizani, and J.-S. Oh, "Semisupervised deep reinforcement learning in support of IoT and smart city services," *IEEE Internet of Things Journal*, vol. 5, pp. 624-635, 2018.

[28] J. Chung, M. Donahoe, C. Schmandt, I.-J. Kim, P. Razavai, and M. Wiseman, "Indoor location sensing using geo-magnetism," in *Proceedings of the 9th international conference on Mobile systems, applications, and services*, 2011, pp. 141-154.

[29] J. Song, H. Jeong, S. Hur, and Y. Park, "Improved indoor position estimation algorithm based on geo-magnetism intensity," in *Indoor Positioning and Indoor Navigation (IPIN), 2014 International Conference on*, 2014, pp. 741-744.

[30] P. Barsocchi, A. Crivello, D. La Rosa, and F. Palumbo, "A multisource and multivariate dataset for indoor localization methods based on WLAN and geo-magnetic field fingerprinting," in *Indoor Positioning and Indoor Navigation (IPIN), 2016 International Conference on*, 2016, pp. 1-8.

[31] G. Berkovich, "Accurate and reliable real-time indoor positioning on commercial smartphones," in *Indoor Positioning and Indoor Navigation (IPIN), 2014 International Conference on*, 2014, pp. 670-677.

[32] R. Faragher and R. Harle, "Location fingerprinting with bluetooth low energy beacons," *IEEE journal on Selected Areas in Communications*, vol. 33, pp. 2418-2428, 2015.

[33] A. R. Pratama and R. Hidayat, "Smartphone-based pedestrian dead reckoning as an indoor positioning system," in *System Engineering and Technology (ICSET), 2012 International Conference on*, 2012, pp. 1-6.

[34] X. Chen and Z. Gao, "Indoor ultrasonic positioning system of mobile robot based on TDOA ranging and improved trilateral algorithm," in *Image, Vision and Computing (ICIVC), 2017 2nd International Conference on*, 2017, pp. 923-927.

[35] J. Tiemann, F. Schweikowski, and C. Wietfeld, "Design of an UWB indoor-positioning system for UAV navigation in GNSS-denied environments," in *Indoor Positioning and Indoor Navigation (IPIN), 2015 International Conference on*, 2015, pp. 1-7.

[36] J. Wang and D. Katabi, "Dude, where's my card?: RFID positioning that works with multipath and non-line of sight," in *ACM SIGCOMM Computer Communication Review*, 2013, pp. 51-62.

[37] J. Jiao, F. Li, Z. Deng, and W. Ma, "A smartphone camera-based indoor positioning algorithm of crowded scenarios with the assistance of deep CNN," *Sensors*, vol. 17, p. 704, 2017.

[38] Y.-S. Kuo, P. Pannuto, K.-J. Hsiao, and P. Dutta, "Luxapose: Indoor positioning with mobile phones and visible light," in *Proceedings of the 20th annual international conference on Mobile computing and networking*, 2014, pp. 447-458.

[39] C. Nagel, T. Becker, R. Kaden, K. Li, J. Lee, and T. H. Kolbe, "Requirements and space-event modeling for indoor navigation," *Open Geospatial Consortium*, 2010.

[40] T. Haute, E. Poorter, P. Crombez, F. Lemic, V. Handziski, N. Wirström, *et al.*, "Performance analysis of multiple Indoor Positioning Systems in a healthcare environment," *International journal of health geographics*, vol. 15, p. 7, 2016.

[41] S. Tao, M. Kudo, H. Nonaka, and J. Toyama, "Camera view usage of binary infrared sensors for activity recognition," in *Pattern Recognition (ICPR), 2012 21st International Conference on*, 2012, pp. 1759-1762.

[42] J. Shotton, A. Fitzgibbon, M. Cook, T. Sharp, M. Finocchio, R. Moore, *et al.*, "Real-time human pose recognition in parts from single depth images," in *Computer Vision and Pattern Recognition (CVPR), 2011 IEEE Conference on*, 2011, pp. 1297-1304.

[43] O. D. Lara and M. A. Labrador, "A survey on human activity recognition using wearable sensors," *IEEE Communications Surveys and Tutorials*, vol. 15, pp. 1192-1209, 2013.

[44] J. R. Kwapisz, G. M. Weiss, and S. A. Moore, "Activity recognition using cell phone accelerometers," *ACM SigKDD Explorations Newsletter*, vol. 12, pp. 74-82, 2011.

[45] D. Zhang, H. Wang, Y. Wang, and J. Ma, "Anti-fall: A non-intrusive and real-time fall detector leveraging CSI from commodity WiFi devices," in *International Conference on Smart Homes and Health Telematics*, 2015, pp. 181-193.

[46] F. Adib, Z. Kabelac, D. Katabi, and R. C. Miller, "3D Tracking via Body Radio Reflections," in *NSDI*, 2014, pp. 317-329.

[47] S. Sigg, U. Blanke, and G. Troster, "The telepathic phone: Frictionless activity recognition from wifi-rssi," in *Pervasive Computing and Communications (PerCom), 2014 IEEE International Conference on*, 2014, pp. 148-155.

[48] Y. Wang, J. Liu, Y. Chen, M. Gruteser, J. Yang, and H. Liu, "E-eyes: device-free location-oriented activity identification using fine-grained wifi signatures," in *Proceedings of the 20th annual international conference on Mobile computing and networking*, 2014, pp. 617-628.

[49] W. Wang, A. X. Liu, M. Shahzad, K. Ling, and S. Lu, "Understanding and modeling of wifi signal based human activity recognition," in *Proceedings of the 21st annual international conference on mobile computing and networking*, 2015, pp. 65-76.

[50] K. Ali, A. X. Liu, W. Wang, and M. Shahzad, "Keystroke recognition using wifi signals," in *Proceedings of the 21st Annual International Conference on Mobile Computing and Networking*, 2015, pp. 90-102.

[51] S. Tan and J. Yang, "WiFinger: leveraging commodity WiFi for fine-grained finger gesture recognition," in *Proceedings of the 17th ACM International Symposium on Mobile Ad Hoc Networking and Computing*, 2016, pp. 201-210.

[52] F. Adib and D. Katabi, *See through walls with WiFi!* vol. 43: ACM, 2013.

[53] Q. Pu, S. Gupta, S. Gollakota, and S. Patel, "Whole-home gesture recognition using wireless signals," in *Proceedings of the 19th annual international conference on Mobile computing & networking*, 2013, pp. 27-38.

[54] M. Scholz, T. Riedel, M. Hock, and M. Beigl, "Device-free and device-bound activity recognition using radio signal strength," in *Proceedings of the 4th augmented human international conference*, 2013, pp. 100-107.

[55] D. M. Levine, S. R. Lipsitz, and J. A. Linder, "Trends in seniors' use of digital health technology in the united states, 2011-2014," *Jama*, vol. 316, pp. 538-540, 2016.

[56] M. Sridharan, J. Bigham, C. Phillips, and E. Bodanese, "Collaborative location estimation for confined spaces using magnetic field and inverse beacon positioning," in *SENSORS, 2017 IEEE*, 2017, pp. 1-3.

[57] K. A. Nguyen, C. Watkins, and Z. Luo, "Co-location Epidemic Tracking on London Public Transports Using Low Power Mobile Magnetometer," *arXiv preprint arXiv:1704.00148*, 2017.

[58] S. Krishnan, P. Sharma, Z. Guoping, and O. H. Woon, "A UWB based localization system for indoor robot navigation," in *Ultra-Wideband, 2007. ICUWB 2007. IEEE International Conference on*, 2007, pp. 77-82.

[59] J. Shackleton, B. VanVoorst, and J. Hesch, "Tracking people with a 360-degree lidar," in *Advanced Video and Signal Based Surveillance (AVSS), 2010 Seventh IEEE International Conference on*, 2010, pp. 420-426.

[60] C. Fuchsberger, J. Hunter, and P. McCue, "Testing Asbru guidelines and protocols for neonatal intensive care," in *Conference on Artificial Intelligence in Medicine in Europe*, 2005, pp. 101-110.

[61] U. Naeem and J. Bigham, "A comparison of two hidden markov approaches to task identification in the home environment," in *Pervasive Computing and Applications, 2007. ICPCA 2007. 2nd International Conference on*, 2007, pp. 383-388.

[62] R. Kosara, S. Miksch, Y. Shahar, and P. Johnson, "AsbruView: capturing complex, time-oriented plans—beyond flow charts," in *Diagrammatic Representation and Reasoning*, ed: Springer, 2002, pp. 535-549.

[63] R. Zurawski and M. Zhou, "Petri nets and industrial applications: A tutorial," *IEEE Transactions on industrial electronics*, vol. 41, pp. 567-583, 1994.

[64] W. van der Aalst, "How to handle dynamic change and capture management information?," in *4th International Conference on Cooperative Information Systems, Edinburgh, Scotland*.

[65] S. Nasreen, M. A. Azam, U. Naeem, M. A. Ghazanfar, and A. Khalid, "Recognition Framework for Inferring Activities of Daily Living Based on Pattern Mining," *Arabian Journal for Science and Engineering*, vol. 41, pp. 3113-3126, 2016.

[66] Z. Wang, B. Guo, Z. Yu, and X. Zhou, "Wi-Fi CSI-Based Behavior Recognition: From Signals and Actions to Activities," *IEEE Communications Magazine*, vol. 56, pp. 109-115, 2018.

[67] K. A. Nguyen and Z. Luo, "Dynamic route prediction with the magnetic field strength for indoor positioning," *International Journal of Wireless and Mobile Computing*, vol. 12, pp. 16-35, 2017.

[68] J. S. Seybold, *Introduction to RF propagation*: John Wiley & Sons, 2005.

[69] J. Petajajarvi, K. Mikhaylov, A. Roivainen, T. Hanninen, and M. Pettissalo, "On the coverage of LPWANs: range evaluation and channel attenuation model for LoRa technology," in *ITS Telecommunications (ITST), 2015 14th International Conference on*, 2015, pp. 55-59.

[70] H.-s. Cho, J. Ji, Z. Chen, H. Park, and W. Lee, "Accurate distance estimation between things: A self-correcting approach," *Open Journal of Internet Of Things (OJIOT)*, vol. 1, pp. 19-27, 2015.

[71] K. Nguyen and Z. Luo, "Evaluation of bluetooth properties for indoor localisation," in *Progress in Location-Based Services*, ed: Springer, 2013, pp. 127-149.

[72] K. Kaemarungsi and P. Krishnamurthy, "Properties of indoor received signal strength for WLAN location fingerprinting," in *Mobile and Ubiquitous Systems: Networking and Services, 2004. MOBIQUITOUS 2004. The First Annual International Conference on*, 2004, pp. 14-23.

[73] R. J. Samworth, "Optimal weighted nearest neighbour classifiers," *The Annals of Statistics*, vol. 40, pp. 2733-2763, 2012.

[74] A. I. McLeod, "Kendall rank correlation and Mann-Kendall trend test," *R Package Kendall*, 2005.

[75] R. Elbakly and M. Youssef, "A robust zero-calibration RF-based localization system for realistic environments," in *Sensing, Communication, and Networking (SECON), 2016 13th Annual IEEE International Conference on*, 2016, pp. 1-9.

[76] J. Handschin, "Monte Carlo techniques for prediction and filtering of non-linear stochastic processes," *Automatica*, vol. 6, pp. 555-563, 1970.

[77] A. Doucet, N. De Freitas, and N. Gordon, "An introduction to sequential Monte Carlo methods," in *Sequential Monte Carlo methods in practice*, ed: Springer, 2001, pp. 3-14.

[78] T. O. Oshin and S. Poslad, "ERSP: An energy-efficient real-time smartphone pedometer," in *Systems, Man, and Cybernetics (SMC), 2013 IEEE International Conference on*, 2013, pp. 2067-2072.

[79] D. Fox, W. Burgard, F. Dellaert, and S. Thrun, "Monte carlo localization: Efficient position estimation for mobile robots," *AAAI/IAAI*, vol. 1999, p. 2.2, 1999.

[80] R. Bellman, "The theory of dynamic programming," RAND Corp Santa Monica CA1954.

[81] F. Duchoň, A. Babinec, M. Kajan, P. Beňo, M. Florek, T. Fico, *et al.*, "Path planning with modified a star algorithm for a mobile robot," *Procedia Engineering*, vol. 96, pp. 59-69, 2014.

[82] D. B. Johnson, "A note on Dijkstra's shortest path algorithm," *Journal of the ACM (JACM)*, vol. 20, pp. 385-388, 1973.

[83] Y.-S. Chen, T.-T. Lo, and W.-C. Ma, "Efficient localization scheme based on coverage overlapping in wireless sensor networks," in *Communications and Networking in China (CHINACOM), 2010 5th International ICST Conference on*, 2010, pp. 1-5.

[84] F.-M. Jhuang, C.-F. Hung, C.-C. Tuan, Y.-C. Wu, and F.-Y. Leu, "An AP selection with RSS standard deviation for indoor positioning in Wi-Fi," in *2015 9th International Conference on Innovative Mobile and Internet Services in Ubiquitous Computing (IMIS)*, 2015, pp. 403-407.

[85] Y. Chen, Q. Yang, J. Yin, and X. Chai, "Power-efficient access-point selection for indoor location estimation," *IEEE Transactions on Knowledge and Data Engineering,* vol. 18, pp. 877-888, 2006.

[86] H. Zou, Y. Luo, X. Lu, H. Jiang, and L. Xie, "A mutual information based online access point selection strategy for WiFi indoor localization," in *Automation Science and Engineering (CASE), 2015 IEEE International Conference on*, 2015, pp. 180-185.

[87] Y. Xu, M. Zhou, and L. Ma, "WiFi indoor location determination via ANFIS with PCA methods," in *Network Infrastructure and Digital Content, 2009. IC-NIDC 2009. IEEE International Conference on*, 2009, pp. 647-651.

[88] A. Ismail, A. Sheta, and M. Al-Weshah, "A mobile robot path planning using genetic algorithm in static environment," *Journal of Computer Science,* vol. 4, pp. 341-344, 2008.

[89] J. Schmidhuber, "Deep learning in neural networks: An overview," *Neural networks,* vol. 61, pp. 85-117, 2015.

[90] X. Glorot and Y. Bengio, "Understanding the difficulty of training deep feedforward neural networks," in *Proceedings of the thirteenth international conference on artificial intelligence and statistics*, 2010, pp. 249-256.

[91] A. H. Salamah, M. Tamazin, M. A. Sharkas, and M. Khedr, "An enhanced WiFi indoor localization system based on machine learning," in *Indoor Positioning and Indoor Navigation (IPIN), 2016 International Conference on*, 2016, pp. 1-8.

[92] B. Karlik and A. V. Olgac, "Performance analysis of various activation functions in generalized MLP architectures of neural networks," *International Journal of Artificial Intelligence and Expert Systems,* vol. 1, pp. 111-122, 2011.

[93] S. Ruder, "An overview of gradient descent optimization algorithms," *arXiv preprint arXiv:1609.04747*, 2016.

[94] R. E. Kalman, "A new approach to linear filtering and prediction problems," *Journal of basic Engineering,* vol. 82, pp. 35-45, 1960.

[95] G. Bishop and G. Welch, "An introduction to the Kalman filter," *Proc of SIGGRAPH, Course,* vol. 8, p. 59, 2001.

[96] K. Fujii, "Extended kalman filter," *Refernce Manual,* 2013.

[97] Y. Li, Y. Zhuang, H. Lan, X. Niu, and N. El-Sheimy, "A profile-matching method for wireless positioning," *IEEE communications letters*, vol. 20, pp. 2514-2517, 2016.

[98] G. A. ten Holt, M. J. Reinders, and E. Hendriks, "Multi-dimensional dynamic time warping for gesture recognition," in *Thirteenth annual conference of the Advanced School for Computing and Imaging*, 2007, p. 1.

[99] D. J. Berndt and J. Clifford, "Using dynamic time warping to find patterns in time series," in *KDD workshop*, 1994, pp. 359-370.

[100] A. Ismail and A. Vigneron, "A new trajectory similarity measure for GPS data," in *Proceedings of the 6th ACM SIGSPATIAL International Workshop on GeoStreaming*, 2015, pp. 19-22.

[101] I. Sutskever, O. Vinyals, and Q. V. Le, "Sequence to sequence learning with neural networks," in *Advances in neural information processing systems*, 2014, pp. 3104-3112.

[102] G. Rote, "Computing the minimum Hausdorff distance between two point sets on a line under translation," *Information Processing Letters*, vol. 38, pp. 123-127, 1991.

[103] T. Colleens and J. Colleens, "Occupancy grid mapping: An empirical evaluation," in *Control & Automation, 2007. MED'07. Mediterranean Conference on*, 2007, pp. 1-6.

[104] J. E. Bresenham, "Incremental line compaction," *The Computer Journal*, vol. 25, pp. 116-120, 1982.

[105] M. Ester, H.-P. Kriegel, J. Sander, and X. Xu, "Density-based spatial clustering of applications with noise," in *Int. Conf. Knowledge Discovery and Data Mining*, 1996.

[106] G. Stylianou, "Stay-point Identification as Curve Extrema," *arXiv preprint arXiv:1701.06276*, 2017.

[107] A. Garulli, A. Giannitrapani, A. Rossi, and A. Vicino, "Mobile robot SLAM for line-based environment representation," in *IEEE Conference on Decision and Control*, 2005, p. 2041.

[108] J. Sturm, N. Engelhard, F. Endres, W. Burgard, and D. Cremers, "A benchmark for the evaluation of RGB-D SLAM systems," in *Intelligent Robots and Systems (IROS), 2012 IEEE/RSJ International Conference on*, 2012, pp. 573-580.

[109] S. Knauth and A. Koukofikis, "Smartphone positioning in large environments by sensor data fusion, particle filter and FCWC," in *Indoor Positioning and Indoor Navigation (IPIN), 2016 International Conference on*, 2016, pp. 1-5.

[110] Z. Chen, H. Zou, H. Jiang, Q. Zhu, Y. C. Soh, and L. Xie, "Fusion of WiFi, smartphone sensors and landmarks using the Kalman filter for indoor localization," *Sensors*, vol. 15, pp. 715-732, 2015.

[111] J. Tisdale, Z. Kim, and J. K. Hedrick, "Autonomous UAV path planning and estimation," *IEEE Robotics & Automation Magazine*, vol. 16, 2009.

[112] L. Lei, H. Wang, and Q. Wu, "Improved genetic algorithms based path planning of mobile robot under dynamic unknown environment," in *Mechatronics and Automation, Proceedings of the 2006 IEEE International Conference on*, 2006, pp. 1728-1732.

[113] K. A. Nguyen and Z. Luo, "On assessing the positioning accuracy of Google Tango in challenging indoor environments," in *Indoor Positioning and Indoor Navigation (IPIN), 2017 International Conference on*, 2017, pp. 1-8.

[114] R. Socher, M. Ganjoo, C. D. Manning, and A. Ng, "Zero-shot learning through cross-modal transfer," in *Advances in neural information processing systems*, 2013, pp. 935-943.

[115] M. Z. T. L. M. Abu, A. Y. T. H. Zhao, and A. T. D. Katabi, "Through-Wall Human Pose Estimation Using Radio Signals."

[116] H.-S. Fang, Y. Xu, W. Wang, X. Liu, and S.-C. Zhu, "Learning pose grammar to encode human body configuration for 3D pose estimation," in *Proc. of the AAAI Conference on Artificial Intelligence*, 2018.

Appendix A

Table 11 Some representative positioning companies and its solution (public data)

Solutions	Techniques	Accuracy	Application
WiFiSLAM	WiFi	2.5 m	Indoor LBS
Estimote	BLE	2 m	Indoor LBS
Meridian	WiFi/BLE	1~3 m	Indoor Navigation
Sensewhere	WiFi/BLE	< 10 m	Indoor LBS
Iway	WiFi/GSM	2~3 m	Indoor LBS
Loctronix	GSM	15 m	Emergency Services
Pointr	BLE	1~3 m	Indoor LBS
9Solutions	BLE/RFID	1~2 m	Security/Health
NaciFloor	RFID	50 cm	Robots
Ubisense	UWB	15 cm	Indoor LBS
Zebra	UWB/RFID	< 1 m	Outdoor/Indoor LBS
Prozyx	UWB+IMU	10 cm	Positioning Modules
ByteLight	LED	5-10 cm	Indoor LBS
IndoorAtlas	Magnetism	1~3 m	Indoor LBS
Cricket	Ultrasonic	1~3 cm	Indoor Navigation
Velodyne	Lidar	1~3 cm	Positioning Modules
LPR-2D	Radar	20 cm	Outdoor/Indoor LBS
Google VPS	Camera	< 3 m	Outdoor/Indoor LBS

Appendix B

This section describes all the training trajectories used in Chapter 5.

Class A-1 (7.5 m)

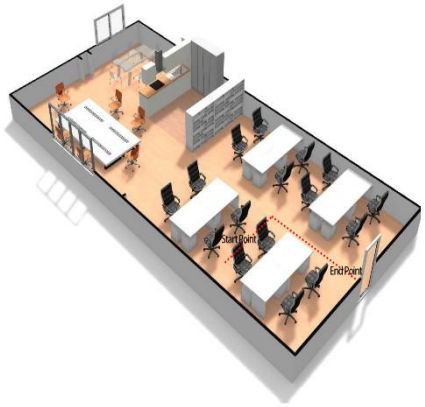

Class A-2 (6.5 m)

Class A-3 (12.5 m)

Class A-4 (8 m)

Class A-5 (9 m)

Class A-6 (16 m)

Class A-7 (10 m)

Class A-8 (11 m)

Class A-9 (18 m)

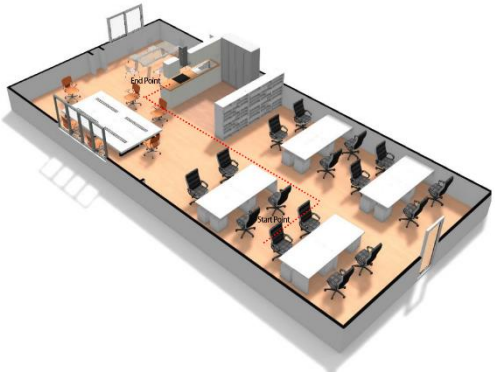

Class A-10 (13.5 m)

Class A-11 (14.5 m)

Class A-12 (21.5 m)

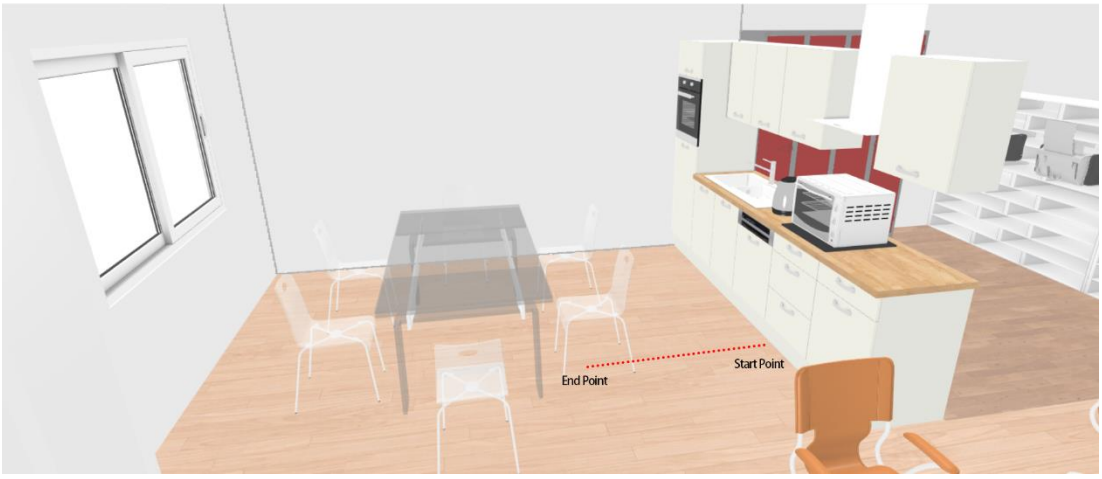

Class B-13 (2 m)

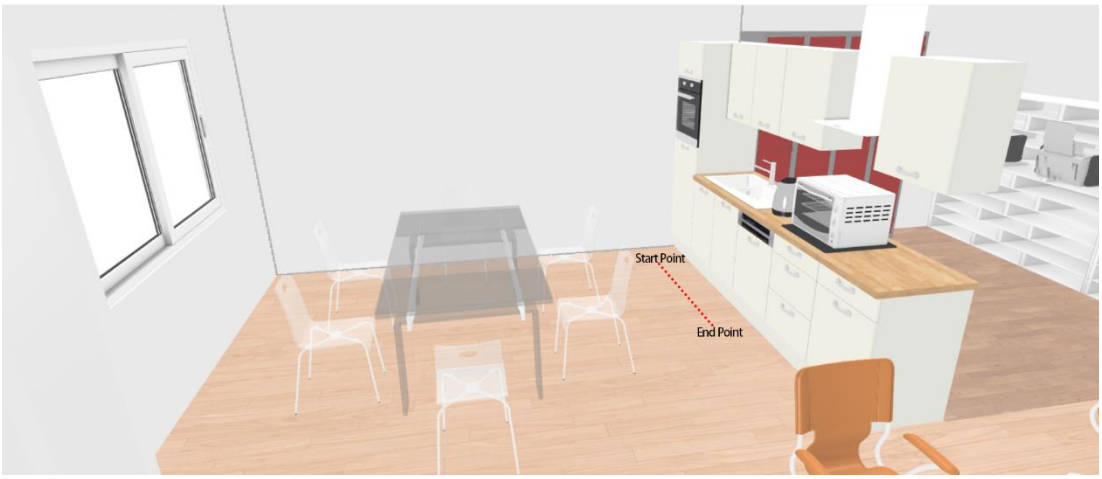

Class B-14 (1.5 m)

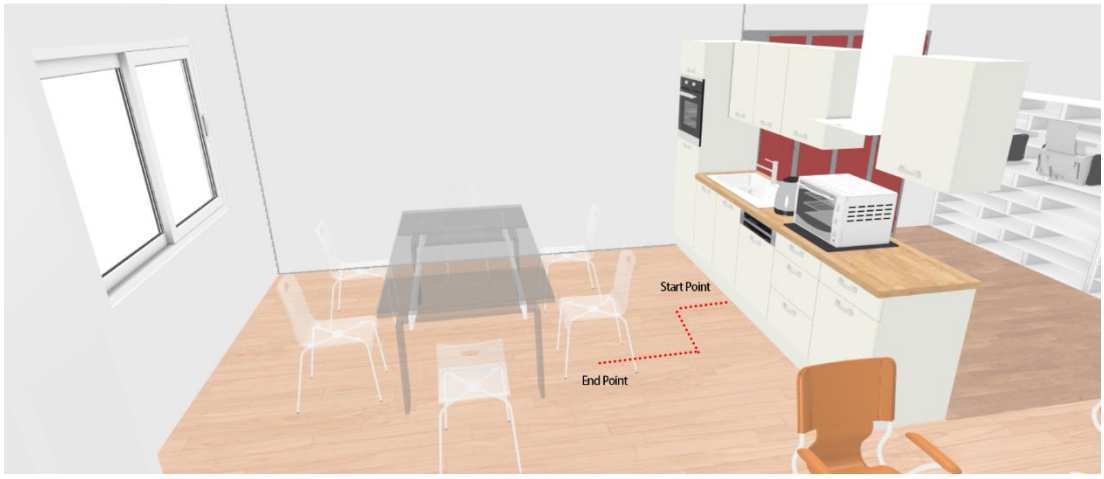

Class B-15 (2.5 m)

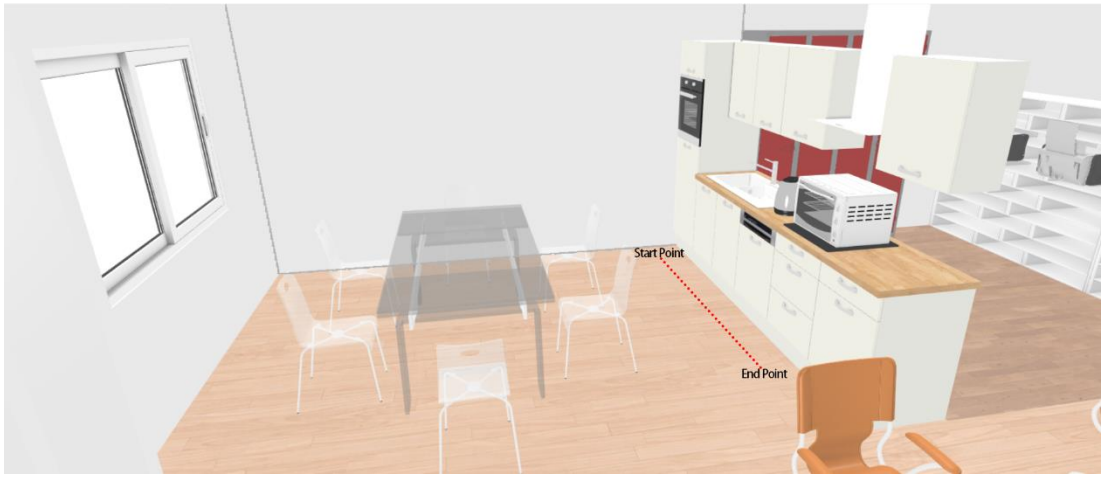

Class B-16 (2 m)

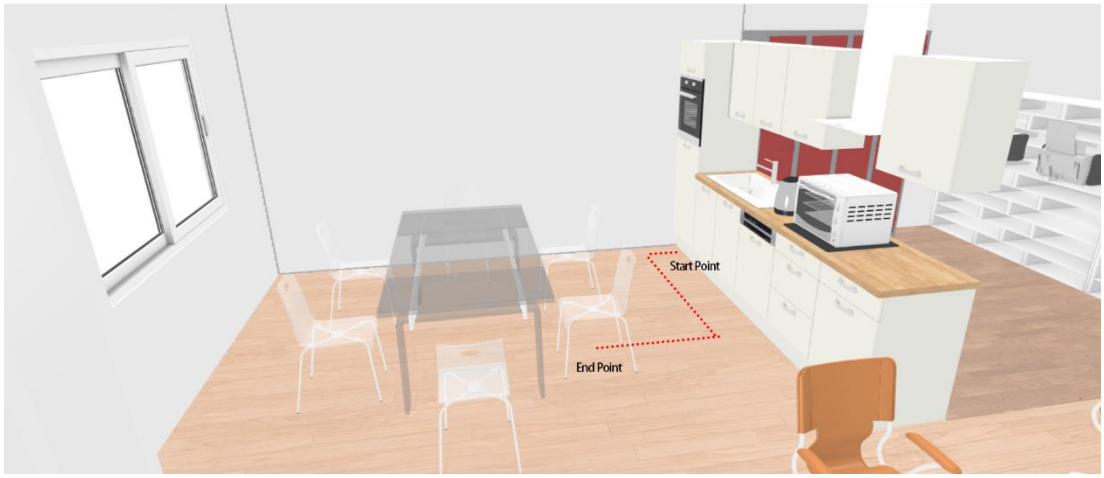

Class B-17 (3.5 m)